Compilation of the Static Dielectric Constant of Inorganic Solids

K. F. Young and H. P. R. Frederikse

Institute for Materials Research, National Bureau of Standards, Washington, D.C. 20234

This compilation contains values of the static dielectric constant of more than 300 inorganic solids. The temperature and frequency of the measurements are listed and the magnitude of the loss tangent is indicated if known. For ninety materials—including most ferroelectrics and antiferroelectrics and several oxides and halides—additional information is presented in the form of graphs depicting the temperature dependence of the dielectric constant. In a few cases the frequency and pressure dependences are also shown. The basic principles and formulas pertinent to the field of dielectrics are reviewed in a short introduction. This part also mentions several measuring techniques and indicates the criteria used for data selection.

Key words: Dielectric constant; dielectric loss; permittivity; static dielectric constant.

Contents

1. Introduction

1.1. Relevance and Sources

The dielectric constant plays an important role in many physical processes and often has to be considered in the evaluation of a material for engineering purposes [1–5] [1]. The analysis of infrared lattice modes, electron-lattice coupling, donor and acceptor activation energies in semiconductors, surface layer properties, plasmon frequencies, electron scattering in solids, etc., all require a knowledge of the dielectric constant. The potential uses of a solid in many technical applications such as insulating coatings, transducers, and capacitors are strongly determined by its dielectric properties. Hence, there is a need for reliable data on the dielectric constants and losses of a wide range of inorganic solids.

The basis of this compilation is a list of dielectric constants originally compiled by S. O. Morgan for the first edition of the AIP–Handbook (1957), [13] updated in the second edition (1963) by J. H. Wasilik, and more recently in the third edition (1972) by K. F. Young. Subsequently this list was considerably expanded by adding information obtained with the aid of two bibliographies: one on Ferroelectrics compiled by Thomas Connolly (Oak Ridge) and Errett Turner (Bell Laboratories), and the other on Electronic Properties of Materials compiled under the auspices of the Electronic Properties Information Center (Hughes Aircraft Company, Culver City, California). Other data have been gathered from "Ferroelectric Crystals" (Jona and Shirane), and "Ferroelectricity" (Merz and Fattuzzo) as well as data brochures from commercial crystal suppliers. The present compilation lists 316 compounds, and entries were made up to January 1972.

[1] Figures in brackets indicate the literature references at the end of this Introduction.

Copyright © 1973 by the U.S. Secretary of Commerce on behalf of the United States. This copyright will be assigned to the American Institute of Physics and the American Chemical Society, to whom all requests regarding reproduction should be addressed.

1.2. Definitions

When a homogeneous dielectric medium is inserted in a capacitor with vacuum capacitance C_0, the capacitor can store more charge and its capacitance is increased to C. The ratio $C/C_0 = \epsilon$ defines the (relative) dielectric constant of the medium. The increased storage capacity is a result of the appearance of polarization charges at the electrode surfaces (which do not contribute to the electric field). This phenomenon is known as dielectric polarization.

The charges are distributed over the surfaces of the electrodes. If the charge density is given by q and the surface area is A, the total charge Q can be written as

$$Q = \int_A q dA. \tag{1}$$

Only the free charge density q/ϵ contributes to the voltage across the capacitor, while the polarization charge density $q(1 - 1/\epsilon)$ is neutralized at the electrode surfaces.

At this point it is common to introduce three field vectors **D**, **E**, and **P**. The electric flux density or dielectric displacement **D**, is related to the (true) charge such that, in a capacitor of effectively infinite extent, the surface-charge density is equal to the normal component of **D**:

$$qdA = D_n dA. \tag{2}$$

Furthermore, the free-charge density determines the electric field strength or field intensity **E** as follows:

$$(q/\epsilon)dA = \epsilon_0 E_n dA. \tag{3}$$

where E_n is the normal component of **E**, and ϵ_0 is the permittivity of free space. Finally, the bound charge density is connected with the polarization, **P**. For the normal component of **P** one can write:

$$q(1-1/\epsilon)dA = P_n dA. \tag{4}$$

From (1), (2), (3), and (4) it then follows that:

$$\mathbf{D} = \epsilon\,\epsilon_0 \mathbf{E} \tag{5}$$

and

$$\mathbf{P} = \mathbf{D} - \epsilon_0 \mathbf{E} = \epsilon_0(\epsilon - 1)\mathbf{E} = \chi \epsilon_0 \mathbf{E}. \tag{6}$$

The parameter $\chi = \epsilon - 1$ is called the dielectric susceptibility.

The field $\mathbf{E}_{loc}$ acting on an atom within the material in the capacitor is given by:

$$\mathbf{E}_{loc} = \mathbf{E} + \mathbf{E}_L + \mathbf{E}_d, \tag{7}$$

where **E** = applied field, $\mathbf{E}_L$ = Lorentz field, due to polarization charges on the inside of the fictitious Lorentz cavity, and $\mathbf{E}_d$ = dipole field, due to dipoles within the Lorentz cavity. If the Lorentz cavity is a sphere, the $\mathbf{E}_L$ is equal to $\mathbf{P}/3\epsilon_0$. The last term reduces to zero for isotropic media and for cubic crystals (when every ion occupies a center of symmetry). Hence for our case:

$$\mathbf{E}_{loc} = \mathbf{E} + \mathbf{P}/3\epsilon_0. \tag{8}$$

This local field polarizes the individual atoms or ions and produces dipoles of magnitude

$$p_i = \alpha_i E_{loc}. \tag{9}$$

α_i defines the polarizability. For N_i atoms or ions per unit volume of type i, the polarization, **P**, can be written as:

$$\mathbf{P} = \sum_i N_i p_i = \mathbf{E}_{loc} \sum_i N_i \alpha_i \tag{10}$$

From eqs (8) and (10) one finds the susceptibility

$$\chi = \frac{\mathbf{P}}{\epsilon_0 \mathbf{E}} = \frac{\sum_i N_i \alpha_i}{\epsilon_0 \left(1 - \frac{1}{3\epsilon_0}\sum_i N_i \alpha_i\right)} = \epsilon - 1. \tag{11}$$

Solving for $\sum_i N_i \alpha_i$ yields the Clausius-Mosotti relation:

$$\frac{\epsilon - 1}{\epsilon + 2} = \frac{1}{3\epsilon_0} \cdot \sum_i N_i \alpha_i. \tag{12}$$

The polarizabilities α_i in the expressions for the polarization, **P**, and for the susceptibility, χ, and in the Clausius-Mosotti relation may refer to electronic or ionic polarization. At optical frequencies the dielectric constant is equal to n^2 (the square of the index of refraction). It should be realized that the derivation of these quantities is based on the assumption of point charges at the lattice points of a crystalline solid. This is, of course, a rather unrealistic assumption, especially for covalent materials.

The above formulas are presented in the International System of Units (SI). In the cgs system they take the following form:

$$\mathbf{D} = \epsilon \mathbf{E}, \tag{5'}$$

$$\mathbf{P} = (\epsilon - 1/4\pi)\mathbf{E} = \chi \mathbf{E}, \tag{6'}$$

$$\mathbf{E}_{loc} = \mathbf{E} + (4\pi/3)\mathbf{P}, \tag{8'}$$

$$\chi = \frac{\sum_i N_i\alpha_i}{1-(4\pi/3)\sum_i N_i\alpha_i}, \qquad (11')$$

and

$$(\epsilon-1)/(\epsilon+2) = (4\pi/3)\sum_i N_i\alpha_i. \qquad (12')$$

In the SI system, permittivity is expressed in the unit farad per meter (F/m). The permittivity of free space is

$$\epsilon_0 = (1/36\,\pi)\times 10^{-9} \simeq 8.854\times 10^{-12}\,\mathrm{F/}m.$$

Usually this is referred to as the dielectric constant. In the cgs system the relative dielectric constant, ϵ, is a pure number and is equal to the relative permittivity, ϵ_r, in the SI system. However, in most of the literature referred to in this survey, the relative permittivity is called the dielectric constant and is expressed as ϵ. This convention is also followed here.

So far the dielectric constant has been treated as a scalar quantity. Actually, the relation between **D** and **E** is a tensor relationship and the dielectric constant is a second-rank symmetric tensor with six independent components ϵ_{ij}. For the different crystal symmetries the form of the tensor and the number of independent components is given in table 1.

The formulas (1)–(12) are derived on the basis of response of the medium to a static electric field. However, if one applies a time dependent field it appears that the displacement cannot follow the field instantaneously. This is a consequence of the fact that no material is "perfect," but instead exhibits inertial effects and losses. Suppose one applies an alternating field $\mathbf{E} = \mathbf{E}_0 e^{i\omega t}$. The resulting displacement will show a lag represented by the phase angle δ and will take the form:

$$\mathbf{D} = \mathbf{D}_0 e^{i(\omega t-\delta)}.$$

Hence the relation between **D** and **E** is conveniently described by a complex dielectric constant

$$\epsilon = \epsilon' - i\epsilon'', \qquad (13)$$

and

$$\epsilon = (\mathbf{D}_0/\mathbf{E}_0)\,e^{-i\delta} = (\mathbf{D}_0/\mathbf{E}_0)(\cos\delta - i\sin\delta). \qquad (14)$$

The real and imaginary parts of the dielectric constant can now be written as follows:

$$\epsilon' = (\mathbf{D}_0/\mathbf{E}_0)\cos\delta, \qquad (15a)$$

and

$$\epsilon'' = (\mathbf{D}_0/\mathbf{E}_0)\sin\delta. \qquad (15b)$$

The tangent of the loss angle is given by:

$$\epsilon''/\epsilon' = \tan\delta. \qquad (16)$$

TABLE 1. Crystal symmetry and tensor form

System	Characteristic Symmetry	Number of Components	Form of the tensor
Cubic	4 3-fold axes	1	$\epsilon\ 0\ 0$ $0\ \epsilon\ 0$ $0\ 0\ \epsilon$
Tetragonal Hexagonal Trigonal	1 4-fold axis 1 6-fold axis 1 3-fold axis	2	$\epsilon_1\ 0\ 0$ $0\ \epsilon_1\ 0$ $0\ 0\ \epsilon_3$
Orthorhombic	3 mutually perpendicular 2-fold axes; no higher order axes	3	$\epsilon_1\ 0\ 0$ $0\ \epsilon_2\ 0$ $0\ 0\ \epsilon_3$
Monoclinic	1 2-fold axis	4	$\epsilon_{11}\ 0\ \epsilon_{31}$ $0\ \epsilon_{22}\ 0$ $\epsilon_{31}\ 0\ \epsilon_{33}$
Triclinic	One center of symmetry or no symmetry	6	$\epsilon_{11}\ \epsilon_{21}\ \epsilon_{31}$ $\epsilon_{21}\ \epsilon_{22}\ \epsilon_{32}$ $\epsilon_{31}\ \epsilon_{32}\ \epsilon_{33}$

1.3. Measurement Techniques

The principal method for determining the real and imaginary parts of the dielectric constant is the comparison of the capacity of an empty (air-filled) capacitor (C_0) with that of the same capacitor containing the dielectric medium (C). In the frequency range 10^2 to 10^7 Hz one often uses the Schering bridge (somewhat analogous to a Wheatstone bridge). Three arms of the bridge contain variable and standard resistors and and capacitors, while the substance to be measured can be inserted in a capacitor which forms the fourth arm

of the bridge. The determination of the dielectric constant and loss from the measured capacitances and resistances with and without the medium is straightforward. Refinements and modifications of this method can be found in many books and publications [1,2,6,7].

For somewhat higher frequencies (10–100 MHz) the resonant circuit method is often used. In this case the capacitor (with the dielectric medium) is made part of an *LC* circuit which is loosely coupled to a generator. The circuit is made to resonate by means of a tuning capacitor before and after removal of the substance [1,2].

In the frequency interval between 100 MHz and 1 GHz one often uses the transmission line technique. In this method the specimen is made the terminating impedance of a coaxial line, producing a standing wave pattern. From the positions and magnitudes of the maxima and minima one can determine the dielectric constant [1].

At still higher frequencies, in the microwave range, the dielectric constant and losses can be measured by transmission line methods or by detecting the perturbation of a cavity. In the latter case, the real part ϵ' can be derived from the shift of the resonant frequency, while an analysis of the change of the height (or width) of the resonant line yields the imaginary part ϵ'' [8, 9].

Dielectric constants of constrained piezoelectric materials are different from those that are not constrained. If the crystal is held rigidly so that displacement in the direction of the applied field is prevented, then the dielectric constant is measured under constant strain and is called the "clamped" dielectric constant, ϵ^S. If the constraint is removed, additional energy is stored in mechanical form producing an increase in the dielectric constant. The effect is greatest when the crystal is completely free to move and yields the "unclamped" dielectric constant measured under constant stress, ϵ^T [12].

1.4. Frequency Dependence

The dielectric constants of most substances show considerable variation with frequency (dispersion). In the high frequency range ($\omega > 10^{14}$ Hz) the dielectric constant has the optical value $\epsilon_\infty = n^2$. With decreasing frequency one finds the infrared dispersion range around $\omega = 10^{13}$ Hz where the dielectric "constant" increases considerably until it reaches a new constant level. For some materials this level is maintained down to very low frequencies, while others show a second dispersion in the microwave, the UHF range, or even lower.

The frequency dependence of the dielectric constant arises from the fact that the polarizability of the medium is caused by different mechanisms (see fig. 1). One can write the total polarizability as the sum of four contributions:

$$\alpha = \alpha_{el} + \alpha_{ion} + \alpha_{dip} + \alpha_{int}. \quad (17)$$

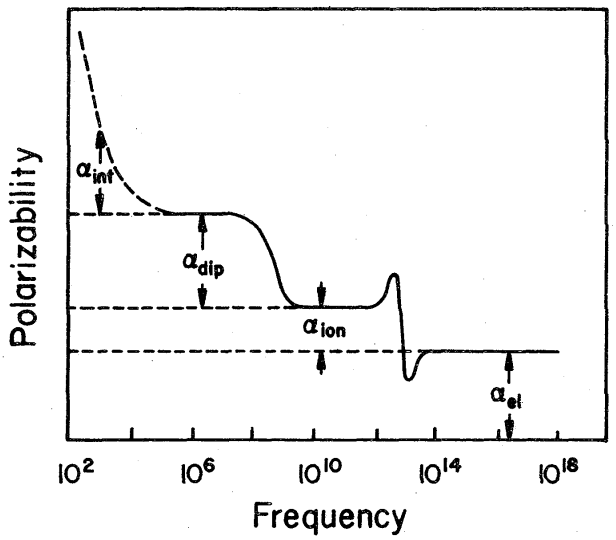

FIGURE 1. Frequency dependence of the polarizability showing several contributing mechanisms.

The electronic contribution α_{el} results from the displacement of the electron cloud relative to the nucleus. Applying the Clausius-Mosotti relation to several different groups of crystals, one can calculate the electronic polarizability of many ions. The values range from 0.0013×10^{-24} cm^3 for C^{4+} to 14×10^{-24} cm^3 for Te^{2-} (in cgs units) [10].

The second term in eq (17) is the ionic polarizability, α_{ion}. This part is a consequence of the displacement of one ion with respect to other ions under the influence of an applied field. Infrared radiation is capable of exciting some of the resonant modes of the medium, giving rise to strong absorption and reflection. At higher frequencies the ions cannot follow the field any more and the ionic polarizability vanishes.

A third contribution originates from the presence of permanent dipoles in the host lattice. These dipoles will be oriented by the applied field up to frequencies of the order of 10^{10} Hz in some cases. This portion of α is known as the dipolar or orientational polarizability α_{dip}.

Real substances contain defects such as grain boundaries, voids, dislocations, clusters of vacancies, interstitials or impurities which can be the source of large accumulations of charges in the bulk of the dielectric. Similar effects occur in nearly all semiconductors and slightly conducting insulators at the electrode-crystal interface. Charges may pile up at the electrode and produce a double layer. Such a barrier layer may result from migrating ions which can not leave the dielectric (blocking electrode) or from trapped electrons or holes (Schottky layer). It is often very difficult to determine if the space charge accumulation is ionic or electronic in nature.

Another source of polarization is caused by random or layered inhomogeneities in the dielectric. This com-

ponent can be easily calculated for simple geometries and is known as the Maxwell-Wagner polarization.

All these mechanisms contribute to the interfacial polarizability α_{int}. As a result one often observes at low frequencies dielectric constants much in excess of the real value for the pure bulk material. (The real value of the dielectric constant excludes the interfacial polarization.) Because of this effect it usually is impossible to measure the static dielectric constant in the low frequency range; for the great majority of substances the measurement has been performed at 10^3 Hz or higher (sometimes as high as 10^8 or 10^9 Hz).

Dielectrics can be divided into three groups on the basis of the polarizability of the host lattice: (1) Nonpolar or covalent materials which do not contain either induced or permanent dipoles. These solids show no dispersion below the optical range; hence the static dielectric constant is equal to the optical dielectric constant ($\epsilon_{op}=n^2$) over the entire frequency range. (2) Polar materials which comprise only induced dipoles. (3) Materials of either kind containing permanent dipoles (mainly molecular crystals).

1.5. Temperature Dependence

Only materials of the groups (1) and (2) mentioned above (covalent solids and ionic substances with inversion symmetry) obey the Clausius-Mosotti expression:

$$(\epsilon-1)/(\epsilon+2)=(1/3)(\alpha_m/V), \qquad (12'')$$

where (α_m/V) is the polarizability per unit volume. The temperature dependence of the dielectric constant is easily obtained by differentiating (12″) with respect to T at constant pressure P:

$$\frac{1}{(\epsilon-1)(\epsilon+2)}\left(\frac{\partial\epsilon}{\partial T}\right)_P=-\frac{1}{3V}\left(\frac{\partial V}{\partial T}\right)_P$$

$$+\left[\frac{1}{\alpha_m}\left(\frac{\partial\alpha_m}{\partial P}\right)_T\Big/\frac{1}{V}\left(\frac{\partial V}{\partial P}\right)_T\right]\frac{1}{3V}\left(\frac{\partial V}{\partial T}\right)_P$$

$$+\frac{1}{3\alpha_m}\left(\frac{\partial\alpha_m}{\partial T}\right)_V=K+L+M. \qquad (18)$$

The first term K describes the direct effect of volume expansion, the second term L represents the increase of the polarizability of a given number of particles as a result of the expanding volume, and the third term M indicates the temperature dependence of the polarizability itself (at constant volume).

It is important to be able to separate the volume-dependent terms and the direct temperature effect. For materials with high ϵ the temperature dependence is almost entirely determined by the last term M in eq (18). This term can be written as follows:

$$M=\frac{1}{(\epsilon-1)(\epsilon+2)}\left(\frac{\partial\epsilon}{\partial T}\right)_V=\frac{1}{(\epsilon-1)(\epsilon+2)}\left\{\left(\frac{\partial\epsilon}{\partial T}\right)_P-\frac{\left(\frac{\partial\epsilon}{\partial P}\right)_T\cdot\left[\frac{1}{V}\frac{\partial V}{\partial T}\right]_P}{\frac{3}{V}\left(\frac{\partial V}{\partial P}\right)_T}\right\}. \qquad (19)$$

This equation shows that in order to calculate the different contributions to the temperature dependence of ϵ one needs to know the thermal expansion coefficient $1/V)(\partial V/\partial T)_P$, the compressibility $-(1/V)(\partial V/\partial P)_T$, the pressure dependence of the dielectric constant $(\partial\epsilon/\partial P)_T$, its over-all temperature dependence $(\partial\epsilon/\partial T)_P$, and finally ϵ itself.

Many strongly polarizable materials (large ϵ) do not follow the Clausius-Mosotti formula. For such materials either a Curie law, $\epsilon=C/T$, or a Curie-Weiss law, $\epsilon=C/(T-T_C)$, holds where C is the Curie constant and T_C is the Curie temperature. In that case

$$(1/\epsilon^2)(\partial\epsilon/\partial T)_P=-(1/C). \qquad (20)$$

Bosman and Havinga [11] have discovered an interesting experimental relationship between the dielectric constant and its temperature dependence which holds for a surprisingly large and diversified number of materials (see fig. 2). It appears that $(\partial\epsilon/\partial T)_P/[(\epsilon-1)(\epsilon+2)]$ is positive for all substances with dielectric

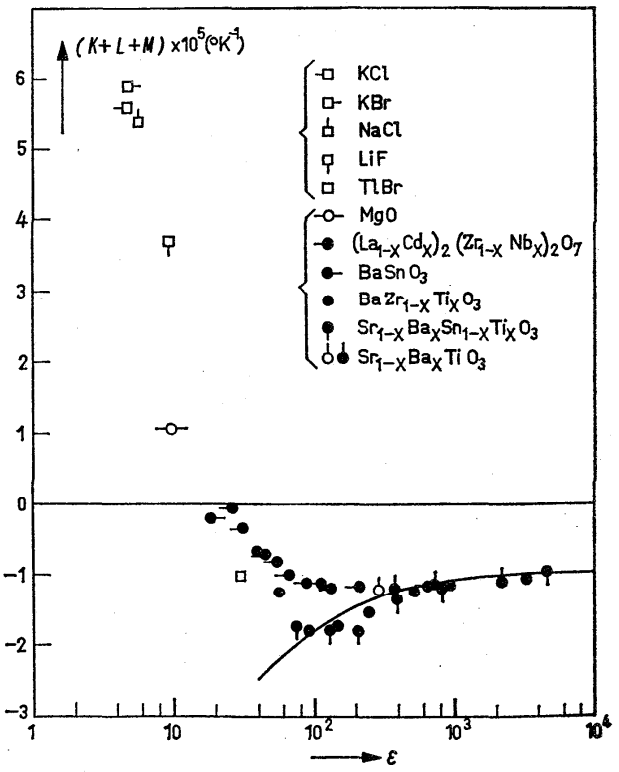

FIGURE 2. The temperature dependence of the dielectric constant, $K+L+M=[1/(\epsilon-1)(\epsilon+2)](\partial\epsilon/\partial T)_P$, as a function of ϵ for a number of cubic compounds at room temperature.

Open symbols mark single crystals; full symbols, ceramics.

constants smaller than ≈ 20, and negative when $\epsilon > 20$.

Ferroelectrics and antiferroelectrics, piezoelectrics, and other crystals that undergo phase changes usually show very large and abrupt variations of the dielectric constant as a function of temperature. The change of ϵ at the transition point depends strongly on the nature of the phase transition. Impurities, defects, domain boundaries greatly influence the measurement of large dielectric constants. Hence one finds considerable variations in the measured values of ϵ in the region of the Curie temperature(s).

1.6. Dielectric Losses

In the previous sections the discussion has been limited to the real part of static dielectric constant, its frequency behavior, temperature dependence, etc. of the perfect intrinsic material without any defects or impurities. This section deals with extrinsic dielectric effects due to polarizable admixtures or irregularities (usually in amounts much smaller than 1%), which produce primarily contributions to the imaginary part of the dielectric constant.

Many polar and non-polar materials contain small numbers of dipoles (e.g., OH^- in oxides, divalent ions associated with vacancies in alkali halides, etc.). For small concentrations the effect of these dipoles is not sufficient to produce readily measurable changes in the real part of the dielectric constant, but they do give rise to increased dielectric losses in certain temperature and frequency regions depending on the relaxation frequency. The loss factor $\tan \delta$ sometimes has the characteristic Debye form, $\omega\tau/(1+\omega^2\tau^2)$, where τ is the relaxation time. Measurements of $\tan \delta$ as a function of frequency for different temperatures make it possible to determine the activation energy and relaxation time of dipolar orientational processes. If just one kind of dipole is involved, a well-defined Debye peak may be observed associated with a single relaxation time. However, often many dipoles of different strengths contribute to the dielectric loss and the process has to be described by a distribution of relaxation times.

Up to this point the dielectric has been treated as a perfect insulator. However, all solids are electrical conductors to a greater or lesser degree. The charge carriers may be electrons or holes, or, at high temperatures, ions. The conductivity will contribute to the loss factor an amount $(\tan \delta)_c = \sigma/\epsilon'\omega$; the quantity σ is practically frequency independent and equal to the dc conductivity. It should be stressed that the conduction loss, $(\tan \delta)_c$, is inversely proportional to ω and tends to infinity for $\omega \to 0$. Debye-type losses, on the other hand, show a maximum at the relaxation frequency ω_0 and decrease as $1/\omega$ for $\omega \gg \omega_0$. For frequencies larger than ω_0 the behavior of dipolar and conduction losses will approximate each other; only measurements performed at sufficiently low frequencies to detect the relaxation maximum will make it possible to distinguish between the two phenomena.

1.7. Data Evaluation

The number of measurements reported for each solid in this compilation is most often one or two; three or more independent determinations are quite rare. Thus, the evaluation of data is made primarily on the basis of the measurement procedures used and the best available evidence regarding indications of purity and degree of perfection of the samples measured. The most important experimental criteria are the frequency range over which measurements were made and the magnitude of the dielectric losses. In general, the reliability can be judged only if measurements were made over a frequency range wide enough to ensure that the extrapolation value is the intrinsic dc dielectric constant. For measurements made at a single frequency, the reliability increases with the magnitude of the frequency used up to—but not including—the infrared range. In those cases for which $\tan \delta$ of an insulating sample has been determined as a function of frequency, values less than 10^{-4} may be taken to indicate that measurements were made on a highly perfect and pure specimen. However, if $\tan \delta > 0.1$, the real part of the dielectric constant may differ by 5–10 percent from the true value of the static dielectric constant. In most cases, these values were included only if no other data were available. Other criteria for evaluation involve the form of the sample as well as the type of electrodes. Single crystal data are listed in preference to data obtained on polycrystalline samples; values obtained from measurements on powders have been discarded unless the measurements were made in the microwave frequency range. Some reported values were eliminated because the electrode properties are likely to have resulted in interfacial polarization effects.

For measurements that have been made in the parallel plate capacitor configuration, the parameter which usually limits the precision is the measurement of the distance between the plates. The usual calculation made is $\epsilon = \frac{Cd}{\epsilon_0 A}$, where C is the measured capacitance, A is the area of the plates, d is the distance between the plates, and ϵ_0 is the permittivity of free space. In order to produce a large, easily measured capacitance, the specimen is made with large area and small thickness. The errors in d are in the absolute thickness measurement and non-parallelism of the two surfaces of area A. Because most sample dimensions are on the order of $A \approx 1$ cm^2 and $d \approx 1$ mm which can only be measured to within about 10μ, it follows that few values of ϵ are accurate to better than 1 percent.

1.8. Presentation of Data

The substances for which data have been collected are listed alphabetically in column 1 of table 2 ac-

cording to their chemical formulas. The second column contains the common name of the solid. A Compound Index has been included as an appendix to facilitate finding data on certain materials with well-known common names but with less familiar chemical composition (e.g., HMTA—hexamethylene tetramine). The third column presents the actual values of the dielectric constant (or its tensor elements when known) measured at the temperature and frequency indicated in columns 4 and 5, respectively. An entry "r.t." in column 4 indicates that the source does not specify the measuring temperature better than "room temperature." Occasionally the author(s) do(es) not mention either the temperature or the frequency of measurement. In these cases neither of these two quantities has been specified in the table, although it is likely that the temperature of the measurement was room temperature.

The abbreviation "i.r." in column 5 means that the value of ϵ has been obtained from refractive index data in the infrared spectral range just below the frequencies corresponding to the lattice vibrational bands. These values correspond, of course, to results from "unclamped" measurements (ϵ^T).

When the material is sufficiently dipolar to produce a classical Cole-Cole plot (ϵ' vs ϵ'' is a semi-circle), then the extrapolated low-frequency dielectric constant is called the limiting value and is designated by "lim" in column 5. Column 6 supplies information concerning the dielectric losses of the material. Literature references and the indication of additional information are given in the last two columns (7 and 8). The figure in the last column refers to the figure number in this compilation where more extensive data concerning the dielectric behavior of the material can be found. This information usually takes the form of one or more graphs presenting the temperature dependence, the frequency dependence, the pressure dependence of the dielectric constant, the loss angle as a function of frequency or temperature, the Curie temperature or other transition temperatures, etc.

1.9. *General References*

[1] Anderson, J. C., Dielectrics (Reinhold Publishing Company, New York, 1964).

[2] von Hippel, A. R., Dielectrics and Waves (John Wiley and Sons, New York, 1954).

[3] Fröhlich, H., Theory of Dielectrics (Oxford University Press, New York, 1958).

[4] Kittel, Charles, Introduction to Solid State Physics, 4th edition (John Wiley and Sons, New York, 1971), Chapter 13.

[5] Brown, F. C., The Physics of Solids (W. A. Benjamin Inc., New York, 1967), Chapter 7.

[6] Parker, R. A., and Wasilik, J. H., Phys. Rev. **120,** 1631 (1960).

[7] Young, K. F., and Frederikse, H. P. R., J. Appl. Phys. **40,** 3115 (1969).

[8] Sabisky, E. S., and Gerritsen, A. J., J. Appl. Phys. **33,** 1450 (1962).

[9] Bussey, H. E., Digest of the Literature on Dielectrics, Volume 24, 1960 (National Academy of Sciences, Washington, D.C., 1962).

[10] Tessman, J., Kahn, A. H., and Shockley, W., Phys. Rev. **92,** 890 (1953).

[11] Bosman, A. J., and Havinga, E. E., Phys. Rev. **129,** 1593 (1963).

[12] Mason, W. P., Piezoelectric Crystals and Their Application to Ultrasonics (D. Van Nostrand Company, Inc., New York, 1950).

[13] Morgan, S. O., American Institute of Physicists Handbook, 1st edition (McGraw-Hill Book Company, New York, 1957).

J. Phys. Chem. Ref. Data, Vol. 2, No. 2, 1973

2. Table of Dielectric Constants of Inorganic Solids

Formula	Name	ε_{ijk}	T (K)	ν (Hz)	tan δ x10^{-4}	Reference	Add'l Info. (Fig. No.)
Ag_3AsS_3	Silver thioarsenate (Proustite)	ε_{11}^T=16.5, ε_{11}^S=14.5	--	2×10^7		185	
		ε_{33}^T=20.0, ε_{33}^S=18.0	--	--		185	
AgBr	Silver bromide	12.50	r.t.	--		154	119
AgCN	Silver cyanide	5.6	--	10^6		216	
AgCl	Silver chloride	11.15	r.t.	--		154	119
$AgNO_3$	Silver nitrate	9.0	293	5×10^5		52	
$AgNa(NO_2)_2$	Silver sodium nitrite	4.5±0.5	r.t.	9.4×10^9	<100	61	
Ag_2O	Silver oxide	8.8	--	--		154, 83	
$(AlF)_2SiO_4$	Aluminum fluosilicate (topaz)	ε_{11}=6.62	297	7×10^3		195	
		ε_{22}=6.58	297	7×10^3		195	
		ε_{33}=6.95	297	7×10^3		195	
Al_2O_3	Aluminum oxide (alumina)	$\varepsilon_{11}=\varepsilon_{22}$=9.34	298	10^2-8×10^9		191	89-92
		ε_{33}=11.54	298	10^2-8×10^9		191	
$AlPO_4$	Aluminum phosphate	ε_{11}^T=6.05	r.t.	10^3		123	
AlSb	Aluminum antimonide	11.21	300	i.r.		206, 137	
		12.04	r.t.	i.r.		75	
AsF_3	Arsenic trifluoride	5.7	--	--		120	
BN	Boron nitride	7.1	r.t.	i.r.		206	
$BaCO_3$	Barium carbonate	8.53	291	2×10^5		170	

Formula	Name	ε_{ijk}	T (K)	ν (Hz)	tan δ $\times 10^{-4}$	Reference	Add'l. Info. (Fig. No.)
$Ba(COOH)_2$	Barium formate	$\varepsilon_{11}=7.9$	r.t.	10^3		123	
		$\varepsilon_{22}=5.9$	r.t.	10^3		123	
		$\varepsilon_{33}=7.5$	r.t.	10^3		123	
$BaCl_2$	Barium chloride	9.81	--	--		99	
$BaCl_2 \cdot 2H_2O$	Barium chloride dihydrate	9.00	r.t.	10^3		99	
BaF_2	Barium fluoride	7.3592±0.0007	300	10^3		5	
		7.32	292	$5x(10^2-10^{11})$		118	127
$Ba(NO_3)_2$	Barium nitrate	4.95	292	$2x10^5$		170	
$Ba_2NaNb_5O_{15}$	Barium sodium niobate ("Bananas")	$\varepsilon_{11}^S=222$, $\varepsilon_{11}^T=235$	296	--		197,198	38
		$\varepsilon_{22}^S=227$, $\varepsilon_{22}^T=247$	296	--		197,198	38
		$\varepsilon_{33}^S=32$, $\varepsilon_{33}^T=51$	296	--		197,198	38
BaO	Barium oxide (baria)	34±1	248, 333	$60 x10^7$		21	93
BaO_2	Barium peroxide	10.7	r.t.	$2x10^6$		72	
BaS	Barium sulfide	19.230	--	$7.25x10^6$		173	
$BaSO_4$	Barium sulfate	11.4	288	10^8		216	
$BaSnO_3$	Barium stannate	18	298	$25x10^5$		27	
$BaTiO_3$	Barium titanate	$\varepsilon_{11}^T=3600$	298	10^5		202	26a,b,c
		$\varepsilon_{11}^S=2300$	298	$2.5x10^8$		202	26a,b,c
		$\varepsilon_{33}^T=150$	298	10^5		202	26a,b,c
		$\varepsilon_{33}^S=80$	298	$2.5x10^8$		202	26a,b,c
$Ba_6Ti_2Nb_8O_{30}$	Barium titanium niobate	$\varepsilon_{11}=\varepsilon_{22}\approx 190$	298	--		88	40
		$\varepsilon_{33}\approx 220$	298	--		88	40

Formula	Name	ε_{ijk}	T (K)	ν (Hz)	tan δ $\times 10^{-4}$	Reference	Add'l. Info. (Fig. No.)
$BaWO_4$	Barium tungstate	$\varepsilon_{11}=\varepsilon_{22}=35.5\pm0.2$	297.5	1.59×10^3	<10	29	
		$\varepsilon_{33}=37.2\pm0.2$	297.5	1.59×10^3	<10	29	
$BaZrO_3$	Barium zirconate	43	--	--		68	
$Be_3Al_2Si_6O_{18}$	Beryllium aluminum silicate (Beryl)	$\varepsilon_{33}=5.95$	297	7×10^3		195	
		$\varepsilon_{11}=\varepsilon_{22}=6.86$	297	7×10^3		195	
$BeCO_3$	Beryllium carbonate	9.7	291	2×10^5		170	
BeO	Beryllium oxide (beryllia)	7.35±0.2	293	2×10^6		82	
		$\varepsilon_{33}=7.66$	--	--		110	
$BiFeO_3$	Bismuth iron oxide	40±3	300	9.4×10^9	700±140	108	53
$Bi_{12}GeO_{20}$	Bismuth germanate	$\varepsilon_{11}^S=38$	r.t.	--		13	
$Bi(GeO_4)_3$	Bismuth germanate	16	293	--		137, 171	
Bi_2O_3	Bismuth sesquioxide	18.2	r.t.	2×10^6		156	
$Bi_4Ti_3O_{12}$	Bismuth titanate	135-220	r.t.	10^3		184	
		112	r.t.	10^3	29	190	
C	Diamond	5.5±0.3	--	--		168	
	Type I	5.87±0.19	300	10^3		63	
	Type IIa	5.66±0.04	300	10^3		63	
$C_4H_4O_6$	Tartaric acid	$\varepsilon_{11}=\varepsilon_{22}=4.3$	298	--		123	
		$\varepsilon_{33}=4.5$	298	--		123	
		$\varepsilon_{13}=0.55$	298	--		123	

Formula	Name	ε_{ijk}	T (K)	ν (Hz)	tan δ x10^{-4}	Reference	Add'l. Info. (Fig. No.)
$C_6H_{14}N_2O_6$	Ethylene diamine tartrate (EDT)	ε_{11}^T=5.0	293	--		123	
		ε_{22}^T=8.3	293	--		123	
		ε_{33}^T=6.0	293	--		123	
		ε_{13}^T=0.7	293	--		123	
$C_6H_{12}O_6NaBr$	Dextrose sodium bromide	ε_{11}^T=4.0	--	10^3		123	
$(CH_3NH_3)Al(SO_4)_2 \cdot 2H_2O$	Methyl ammonium alum (MASD)	19	197	--		92	74
$Ca_2B_6O_{11} \cdot 5H_2O$	Colemanite	ε_{11}=20	253-293	10^3		110	
		ε_{33}=25	293	10^3		204	83
$CaCO_3$	Calcium carbonate	ε_{11}=8.67	--	9.4×10^{10}		47	
		ε_{22}=8.69	--	9.4×10^{10}		47	
		ε_{33}=8.31	--	9.4×10^{10}		47	
		$\varepsilon_{11}=\varepsilon_{22}$=8.5	--	10^8		167	
		ε_{33}=8.0	--	10^8		167	
		9.15	291	2×10^5		170	
$CaCeO_3$	Calcium cerate	21	--	--		68	
CaF_2	Calcium fluoride	6.7986±0.0007	300	10^3		5	
		6.76	--	10^5		89	
		6.81	300	$5 \times (10^2 - 10^{11})$		116	125
		$\varepsilon_{11}=\varepsilon_{22}$=8.70	--	1.6×10^6		129	
		ε_{33}=8.20	--	1.6×10^6		129	

Formula	Name	ε_{ijk}	T (K)	ν (Hz)	tan δ $\times 10^{-4}$	Reference	Add'l. Info. (Fig. No.)
$CaMoO_4$	Calcium molybdate	$\varepsilon_{11}=\varepsilon_{22}=24.0\pm0.2$	297.5	<10		29	
		$\varepsilon_{33}=20.0\pm0.2$	297.5	<10		29	
$Ca(NO_3)_2$	Calcium nitrate	6.54	292	2×10^5		170	
$CaNb_2O_6$	Calcium niobate	$\varepsilon_{11}=22.8\pm1.9$	r.t.	$(5-500)\times10^3$		51	
$Ca_2Nb_2O_7$	Calcium pyroniobate	~45	--	5×10^7		157	41
CaO	Calcium oxide	11.8 ± 0.3	283	2×10^6		82	
CaS	Calcium sulfide	6.699	--	7.251×10^6		173	
$CaSO_4\cdot2H_2O$	Calcium sulfate dihydrate	$\varepsilon_{11}=5.10$	--	--		47	
		$\varepsilon_{22}=5.24$	--	--		47	
		$\varepsilon_{33}=10.30$	--	--		47	
$CaTiO_3$	Calcium titanate	165	--	--		154	29
$CaWO_4$	Calcium tungstate	$\varepsilon_{11}=\varepsilon_{22}=11.7\pm0.1$	297.5	1.59×10^3		29	
		$\varepsilon_{33}=9.5\pm0.2$	297.5	1.59×10^3		29	
Cd_3As_2	Cadmium arsenide	$\varepsilon_{33}=18.5$	4	--		30	
$CdBr_2$	Cadmium bromide	8.6	293	5×10^5		52	
CdF_2	Cadmium fluoride	8.33 ± 0.08	300	10^5-10^7		212	128-130

Formula	Name	ε_{ijk}	T (K)	ν (Hz)	tan δ x10^{-4}	Reference	Add'l. Info. (Fig. No.)
CdS	Cadmium sulfide	ε_{11}=9.4	--	--		152	
		ε_{33}=10.4	--	--		152	
		$\varepsilon_{11}=\varepsilon_{22}$=8.7	300	i.r.		15	
		ε_{33}=9.25	300	i.r.		15	
		$\varepsilon_{11}=\varepsilon_{22}$=8.37	8	i.r.		15	
		ε_{33}=9.00	8	i.r.		15	
		ε_{11}^{T}=8.48	77	10^4		20	
		ε_{33}^{T}=9.48	77	10^4		20	
		ε_{11}^{S}=9.02, ε_{11}^{T}=9.35	298	10^4		90	
		ε_{33}^{S}=9.53, ε_{33}^{T}=10.33	298	10^4		90	
CdSe	Cadmium selenide	ε_{11}^{S}=9.53, ε_{11}^{T}=9.70	298	10^4		110	
		ε_{33}^{S}=10.2, ε_{33}^{T}=10.65	298	10^4		110	
		ε_{11}^{T}=9.70, ε_{11}^{S}=9.33	298	10^4		20	
		ε_{33}^{T}=10.65, ε_{33}^{S}=10.20	298	10^4		20	
CdTe	Cadmium telluride	$\varepsilon_{11}=\varepsilon_{22}$=10.60±0.15	297	i.r.		116	
		ε_{33}=7.05±0.05	297	i.r.		116	
		$\varepsilon_{11}^{T}=\varepsilon_{11}^{S}$=9.65±2%	77	10^4		20	
$Cd_2Nb_2O_7$	Cadmium pyroniobate	500-580	293	10^3	140	122	
CeO_2	Cerium oxide	7.0	--	2×10^6		72	
		26	--	--		68	
$CoNb_2O_6$	Cobalt niobate	ε_{11}=18.4±0.6	r.t.	(5-500)x10^3	<10	51	
		ε_{22}=21.4±1.1	r.t.	(5-500)x10^3	<10	51	
		ε_{33}=33.0±0.7	r.t.	(5-500)x10^3	<10	51	

Formula	Name	ε_{ijk}	T (K)	ν (Hz)	tan δ $\times 10^{-4}$	Reference	Add'l. Info. (Fig. No.)
CoO	Cobalt oxide	12.9	298	10^2-10^{10}	~10	149	94,96,97
		10.0	--	6×10^{10}		165	
$CoWO_4$	Cobalt tungstate	ε_{22}=19	298	10^3	3,000	51	
		ε_{33}=32	298	10^3	40,000	51	
Cr_2O_3	Chromic sesquioxide	$\varepsilon_{11}=\varepsilon_{22}$=13.3	298.5	10^3		55	98
		ε_{33}=11.9	298.5	10^3		55	98
		8	315	6×10^{10}		165	
$CsAl(SO_4)_2\cdot12H_2O$	Cesium alum	5.0	--	$20\text{-}20\times10^3$		114	
CsBr	Cesium bromide	6.51	253	2×10^6		94	
		6.38	298	1.6×10^3		94	
		6.34	--	9.4×10^{10}		47	
Cs_2CO_3	Cesium carbonate	6.53	291	2×10^5		170	
CsCl	Cesium chloride	7.20	222	2×10^6		94	
		6.34	292	2×10^5		83	
		7.2	298	--		77	
$Cs_2H_2AsO_4$	Cesium dihydrogen arsenate (CDA)	ε_{11}=58	--	--		215	Table A
		ε_{33}=34	--	--		215	Table A
		4.8	273	9.5×10^9		111	
$Cs_2H_2PO_4$	Cesium dihydrogen phosphate (CDP)	6.15	285	9.5×10^9		111	Table A
$CsH_3(SeO_3)_2$	Cesium trihydrogen selenite	ε_{11}=80	273	10^5		119	78
		ε_{22}=63	273	10^5		119	78
		ε_{33}=12	273	10^5		119	78

Formula	Name	ε_{ijk}	T (K)	ν (Hz)	tan δ x10^{-4}	Reference	Add'l. Info. (Fig. No.)
CsI	Cesium iodide	6.15	285	9.5×10^{9}		111	
		5.65	298	10^{6}		83	
		6.31	298	1.6×10^{3}		93	
$CsNO_3$	Cesium nitrate	$\varepsilon_{11}=\varepsilon_{22}=9.4$	r.t.	5×10^{5}		178	
		$\varepsilon_{33}=8.3$	r.t.	5×10^{5}		178	
$CsPbCl_3$	Cesium lead chloride	14.37	300	10^{5}-10^{6}		40	54,55
CuBr	Cuprous bromide	8.0	293	5×10^{5}		52	
CuCl	Cuprous chloride	9.8±0.5	--	10^{3}		17, 110	
		8.4±0.5	--	9.4×10^{9}		17, 110	
CuO	Cupric oxide	18.1	r.t.	2×10^{6}		72	
Cu_2O	Cuprous oxide (Cuprite)	7.60±0.06	r.t.	10^{5}		133	99
$CuSO_4\cdot5H_2O$	Cupric sulfate pentahydrate	6.60		--		99	
EuF_2	Europium fluoride	7.7±0.2	298	$(1\text{-}300)\times10^{3}$		11	
$Eu_2(MoO_4)_3$	Europium molybdate	9.5	298	--		26	
EuS	Europium sulfide	13.10±0.04	80	$5\times(10^{2}\text{-}10^{5})$		36	
FeO	Ferrous oxide	14.2	r.t.	2×10^{6}		72	
		12.7	--	6×10^{10}		165	100
Fe_2O_3 - α	Ferric sesquioxide (hematite)	12	--	6×10^{10}		165	
Fe_2O_3 - γ		4.5	--	10^{5}-10^{7}		91	
Fe_3O_4	Ferrosoferric oxide (magnetite)	20	--	10^{5}-10^{7}		91	

Formula	Name	ε_{ijk}	T (K)	ν (Hz)	tan δ $\times 10^{-4}$	Reference	Add'l Info. (Fig. No.)
GaAs	Gallium arsenide	13.13	300	--		206	
		12.90	4	i.r.		75	
		12.95±0.10	r.t.	$(8.5\text{-}70)\times 10^{9}$		37	
GaP	Gallium phosphide	10.18	--	--		206	
		11.1	r.t.	--		14	
		10.8±0.2	--	i.r.		104	
		10.75±0.1	1.6	i.r.		142	
GaSb	Gallium antimonide	15.69	--	--		206	
		15.7	4	i.r.		75	
		$\varepsilon_{11}=\varepsilon_{22}=10.2, 9.80$	r.t.	i.r.		113	
		$\varepsilon_{33}= 7.6$	r.t.	i.r.		113	
		$\varepsilon_{33}= 8.0\pm0.3$	r.t.	--		113	
		7±1	--	--		32	
$Gd_2(MoO_4)_3$	Gadolinium molybdate	10	298	--		26	
		9.5	298	10^{3}		44	87
Ge	Germanium	13.62±0.15	r.t.	35×10^{9}		64	
		16.0±0.3	4	9.2×10^{9}		45	
		15.8±0.2	--	$500\text{-}3\times 10^{10}$		49	
		$\varepsilon_{11}=\varepsilon_{22}=12.7$	r.t.	34×10^{9}		107	
		$\varepsilon_{33}=12.8$	r.t.	34×10^{9}		107	
GeO_2	Germanium dioxide	$\varepsilon_{11}=\varepsilon_{22}= 7.44$	--	i.r.		172	

Formula	Name	ε_{ijk}	T (K)	ν (Hz)	tan δ x10^{-4}	Reference	Add'l. Info. (Fig. No.)
HIO_3	Iodic acid	ε_{11}=7.5	--	10^3		123	
		ε_{22}=12.4	--	10^3		123	
		ε_{33}=8.1	--	10^3		123	
$H\text{-}NH_4(ClCH_2COO)_2$	Hydrogen ammonium dichloroacetate	$\varepsilon_{[102]}$=5.9	--	10^5		87	84-86
H_2O	Ice I (P = 0 kbar)	99	243	Lim		207	112-115
	Ice III (P = 3 kbar)	117	243	Lim		207	112-115
	Ice V (P = 5 kbar)	114	243	Lim		207	112-115
	Ice VI (P = 8 kbar)	193	243	Lim.		207	112-115
HgCl	Mercurous chloride (Calumel)	$\varepsilon_{11}=\varepsilon_{22}$=14.0	--	10^{12}		114	
$HgCl_2$	Mercuric chloride	6.5	--	10^{12}		114	
HgS	Mercurous sulfide (Cinnabar)	$\varepsilon_{11}=\varepsilon_{22}$=18.0	--	i.r.		214	
		ε_{33}=32.5	--	i.r.		214	
HgSe	Mercurous selenide	25.6	r.t.	10^4-10^6		103	
I_2	Iodine	ε_{11}=6	r.t.	5x(10^4-10^7)		175	
		ε_{22}=3	r.t.	5x(10^4-10^7)		175	
		ε_{33}=40	r.t.	5x(10^4-10^7)		175	
InAs	Indium arsenide	14.55±0.3	r.t.	i.r.		116	
		15.15	4	i.r.		75	
InP	Indium phosphide	12.37	--	--		206	
		12.61	r.t.	i.r.		75	
InSb	Indium antimonide	17.88	4	i.r.		75	
$KAl(SO_4)_2 \cdot 12H_2O$	Potassium alum	6.5	--	20-20x10^3		114	

Formula	Name	ε_{ijk}	T (K)	ν (Hz)	$\tan\delta$ $\times 10^{-4}$	Reference	Add'l. Info. (Fig. No.)
KBr	Potassium bromide	4.90±0.02	r.t.	5×10^{3}		48	
		4.78	r.t.	2×10^{6}		47	
		4.90±0.02	r.t.	--		115	
		4.88	300	--		118a	117
		4.53	4.2	--		118a	117
$KBrO_3$	Potassium bromate	7.3	r.t.	2×10^{6}		180	
KCN	Potassium cyanide	6.15	r.t.	2×10^{6}		180	
K_2CO_3	Potassium carbonate	4.96	291	2×10^{5}		170	
$K_2C_4H_4O_6\cdot1/2\ H_2O$	Dipotassium tartrate (DKT)	ε_{11}=6.44	r.t.	--		123	
		ε_{22}=5.80	r.t.	--		123	
		ε_{33}=6.49	r.t.	--		123	
		ε_{13}=0.005	r.t.	--		123	
KCl	Potassium chloride	4.86±0.02	r.t.	5×10^{3}		48	
		4.84±0.02	r.t.	--		117	
		5.90	300	--		154	
		4.50	4.2	--		154	
		4.55	r.t.	2×10^{6}		47	
$KClO_3$	Potassium chlorate	5.1	r.t.	2×10^{6}		180	
$KClO_4$	Potassium perchlorate	5.9	r.t.	2×10^{6}		180	
K_2CrO_4	Potassium chromate	7.3	--	6×10^{7}		216	

Formula	Name	ε_{ijk}	T (K)	ν (Hz)	tan δ x10^{-4}	Reference	Add'l. Info. (Fig. No.)
$KCr(SO_4)_2 \cdot 12H_2O$	Potassium chrome alum	6.5	100-240	175×10^3		208	
KD_2AsO_4	Potassium dideuterium arsenate (KDDA)	ε_{11}=70	298	--		1	18,19
		ε_{33}=31	298	--		1	18,19
KD_2PO_4	Potassium dideuterium phosphate (KDDP)	50±2	297	10^3		176	15-17
KF	Potassium fluoride	6.05	--	2×10^6		208	
		5.46	--	--		76	
$K_4Fe(CN)_6 \cdot 3H_2O$	Potassium ferrocyanide	$\varepsilon_{[110]}$=16	260	--		109	82
		$\varepsilon_{[101]}$=10	260	--		109	
		$\varepsilon_{[010]}$= 4	260	--		109	
KH_2AsO_4	Potassium dihydrogen arsenate (KDA)	31	r.t.	2×10^6		180	13,14 Table A
		ε_{11}=60	298	--	70	1	
		ε_{33}=24	298	--	80	1	
KH_2PO_4	Potassium dihydrogen phosphate (KDP)	46	298	10^3		123	12 Table A
		ε_{33}^T=50	297	10^3		176	
		ε_{11}=42	r.t.	--		34	
		ε_{33}=21	r.t.	--		34	
K_2HPO_4	Dipotassium monohydrogen orthophosphate	9.05	r.t.	2×10^6		180	
KI	Potassium iodide	5.00	r.t.	9.4×10^{10}		47	
		5.10±0.02	r.t.	5×10^3		52	

Formula	Name	ε_{ijk}	T (K)	ν (Hz)	tan δ $\times 10^{-4}$	Reference	Add'l. Info. (Fig. No.)
KIO_3	Potassium iodate	170	255	10^5		79	67
		10	293	10^5		79	67
		$\varepsilon_{[\bar{1}01]} \approx 40,70$	r.t.	10^5		78	
		16.85	r.t.	2×10^6		108	
$(K,H)Al_3(SiO_4)_3$	Mica (muscovite)	5.4	299	10^2-3×10^9		191	
$(K,H)Mg_3Al(SiO_4)_3$	Mica (Canadian)	$\varepsilon_{11}=\varepsilon_{22}=6.9$	298	10^2-10^4		191	
		$\varepsilon_{33}=7.3$	298	10^4		191	
KNO_2	Potassium nitrite	25	305	--		148	64
KNO_3	Potassium nitrate	4.37	293	2×10^5		170	59,60
		6.6	360	5×10^5		126	
$KNa(C_4D_4O_6)\cdot 4H_2O$	Deuterated rochelle salt	$\varepsilon_{11}=160$	280	900		73	1
$KNa(C_4H_4O_6)\cdot 4H_2O$	Rochelle salt	$\varepsilon_{11}= 65$	280	900		73	1-5
$KNbO_3$	Potassium niobate	500	r.t.	--		174	37
K_3PO_4	Potassium orthophosphate	7.75	r.t.	2×10^6		180	
KSCN	Potassium thiocyanate	7.9	r.t.	2×10^6		180	
K_2SO_4	Potassium sulfate	6.4	r.t.	2×10^6		180	
$K_2S_3O_6$	Potassium trithionate	5.7	293	1.8×10^6		169	
$K_2S_4O_6$	Potassium tetrathionate	5.5	293	1.8×10^6		169	
$K_2S_5O_6\cdot H_2O$	Potassium pentathionate	7.8	293	1.8×10^6		169	
$K_2S_6O_6$	Potassium hexathionate	7.8	293	1.8×10^6		169	

Formula	Name	ε_{ijk}	T (K)	ν (Hz)	tan δ x10^{-4}	Reference	Add'l. Info. (Fig. No.)
K_2SeO_4	Potassium selenate	ε_{11}=5.9	r.t.	10^3		4	79
		ε_{22}=7.7	r.t.	10^3		4	79
		ε_{11}=5.6	80	10^3		4	79
		ε_{22}=7.5	80	10^3		4	79
$KSr_2Nb_5O_{15}$	Potassium strontium niobate	ε_{11}=ε_{11}≈1200	298	--		65	39
		ε_{33}≈ 800	298	--		65	39
$KTaNbO_3$	Potassium tantalate niobate (KTN)	6,000	272	10^4		38	47
		34,000	273	10^4		38	47
		6,000	293	10^4		38	47
$KTaO_3$	Potassium tantalate	242	298	$2x10^5$		201	28,46
$LaScO_3$	Lanthanum scandate	30	--	--		68	
LiBr	Lithium bromide	12.1	--	$2x10^6$		82	
		13.25	--	--		76	
		13.2	--	--		76	
Li_2CO_3	Lithium carbonate	4.9	291	$2x10^5$		170	
LiCl	Lithium chloride	11.05	--	$2x10^6$		52	
		11.95	--	--		76	
		10.62	292	$2x10^5$		170	
LiD	Lithium deuteride	14.0±0.5	--	i.r.		28	
LiF	Lithium fluoride	9.00	298	10^2-10^7		191	
		9.11	353	10^2-10^7		191	
		8.83±0.02	r.t.	$5x10^3$		48	
		9.01±0.03	r.t.	--		117	

Formula	Name	ε_{ijk}	T (K)	ν (Hz)	tan δ x10^{-4}	Reference	Add'l. Info. (Fig. No.)
$LiGaO_2$	Lithium metagallate	ε_{11}^T=7.0, ε_{22}^T=6.0	--	--		90	
		ε_{33}^T=9.5	--	--		12	
		ε_{11}^S=6.8, ε_{22}^S=5.8	--	--		90	
LiH	Lithium hydride	12.9±0.5	--	i.r.		28	
Li^6H	Lithium-6 hydride	13.2±0.5	--	--		28	
Li^7H	Lithium-7 hydride	12.9±0.5	--	--		28	
$LiH_3(SeO_3)_2$	Lithium trihydrogen selenite	29	298	10^4		161	76
		ε_{11}=13.0	--	--		161	76
		ε_{22}=12.9	--	--		161	76
		ε_{33}= 46	--	--		161	76
LiI	Lithium iodide	11.03	--	$2x10^6$		83	
		8.2	--	--		180	
$LiIO_3$	Lithium iodate	ε_{11}=7.9, ε_{33}=5.9	253	$2x10^7$		76	
		$\varepsilon_{11}=\varepsilon_{22}$=65	294.5	10^3		130	68
		ε_{33}=554	298	--		130	68
$LiNH_4C_4H_4O_6 \cdot H_2O$	Lithium ammonium tartrate (LAT)	ε_{11}^T=7.2	298	--		123	6
		ε_{22}^T=8.0	--	--		123	6
		ε_{33}^T=6.9	--	--		123	6
$LiNa_3CrO_4 \cdot 6H_2O$	Lithium trisodium chromate	8.0	--	10^3		123	
$LiNa_3MoO_4 \cdot 6H_2O$	Lithium trisodium molybdate	ε_{11}=6.7	--	10^3		123	
		ε_{33}=5.3	--	10^3		123	
$LiNbO_3$	Lithium niobate	$\varepsilon_{11}=\varepsilon_{22}$=82	298	10^5		136,13	32-35
		ε_{33}=30	298	10^5		136,13	32-35

Formula	Name	ε_{ijk}	T (K)	ν (Hz)	tan δ x10-4	Reference	Add'l Info. (Fig. No.)
$Li_2SO_4 \cdot H_2O$	Lithium sulfate monohydrate	ε_{11}=5.6	298	--		123	
		ε_{22}=10.3	298	--		123	
		ε_{33}=6.5	298	--		123	
		ε_{13}=0.07	298	--		123	
$LiTaO_3$	Lithium tantalate	$\varepsilon_{11}=\varepsilon_{22}$=53	r.t.	10^5		209	44,45
		ε_{33}=46	r.t.	10^5		209	44,45
		$\varepsilon^S_{11}=\varepsilon^S_{22}$=41	r.t.	--		192	
		ε^S_{33}=43	r.t.	--		192	
		$\varepsilon^T_{11}=\varepsilon^T_{22}$=51	r.t.	--		192	
		ε^T_{33}=45	r.t.	--		192	
$LiTlC_4H_4O_6 \cdot H_2O$	Lithium thallium tartrate (LTT)	$\varepsilon_{11} \approx 20$	80	--			7
$Mg_3B_7O_{13}Cl$	Magnesium borate monochloride (boracite)	ε_{11}=14.1	r.t.	5×10^5		177	
$MgCO_3$	Magnesium carbonate	8.1	291	2×10^5		170	
$MgNb_2O_6$	Magnesium niobate	ε_{11}=16.4±0.5	r.t.	$(5\text{-}500) \times 10^3$		51	
		ε_{22}=20.9±0.5	r.t.	$(5\text{-}500) \times 10^3$		51	
		ε_{33}=32.4±0.5	r.t.	$(5\text{-}500) \times 10^3$		51	
MgO	Magnesium oxide (Periclase)	9.65	298	10^2-10^8		191	101,102
		9.8±0.5	308	2×10^6		82	
$(MgO)_xAl_2O_3$	Spinel	8.6	--	--		129	
$MgSO_4$	Magnesium sulfate	8.2	--	--		154	
$MgSO_4 \cdot 7H_2O$	Magnesium sulfate septa hydrate	5.46	--	--		99	
$MgTiO_3$	Magnesium titanate	18	--	--		154	30

Formula	Name	ε_{ijk}	T (K)	ν (Hz)	tan δ x10^{-4}	Reference	Add'l. Info. (Fig. No.)
$MgWO_4$	Magnesium tungstate	ε_{11}=18.0±1	r.t.	(5-500)x10^3	<10	51	
		ε_{22}=18.0±1	r.t.	(5-500)x10^3	<10	51	
$MnNb_2O_6$	Manganese niobate	ε_{11}=17.4±2	r.t.	(5-500)x10^3	<10	51	
		ε_{22}=16.1±0.5	r.t.	(5-500)x10^3	<10	51	
		ε_{33}=30.7±1	r.t.	(5-500)x10^3	<10	51	
MnO	Manganese oxide (Pyrolusite)	18.0±0.5	r.t.	(1-273)x10^6		222	
		12.8	--	6x10^{10}		165	
MnO_2	Manganese dioxide	~10^4	298	10^4		222	
Mn_2O_3	Manganese sesquioxide	8	--	6x10^{10}		165	
$MnWO_4$	Manganese tungstate	ε_{11}=19.3±1.3	r.t.	(5-500)x10^3	~200	51	
		ε_{22}=14.3±0.5	r.t.	(5-500)x10^3	~ 10	51	
		ε_{33}=16.5±1.1	r.t.	(5-500)x10^3	~500	51	
$N(CH_3)_4HgBr_3$	Tetramethylammonium tribromo mercurate (TTM)	~10	233-373	--		56	
$N(CH_3)_4HgI_3$	Tetramethylammonium triiodo mercurate (TTM)	~10	233-373	--		156	
$N_4(CH_2)_6$	Hexamethylene tetramine (HMTA)	2.6±0.2	--	10^9-10^{10}		17	
$(ND_4)_2BeF_4$	Deuteroammonium fluoberyllate	ε_{11}=10	--	--		85	
		ε_{22}= 9	--	--		85	
		ε_{33}= 9	--	--		85	
$(ND_4)_2SO_4$	Deuteroammonium sulfate	ε_{11}= 9	--	--		85	
		ε_{22}=10	--	--		85	
		ε_{33}= 9	--	--		85	

Formula	Name	ε_{ijk}	T (K)	ν (Hz)	tan δ x10^{-4}	Reference	Add'l. Info. (Fig. No.)
$(NH_2 \cdot CH_2COOH)_3 \cdot H_2SO_4$	Triglycine sulfate (TGS)	ε_{11}=9	273	10^4		84	9
		ε_{22}=30	273	10^4		84	9
		ε_{33}=6.5	273	10^4		84	9
		70	298.5	10^4		146	10
		30	298.5	10^7		146	10
$(NH_2 \cdot CH_2COOH)_3 \cdot H_2SeO_4$	Triglycine selenate (TGSe)	200	293	$.0x10^3$		67	11
$(NH_2CH_2COOH)_3 \cdot H_2BeF_4$	Triglycine fluorberyllate (TGFB)	ε_{22}=12	273	10^4		84	9
$NH_4Al(SO_4)_2 \cdot 12H_2O$	Ammonium alum	6	r.t.	10^{12}		114	
$(NH_4)_2BeF_4$	Ammonium fluoberyllate	9	183-193	10^4, $3.3x10^9$		135	
		$\varepsilon_{11}=\varepsilon_{22}$=7.8	123	10^5		85	75
		ε_{33}=7.1	123	10^5		85	75
		$\varepsilon_{11}=\varepsilon_{22}$=8.8	293	10^5		85	75
		ε_{33}=9.2	293	10^5		85	75
NH_4Br	Ammonium bromide	7.3	r.t.	10^{12}		114	
		7.1	--	$7x10^5$		31	
NH_4I	Ammonium iodide	9.8	--	--		63	
$(NH_4)_2C_2H_4O_6$	Ammonium tartrate	ε_{11}=6.45	r.t.	10^3		123	
		ε_{22}=6.8	r.t.	10^3		123	
		ε_{33}=6.0	r.t.	10^3		123	

Formula	Name	ε_{ijk}	T (K)	ν (Hz)	tan δ x10^{-4}	Reference	Add'l. Info. (Fig. No.)
$(NH_4)_2Cd_2(SO_4)_3$	Ammonium cadmium sulfate	9.8	r.t.	10^4		135	73
		9.8	r.t.	3.3×10^9		135	73
NH_4Cl	Ammonium chloride	6.96	r.t.	--		82	
		6.9	--	7×10^5		31	
$NH_4(ClCH_2COO)$	Ammonium monochloroacetate	5	r.t.	2×10^6		144	
$NH_4Cr(SO_4)_2\cdot12H_2O$	Ammonium chrome alum	6.5	r.t.	175×10^3		208	
NH_4HSO_4	Ammonium bisulfate	165	273	5×10^4		181	71
$NH_4H_2AsO_4$	Ammonium dihydrogen arsenate (ADA)	5.1	265	9.5×10^9		124	
		$\varepsilon_{11}=\varepsilon_{22}=85$	298	10^3	tan δ = 12,000	2	23,24
		$\varepsilon_{33}=22$	--	--	tan δ = 90,000	2	23,24
$NH_4H_2PO_4$	Ammonium dihydrogen phosphate (ADP)	$\varepsilon_{11}=\varepsilon_{22}=56$	--	--		97	20,21
		$\varepsilon_{33}=15.5$	--	--		97	20,21
		$\varepsilon_{11}=\varepsilon_{22}=57.1\pm0.6$	294.5	10^5-35×10^9		158	
		$\varepsilon_{33}=14.0\pm0.3$	294	10^5-36×10^9		158	
$ND_4D_2PO_4$	Ammonium dideuterium phosphate (ADDP)	$\varepsilon_{11}=\varepsilon_{22}=74, \varepsilon_{33}=24$	300	--		125	22
NH_4NO_3	Ammonium nitrate	10.7	322	$(5\text{-}50)\times10^3$		210	61-63
$(NH_4)_2SO_4$	Ammonium sulfate	9.8	293	10^3		135	
		$\varepsilon_{11}=\varepsilon_{22}=8.0$	123	10^5		85	70
		$\varepsilon_{33}=6.3$	123	10^5		85	70
		$\varepsilon_{11}=\varepsilon_{22}=10.0$	293	10^5		85	70
		$\varepsilon_{33}=9.3$	293	10^5		85	70
		10.2	273	10^4-3.3×10^9		188	

Formula	Name	ε_{ijk}	T (K)	ν (Hz)	tan δ x10^{-4}	Reference	Add'l. Info. (Fig. No.)
$(NH_4)_2UO_2(C_2O_4)_2$	Ammonium uranyl oxalate	8.03	--	10^4-3.3x10^9		54	
$(NH_4)_2UO_2(C_2O_4)_2 \cdot 3H_2O$	Ammonium uranyl oxalate trihydrate	6.06	--	10^4-3.3x10^9		54	
NaBr	Sodium bromide	6.28±0.03	r.t.			117	
		6.4	r.t.	2x10^6		82	
		5.99	--	2x10^6		94	
		6.44	298	1.6x10^3		93	
		6.1	--	2x10^6		180	
		6.28					
$NaBrO_3$	Sodium bromate	ε_{11}^T=5.70	298	10^3		124	66
NaCN	Sodium cyanide	7.55	293	10^5		191	
$NaCO_3$	Sodium carbonate	8.75	291	2x10^5		170	
$NaCO_3 \cdot 10H_2O$	Sodium carbonate decahydrate	5.3	--	6x10^7		99	
NaCl	Sodium chloride	5.92±0.02	r.t.	5x10^3		48	
		5.9	298	10^2-10^7		191	
		5.90±0.02	r.t.	--		117	
		5.90	300	--		118a	116
		5.45	4.2	--		118a	116
$NaClO_3$	Sodium chlorate	ε_{11}^T=5.76	301	10^3		123,124	66
		5.28	--	10^3		102	
$NaClO_4$	Sodium perchlorate	5.76	--	10^3		123	
NaF	Sodium fluoride	5.05±0.03	r.t.	--		117	
		5.08±0.02	r.t.	5x10^3		48	

Formula	Name	ε_{ijk}	T (K)	ν (Hz)	tan δ $\times 10^{-4}$	Reference	Add'l. Info. (Fig. No.)
$NaH_3(SeO_3)_2$	Sodium trihydrogen selenite	$\varepsilon_{11} \approx 75$	273	2×10^5		22	77
$NaD_3(SeO_3)_2$	Sodium trideuterium selenite	$\varepsilon_{11} \approx 220$	273	2×10^5		22	77
NaI	Sodium iodide	7.28±0.03	r.t.	--		117	
		6.15	r.t.	2×10^6		180	
$NaK(C_4H_2D_2O_6)\cdot 4D_2O$	Sodium potassium tartrate tetradeutrate	$\varepsilon_{11}=70$	273	10^3		73	1
	(deuterated Rochelle salt)	$\varepsilon_{22}=8.9$	273	10^3		73	1
$NaK(C_4H_4O_6)\cdot 4H_2O$	Sodium potassium tartrate tetrahydrate	$\varepsilon_{11}=170$	273	10^3		73	1
	(Rochelle salt)	$\varepsilon_{22}=9.1$	273	10^3		73	1
		$\varepsilon_{11}=1.95$	273	10^3		163	1
$NaNH_4(C_4H_4O_6)\cdot 4H_2O$	Sodium ammonium tartrate	$\varepsilon_{11}=8.4$	298	--		92	8
	(Ammonium Rochelle salt)	$\varepsilon_{22}=9.2$	298	--		92	8
		$\varepsilon_{33}=9.5$	298	--		92	8
		$\varepsilon_{11}=9.0$	--	10^3		123	
		$\varepsilon_{22}=8.9$	--	10^3		123	
		$\varepsilon_{33}=10.0$	--	10^3		123	
$NaNbO_3$	Sodium niobate	$\varepsilon_{33}=670\pm13$	r.t.	--		43	36
		$\varepsilon_{11}=\varepsilon_{22}=76\pm2$	r.t.	--		43	36
		$\varepsilon_{11}=\varepsilon_{22}=926\pm62$	803	--		43	36

Formula	Name	ε_{ijk}	T (K)	ν (Hz)	tan δ x10^{-4}	Reference	Add'l. Info. (Fig. No.)
$NaNO_2$	Sodium nitrite	ε_{11}=6.8	r.t.	$5x10^5$		178	65
		ε_{22}=6.4	r.t.	$5x10^5$		178	65
		ε_{33}=7.8	r.t.	$5x10^5$		178	65
		ε_{11}=7.4	r.t.	$5x10^5$		110	65
		ε_{22}=5.5	r.t.	$5x10^5$		110	65
		ε_{33}=5.0	r.t.	$5x10^5$		110	65
$NaNO_3$	Sodium nitrate	6.85	292	$2x10^5$		170	
		7	275	--		121	56,57
$NaSO_4$	Sodium sulfate	7.90	--	--		99	
$NaSO_4 \cdot 10H_2O$	Sodium sulfate decahydrate	5.0	--	--		99	
$Na_2S_2O_3 \cdot 5H_2O$	Sodium sulfate pentahydrate	7	250-290	$300-10^4$		186	
$Na_2UO_2(C_2O_4)_2$	Sodium uranyl oxalate	5.18	--	--		54	
$NdAlO_3$	Neodymium aluminate	17.5	--	--		68	
$NdScO_3$	Neodymium scandate	27	--	--		68	
$Ni_3B_7O_{13}I$	Nickel iodine boracite	ε_{11}=14	260	--		6	
$NiNb_2O_6$	Nickel niobate	ε_{11}=16.0±0.5	r.t.	$(5-500)x10^3$	<10	51	
		ε_{22}=23.8±1.8	r.t.	$(5-500)x10^3$	<10	51	
		ε_{33}=31.3±2.5	r.t.	$(5-500)x10^3$	<10	51	
NiO	Nickel oxide	11.9	298	10^5	17,000	149	95-97
		9.7	--	$6x10^{10}$		165	

Formula	Name	ε_{ijk}	T (K)	ν (Hz)	tan δ $\times 10^{-4}$	Reference	Add'l. Info. (Fig. No.)
$NiSO_4 \cdot 6H_2O$	Nickel sulfate hexahydrate	6.2	--	10^3		165	
		$\varepsilon_{11}=6.2$	r.t.	--		123	
		$\varepsilon_{33}=6.8$	r.t.	--		123	
$NiWO_4$	Nickel tungstate	$\varepsilon_{11}=17.4\pm2.4$	r.t.	$(5-500)\times10^3$	<10	51	
		$\varepsilon_{22}=13.6\pm1.0$	r.t.	$(5-500)\times10^3$	<10	51	
		$\varepsilon_{33}=19.7\pm0.6$	r.t.	$(5-500)\times10^3$	<10	51	
P	Phosphorous (red)	4.1	--	10^8		216	
P	Phosphorous (yellow)	3.6	--	10^8		168	
$[P(CH_3)_4]HgBr_3$	Tetramethylphosphonium tribromo mercurate (TTM)	~10	233-373	--		56	
$PbBr_2$	Lead bromide	>30	293	$(0.5-3)\times10^6$		52	
$PbCO_3$	Lead carbonate	18.6	288	10^8		216	
$Pb(C_2H_3O_2)_2$	Lead acetate	2.6	290-295	10^6		216	
$PbCl_2$	Lead chloride	33.5	273	$(0.5-3)\times10^6$		52	
Pb_2CoWO_6	Lead cobalt tungstate	~250	--	--		24	
PbF_2	Lead fluoride	26.3	r.t.	--		9	
$PbHfO_3$	Lead hafnate	390	300	10^5		174	
		185	400	--		164	49
PbI_2	Lead iodide	20.8	293	$(0.5-3)\times10^6$		52	
$Pb_3MgNb_2O_9$	Lead magnesium niobate	10,000	297	--		25	43
$PbMoO_4$	Lead molybdate	$\varepsilon_{11}=34.0\pm0.4$	297.5	1.59×10^3	<10	29	
		$\varepsilon_{33}=40.6\pm0.2$	297.5	1.59×10^3	<10	29	

Formula	Name	ε_{ijk}	T (K)	ν (Hz)	tan δ x10^{-4}	Reference	Add'l. Info. (Fig. No.)
$Pb(NO_3)_2$	Lead nitrate	16.8	--	$(0.5-3)\times10^6$		52	
$PbNb_2O_6$	Lead niobate	$\varepsilon_{33}^T=180$	298	--		194	42
PbO	Lead oxide	25.9	r.t.	2×10^6		72	
		50-60	293	10^6	30-80	18	
PbS	Lead sulfide (Galena)	190	77	i.r.		33	
		200±35	--	i.r.		39	
$PbSO_4$	Lead sulfate	14.3	290-295	10^6		216	
PbSe	Lead selenide	280	--	i.r.		33	
$PbTa_2O_6$	Lead metatantalate	$\varepsilon_{11}=\varepsilon_{22}\approx300$	--	10^4		182	48
		$\varepsilon_{33}=150$	--	10^4		182	48
PbTe	Lead telluride	450	--	i.r.		33	
		400	77	10^4-15×10^4		100	
		430	4.2	10^4-15×10^4		100	
		412±40	--	i.r.		39	
$PbTiO_3$	Lead titanate	~200	r.t.	10^3		151,164b	31a,b,c
$PbWO_4$	Lead tungstate	$\varepsilon_{11}=\varepsilon_{22}=23.6\pm0.3$	297.5	1.59×10^3	<10	29	
		$\varepsilon_{33}=31.0\pm0.4$	297.5	1.59×10^3	<10	29	
$Pb(Zn_{1/3}Nb_{2/3})O_3$	Lead zinc niobate	7	300	10^3,300×10^3		211	
$PbZrO_3$	Lead zirconate	200	400	--		164	50-52
$RbAl(SO_4)_2 \cdot 12H_2O$	Rubidium alum	5.1	--	10^{12}		114	

Formula	Name	ε_{ijk}	T (K)	ν (Hz)	tan δ x10^{-4}	Reference	Add'l. Info. (Fig. No.)
RbBr	Rubidium bromide	4.83	300	--		118b	118
	NaCl structure (1 bar)	4.9	r.t.	--		77	
	CsCl structure (4.6 kbar)	6.5	r.t.	--		77	
Rb_2CO_3	Rubidium carbonate	4.87±0.02	r.t.	$5x10^3$		48	
		4.86±0.02	r.t.	--		117	
		6.73	292	$2x10^5$		170	
RbCl	Rubidium chloride	4.91±0.02	r.t.	$5x10^3$		48	
		4.92±0.02	r.t.	--		117	
$RbCr(SO_4)_2 \cdot 12H_2O$	Rubidium chrome alum	5.0	--	10^{12}		114	
RbF	Rubidium fluoride	5.91	--	$2x10^6$		82	
		6.48	--	--		76	
$RbHSO_4$	Rubidium bisulfate	ε_{11}=7	r.t.	10^5		144	72
		ε_{22}=8	r.t.	10^5		144	72
		ε_{33}=10	r.t.	10^5		144	72
RbH_2AsO_4	Rubidium dihydrogen arsenate (RDA)	3.90	273	$9.5x10^9$	40	111	Table A
		ε_{11}=55	--	--		224	
		ε_{33}=28	--	--		224	
RbH_2PO_4	Rubidium dihydrogen phosphate (RDP)	6.15	285	$9.5x10^9$	400	224	Table A
RbI	Rubidium iodide	4.94±0.02	r.t.	$5x10^3$		48	
		4.91±0.02	r.t.	--		117	
$RbInSO_4$	Rubidium iridium sulfate	6.85	--	--		53	

Formula	Name	ε_{ijk}	T (K)	ν (Hz)	tan δ x10^{-4}	Reference	Add'l. Info. (Fig. No.)
$RbNO_3$	Rubidium nitrate	20-380	403-488	10^6		46	58
		30	488-538	10^6		46	58
S	Sulfur	ε_{11}=3.75	298	10^2-10^3		191	
		ε_{22}=3.95	298	10^2-10^3		191	
		ε_{33}=4.44	298	10^2-10^3		191	
	sublimed	3.69	298	10^2-10^3		191	
$SC(NH_2)_2$	Thiourea	$\varepsilon_{11}=\varepsilon_{33}\approx3$	77-300	10^3		66	80
		ε_{22}=35	300	10^3		66	80
Sb_2O_3	Antimonous sesquioxide	12.8	--	$(1.5\text{-}2)\times10^3$		72	
Sb_2S_3	Antimonous sulfide (stibnite)	$\varepsilon_{11}=\varepsilon_{22}$=15	r.t.	10^3		69	
		ε_{33}=180	r.t.	10^3		69	
Sb_2Se_3	Antimonous selenide	~110	r.t.	$(10\text{-}16.5)\times10^9$		70	
SbSI	Antimonous sulfide iodide	2000	273	10^5		74	81
		$\varepsilon_{11}=\varepsilon_{22}\approx25$	r.t.	10^3-10^5		57	
		$\varepsilon_{33}\approx5\times10^4$	295	10^3-10^5		57	
Se	Selenium	11.0	298	3×10^8		191	
	amorphous	6.60±0.30	298	24×10^9		115	
	crystalline	19.85±0.85	298	24×10^9		115	
		8.7	--	--		160	
	amorphous	6.1-6.4	--	--		3	
	crystalline	$\varepsilon_{11}=\varepsilon_{22}$=7.4	--	--		60	
		ε_{33}=11.4	--	--		60	

Formula	Name	ε_{ijk}	T (K)	ν (Hz)	tan δ x10^{-4}	Reference	Add'l. Info. (Fig. No.)
Se (cont.)	Selenium (monocrystal)	$\varepsilon_{11}=\varepsilon_{22}=11$	300	24×10^{9}		160	
		$\varepsilon_{33}=21$	300	24×10^{9}		160	
	(amorphous)	6.0	298	10^{2}-10^{10}		63	
Si	Silicon	12.1	4.2	10^{7}-10^{9}		150	
		11.94	300	10^{7}-10^{9}		150	
		11.7	7.7	10^{6}		63	
		11.7±0.2	--	500-3×10^{10}		49	
SiC	Silicon carbide	$\varepsilon_{33}=10.2\pm0.2$	293	10^{5}	30	81	
		10.0	--	i.r.		179	
	cubic	9.72	r.t.	i.r.		141	
	6H	$\varepsilon_{11}=\varepsilon_{22}=9.66$	r.t.	i.r.		141	
		$\varepsilon_{33}=10.03$	r.t.	i.r.		141	
		9.7±0.1	1.8	i.r.		141	
Si_3N_4	Silicon nitride	4.2 (film)	r.t.	10^{3}		58	
SiO	Silicon monoxide	5.8	r.t.	10^{3}		58	
SiO_2	Silicon dioxide	$\varepsilon_{11}=4.42$	--	9.4×10^{10}		47	103,106
		$\varepsilon_{22}=4.41$	--	9.4×10^{10}		47	
		$\varepsilon_{33}=4.60$	--	9.4×10^{10}		47	
		$\varepsilon_{11}=\varepsilon_{22}=4.5$	r.t.	--		35	
		$\varepsilon_{33}=4.6$	r.t.	--		35	
$Sm_2(MoO_4)_3$	Samarium molybdate	12	298	--		26	

Formula	Name	ε_{ijk}	T (K)	ν (Hz)	tan δ x10^{-4}	Reference	Add'l. Info. (Fig. No.)
SnO_2	Stannic dioxide	$\varepsilon_{11}=\varepsilon_{22}=14\pm2$	r.t.	10^4-10^{10}	10-10^2	189	
		$\varepsilon_{33}=9.0\pm0.5$	r.t.	10^4-10^{10}	10-10^2	189	
SnSb	Tin antimonide	147	r.t.	10^4-10^6		103	
SnTe	Tin telluride	1770±300	--	i.r.		39	
$Sr(COOH)_2 \cdot 2H_2O$	Strontium formate dihydrate	6.1	--	10^3		123	
$SrCO_3$	Strontium carbonate	8.85	298	$2x10^5$		170	
$SrCl_2$	Strontium chloride	9.19	--	--		99	
		7.69	--	$2x10^6$		99	
$Sr_4Cl_2 \cdot 6H_2O$	Strontium chloride hexahydrate	8.52	--	--		99	
SrF_2	Strontium fluoride	6.465±0.002	300	10^3		5	
		6.50	300	$5x(10^2$-$10^{11})$		118	126
$SrMoO_4$	Strontium molybdate	$\varepsilon_{11}=\varepsilon_{22}=31.7\pm0.2$	297.5	$1.59x10^3$	<10	29	
		$\varepsilon_{33}=41.7$ 0.2	297.5	$1.59x10^3$	<10	29	
$Sr(NO_3)_2$	Strontium nitrate	5.33	292	$2x10^5$		170	
$Sr_2Nb_2O_7$	Strontium niobate	$\varepsilon_{11}=75$	--	10^3		127	
		$\varepsilon_{22}=46$	--	10^3		127	
		$\varepsilon_{33}=43$	--	10^3		127	
SrO	Strontium oxide	13.3±0.3	273	$2x10^6$		82	
SrS	Strontium sulfide	11.310	--	$7.25x10^6$		173	
$SrSO_4$	Strontium sulfate	11.5	--	--		154	

Formula	Name	ε_{ijk}	T (K)	ν (Hz)	tan δ x10^{-4}	Reference	Add'l. Info. (Fig. No.)
$SrTiO_3$	Strontium titanate	332	298	10^3		154	25,26
		2080	78	10^3		200	
$SrWO_4$	Strontium tungstate	$\varepsilon_{11}=\varepsilon_{22}=25.7\pm0.2$	297.5	1.59×10^3	<10	29	
		$\varepsilon_{33}=34.1\pm0.2$	297.5	1.59×10^3	<10	29	
Ta_2O_5	Tantalum pentoxide (tantala)						
	α phase	$\varepsilon_{11}=\varepsilon_{22}=30$	77	10^3		143	108-110
	α phase	$\varepsilon_{33}=65$	77	10^3		143	108-110
	β phase	24	292	10^3		143	108-110
$Tb(MoO_4)_3$	Terbium molybdate	11	298	--		26	
		$\varepsilon_{11}=\varepsilon_{22}=33$	100-200	9.4×10^9		192	
		$\varepsilon_{33}=53$	100-200	9.4×10^9		192	
Te	Tellurium	$\varepsilon_{11}=\varepsilon_{22}=33$	--	--		3	
		$\varepsilon_{33}=54$	--	--		3	
	polycrystalline	27.5	--	i.r.		80	
	monocrystalline	28.0	--	i.r.		80	
ThO_2	Thorium dicxide	18.9±0.4	r.t.	3×10^5		10	
		10.6	r.t.	2×10^6		72	
TiO_2	Titanium dioxide (rutile)	$\varepsilon_{11}=\varepsilon_{22}=86$	300	10^4-10^6		139,140	111
		$\varepsilon_{33}=170$	300	10^4-10^6		139,140	111
Ti_2O_3	Titanium sesquioxide	30	77	6×10^{10}		165	
TlBr	Thallium bromide	30	298	--		27	
		30.0±0.2	293	10^3-10^7		162	120,122,123

Formula	Name	ε_{ijk}	T (K)	ν (Hz)	tan δ $\times 10^{-4}$	Reference	Add'l. Info. (Fig. No.)
TlCl	Thallous chloride	31.9	--	2×10^{6}		52	
		32.2±0.2	293	10^{3}-10^{5}		162	120,123
TlI	Thallous iodide orthorhombic	21.2±0.2	293	10^{4}		162	121,124
	cubic (p=3 kbar)	29.6±0.5	293	10^{4}		162	121,124
		37.3	193	10^{7}		191	
$TlNO_3$	Thallous nitrate	16.5	293	5×10^{5}		52	
		13.5	300-310	10^{9}			
$TlSO_4$	Thallous sulfate	25.5	293	5×10^{5}		52	
UO_2	Uranium dioxide	24	--	3×10^{5}		10	
		21.0±1	143-373	9.4×10^{9}		62	
WO_3	Tungsten trioxide	$\varepsilon_{11}=9\times10^{4}$		--		101	
		$\varepsilon_{22}=4\times10^{4}$				101	
		$\varepsilon_{33}=6\times10^{3}$					
$YMnO_3$	Yttrium manganate	20	r.t.	2×10^{7}		23	
Y_2O_3	Yttrium sesquioxide	10	--	10^{6}		132	
$YbMnO_3$	Ytterbium manganate	20	r.t.	2×10^{7}		23	
Yb_2O_3	Ytterbium sesquioxide	5.0 (film)	r.t.	10^{3}		58	

Formula	Name	ε_{ijk}	T (K)	ν (Hz)	tan δ x10⁻⁴	Reference	Add'l. Info. (Fig. No.)
ZnO	Zinc monoxide	ε_{11}^S=8.33				90	
		ε_{33}^S=8.84				90	
		ε_{11}^T=9.26				90	
		ε_{33}^T=11.0				90	
		ε_{11}=9.26				110	
		ε_{33}=8.2				110	
		8.15	--	3×10^{10}		86	
		8.15	--	i.r.		40	
ZnS	Zinc sulfide	ε_{11}^T=8.08±2%	77	10^4		20	88
		ε_{11}^T=8.32±2%	298	10^4		20	88
		ε_{11}^T=8.14±2%	77	10^4		20	88
		ε_{11}^T=8.37±2%	298	10^4		20	88
		$\varepsilon_{11}^S=\varepsilon_{11}^T$=8.7±1%	r.t.	--		105	
ZnSe	Zinc selenide	$\varepsilon_{11}^T=\varepsilon_{11}^S$=9.12±2%	298	10^4		20	
		8.1±0.3	--	--		7,8	
ZnTe	Zinc telluride	$\varepsilon_{11}^T=\varepsilon_{11}^S$=10.10±2%	--	--		7	
$ZnWO_4$	Zinc tungstate	ε_{22}=16.1±0.5	r.t.	$(5\text{-}500)\times10^3$	<10	51	
ZrO_2	Zirconium dioxide (zirconia)	12.5	r.t.	2×10^6		72	

3. Graphical Data

3.1. Rochelle Salt and Related Tartrates

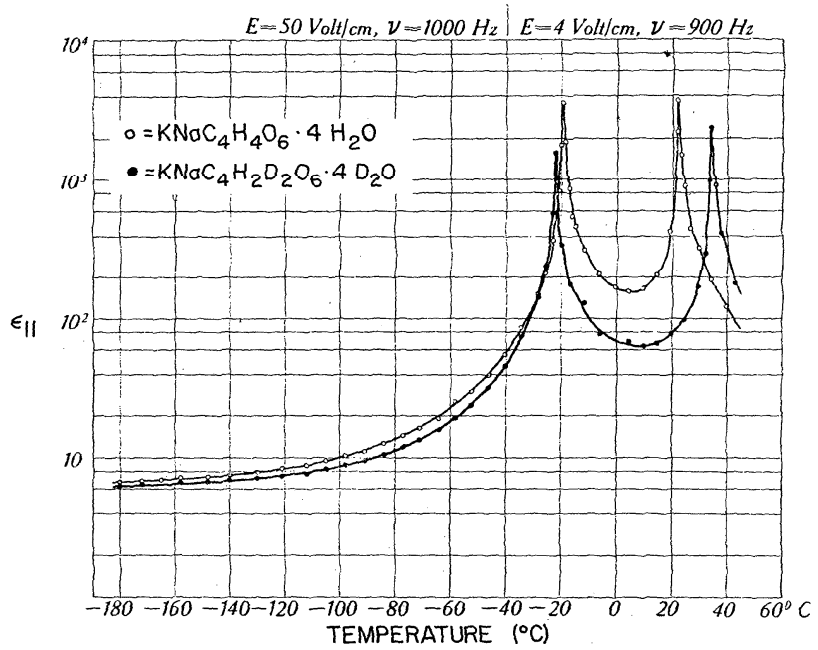

FIGURE 1. $NaKC_4H_4O_6 \cdot 4H_2O$ (Rochelle salt) and $NaKC_4H_2D_2O_6 \cdot 4D_2O$ (deuterated Rochelle salt). The temperature dependences of the dielectric constants of Rochelle salt and deuterated Rochelle salt by Hablützel [73].

Remarks – Rochelle salt has two Curie points: $T_c^l = 255$ K and $T_c^u = 297$ K. Deuterated Rochelle salt has its Curie points shifted: $T_c^l = 251$ K and $T_c^m = 308$ K.

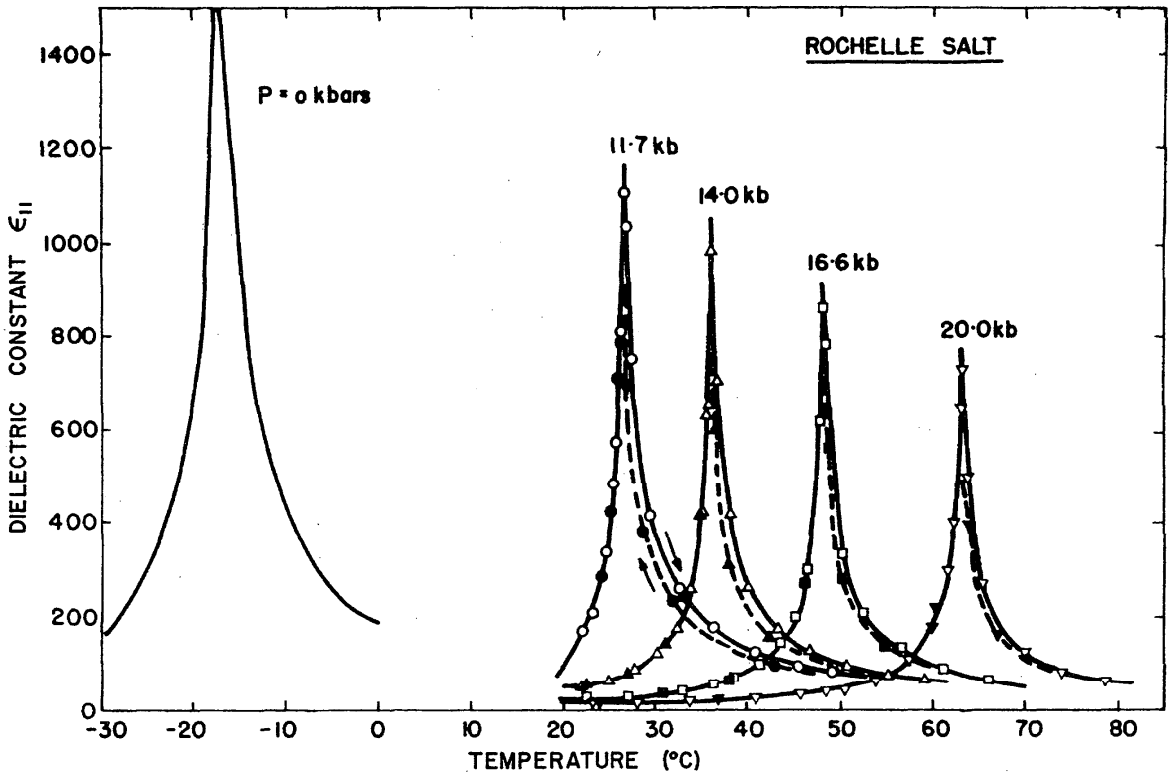

FIGURE 2. $NaKC_4H_4O_6 \cdot 4H_2O$ (Rochelle salt). Temperature dependence of the dielectric constant of Rochelle salt near the lower Curie point at different pressures by Samara [163].

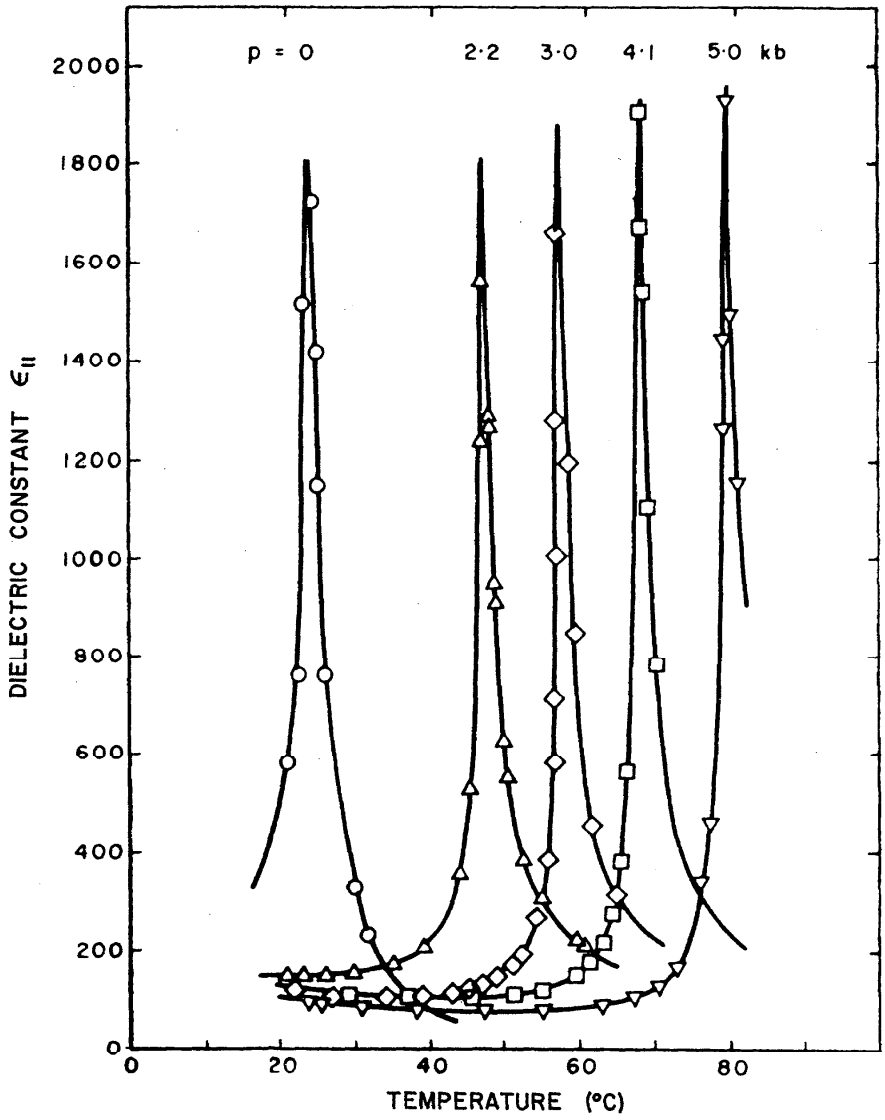

FIGURE 3. $NaKC_4H_4O_6 \cdot 4H_2O$ (Rochelle salt). Temperature dependence of the dielectric constant of Rochelle salt near the upper Curie point at different pressures by Samara [163].

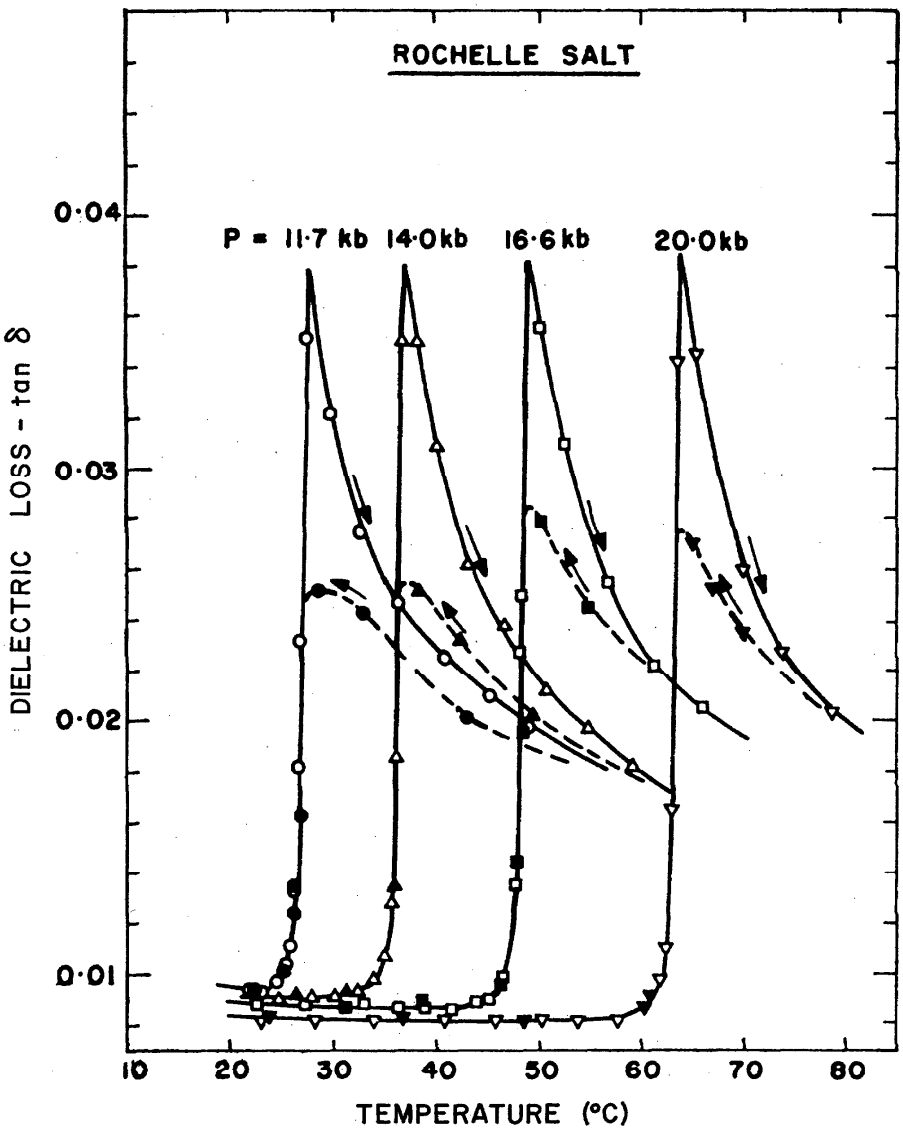

FIGURE 4. $NaKC_4H_4O_6 \cdot 4H_2O$ (Rochelle salt). Temperature dependence of the dielectric loss of Rochelle salt near the lower Curie point at different pressures by Samara [163].

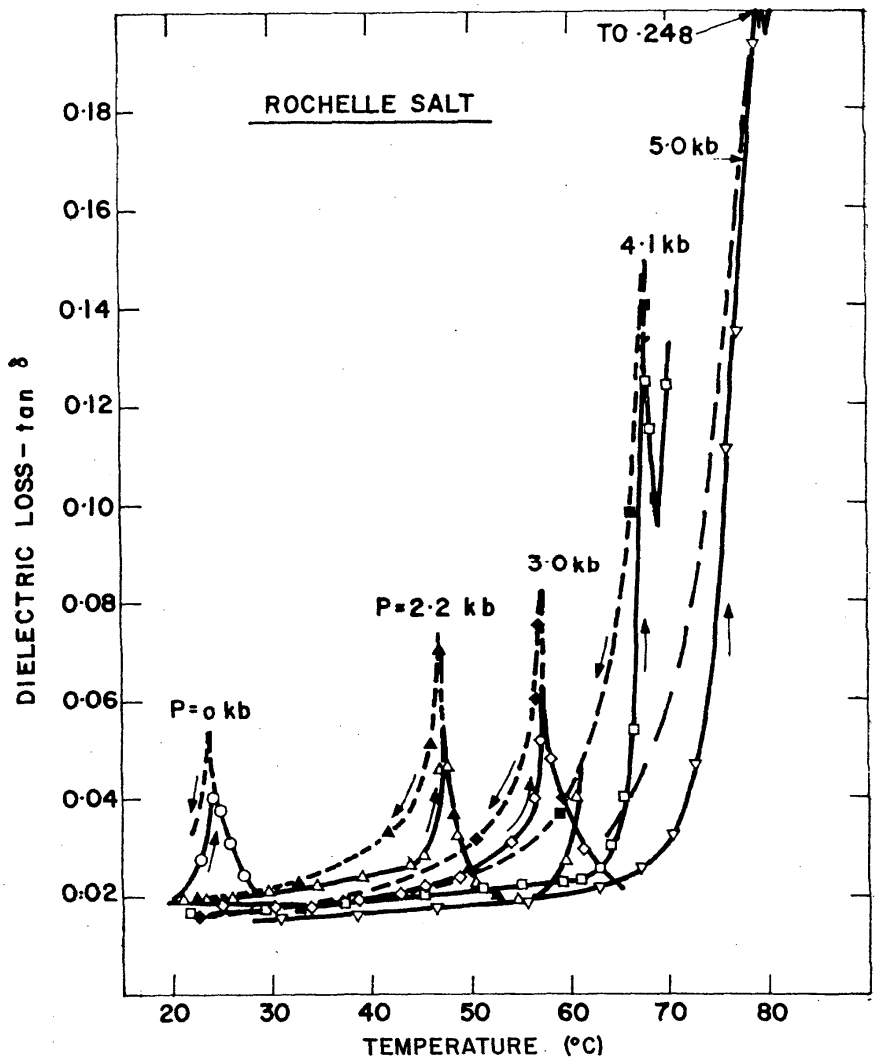

FIGURE 5. $NaKC_4H_4O_6 \cdot 4H_2O$ (Rochelle salt). Temperature dependence of the dielectric loss of Rochelle salt near the upper Curie point at different pressures by Samara [163].

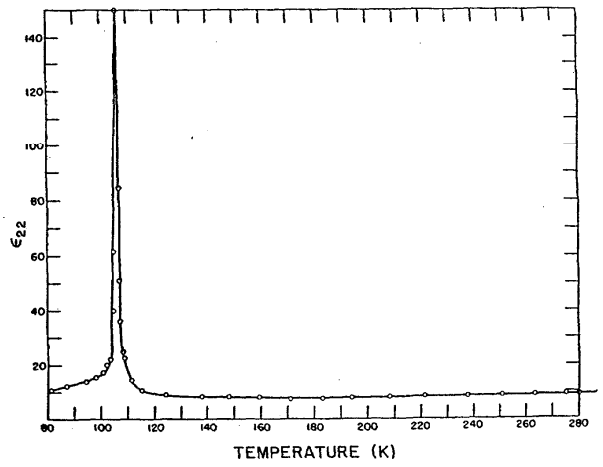

FIGURE 6. $LiNH_4C_4H_4O_6 \cdot H_2O$ (LAT). Temperature dependence of dielectric constant ϵ_{22} of LAT by Merz [138].

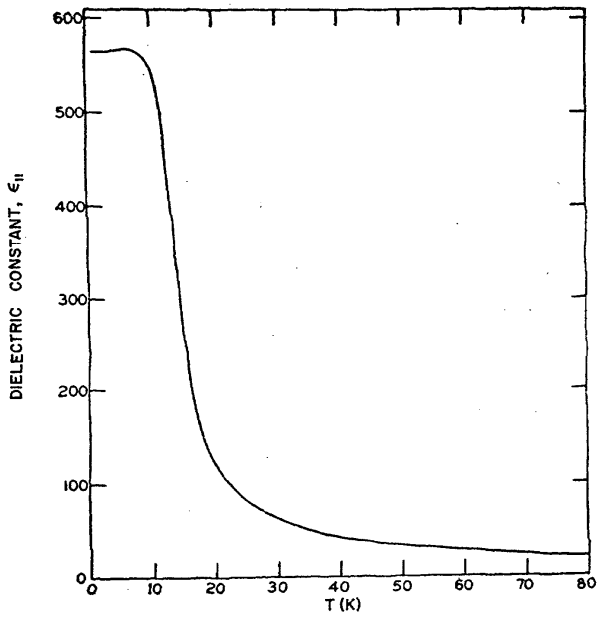

FIGURE 7. $LiTlC_4H_4O_6 \cdot H_2O$ (LTT). Temperature dependence of the dielectric constant ϵ_{11} of LTT by Matthias, et al. [137].

($\nu = 10^3$Hz, $E_a = 5$ V/cm)

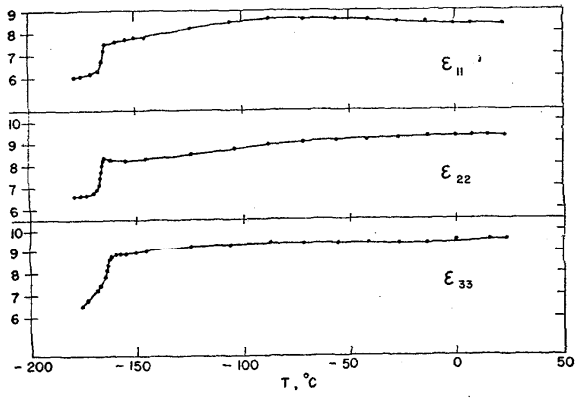

FIGURE 8. $NaNH_4C_4H_4O_6 \cdot 4H_2O$–"ammonium Rochelle salt." Temperature dependence of the dielectric constant of "ammonium Rochelle salt" by Jona, et al. [92].

Remarks—This salt has a $T_c = 109$ K.

3.2. Triglycine Sulfate and Related Compounds

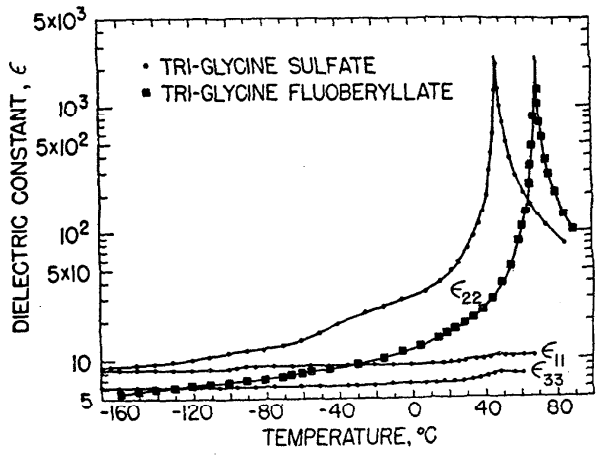

FIGURE 9. $(NH_2CH_2COOH)_3\ H_2SO_4$–Triglycine sulfate (TGS). TGS is isomorphous with TG Selenate and TG Fluorberyllate. The temperature dependences of the dielectric constants ϵ_{11}, ϵ_{22}, and ϵ_{33} for TGS and ϵ for TGFB by Hoshino, et al. [85].

Remarks—Above T_c the dielectric constant is given by $\epsilon = C/(T - T_c)$, where $C = 3280$ and $T_c = 322.57 \pm 0.05$ K. $(NH_2CH_2COOH)_3 \cdot H_2BeF_4$–Tryglycine Fluorberyllate TBFB. $T_c = 346 \pm 0.2$ K was measured by Wieder, et al. [205]. Above T_c the dielectric constant is given by $\epsilon' = C/(T - T_c)$ where $C = 2512 \pm 80$.

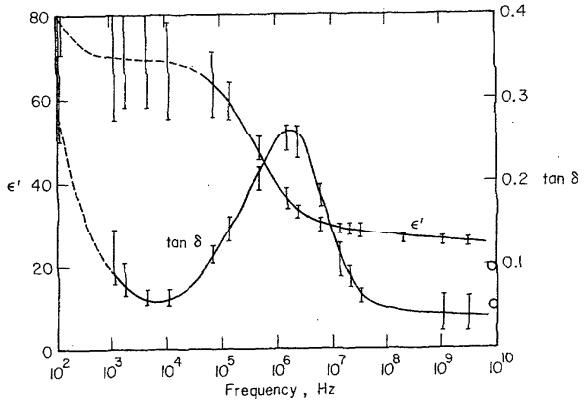

FIGURE 10. $(NH_2CH_2COOH)_3H_2SO_4$ (TGS). The frequency dependences of the dielectric constant and loss tangent of TGS measured at 298.5 K by Petrov [146].

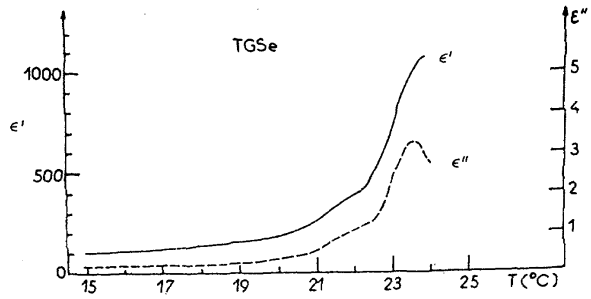

FIGURE 11. $(NH_2CH_2COOH)_3 \cdot H_2SeO_4$–Tryglycine Selenate (TGSe). The temperature dependence of the real and imaginary parts of the dielectric constant ϵ', ϵ'' of TGSe measured at 1592 Hz by Grandjean, et al. [67].

Remarks—For this material $T_c = 295.7$ K was measured by Matthias, et al. [137].

3.3. KDP and Related Phosphates and Arsenates

Table A. KDP and related (anti) ferroelectrics

Compound Formula	Compound name	Curie Temperatures T_c
KH_2PO_4	KDP	123 K
KH_2AsO_4	KDA	97
KD_2PO_4	KDDP	213
KD_2AsO_4	KDDA	162
$NH_4H_2PO_4$*	ADP	148
$NH_4H_2AsO_4$*	ADA	216
$NH_4D_2PO_4$*	ADDP	242, 245
$NH_4D_2AsO_4$*	ADDA	299
$ND_4D_2PO_4$*	A_dDDP	243
$ND_4D_2AsO_4$*	A_dDDA	304
RbH_2PO_4	RDP	146
RbH_2AsO_4	RDA	111
RbD_2PO_4	RDDP	218
RbD_2AsO_4	RDDA	178
$Cs\ H_2PO_4$	CDP	159
$Cs\ H_2AsO_4$	CDA	143
$Cs\ D_2AsO_4$	CDDA	212

*antiferroelectrics

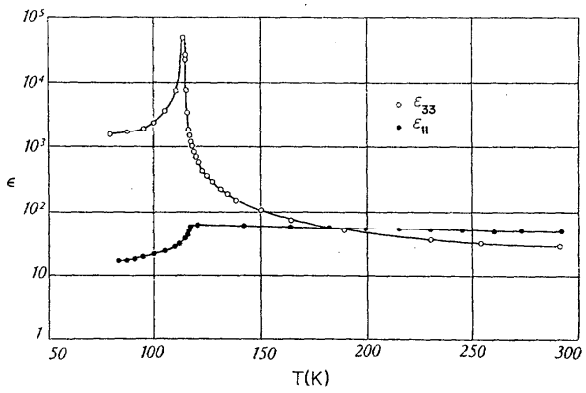

FIGURE 12. KH_2PO_4 (KDP). The temperature dependences of the dielectric constants ϵ_{11}, ϵ_{33} of KDP measured at 800 Hz by Busch [34].

(E_a = 200 V/cm).

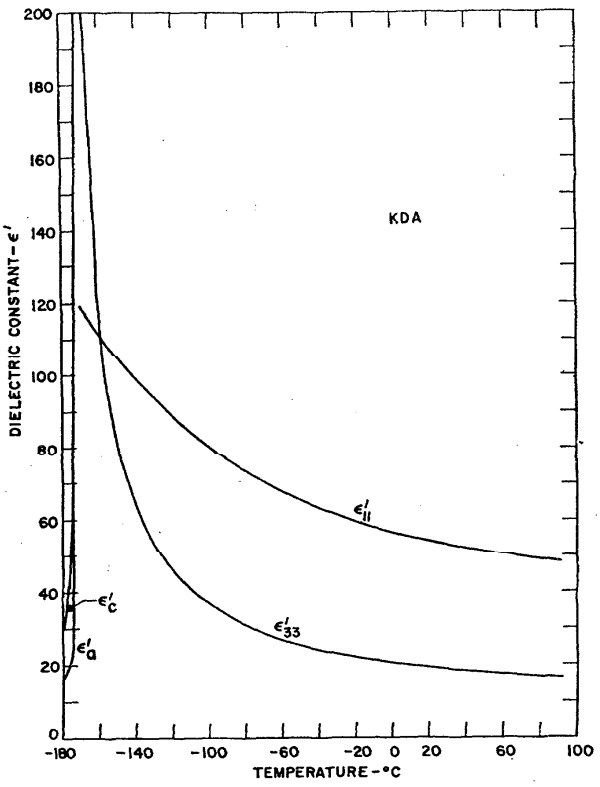

FIGURE 13. KH_2AsO_4 (KDA). Temperature dependences of the dielectric constants $\epsilon_{11}, \epsilon_{33}$ of KDA measured by Adhav [1, 2].

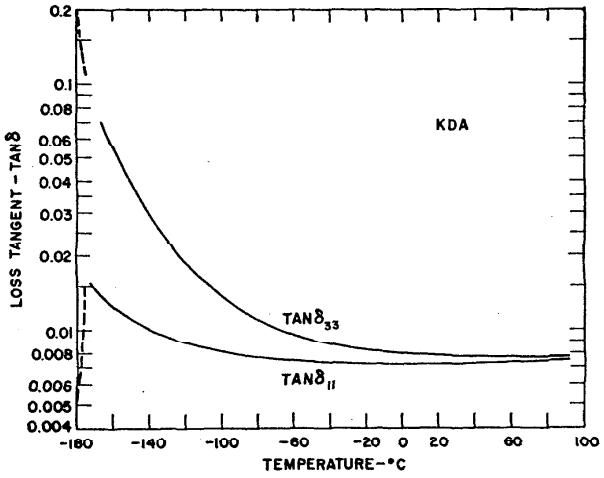

FIGURE 14. KH_2AsO_4 (KDA). Temperature dependences of the dielectric loss tangents tan δ_{11}, tan δ_{33} for KDA as measured by Adhav [1, 2].

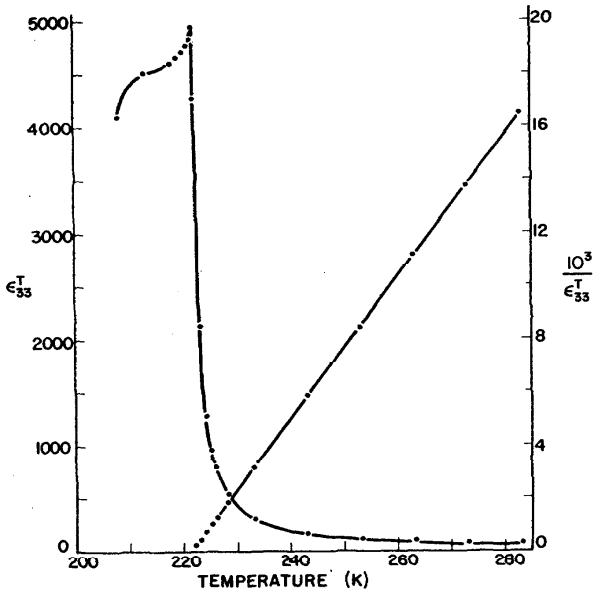

FIGURE 15. KD_2PO_4 (KDDP). Temperature dependence of the dielectric constants ϵ_{33} and its reciprocal for KDDP measured by Sliker, et al. [176].

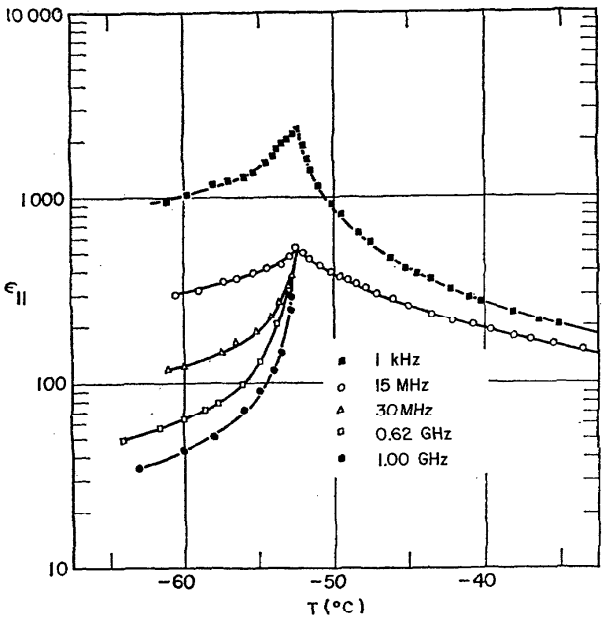

FIGURE 16. KD_2PO_4 (KDDP). Temperature dependences of the dielectric constant for KDDP at different frequencies measured by Hill, et al. [90].

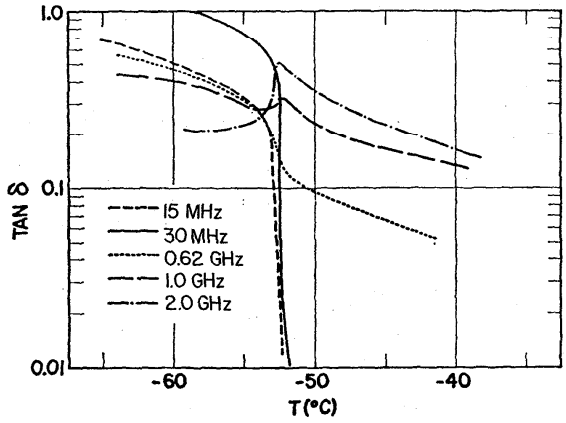

FIGURE 17. KD_2PO_4 (KDDP). Temperature dependence of the dielectric loss tangent for KDDP at different frequencies by Hill, et al. [90].

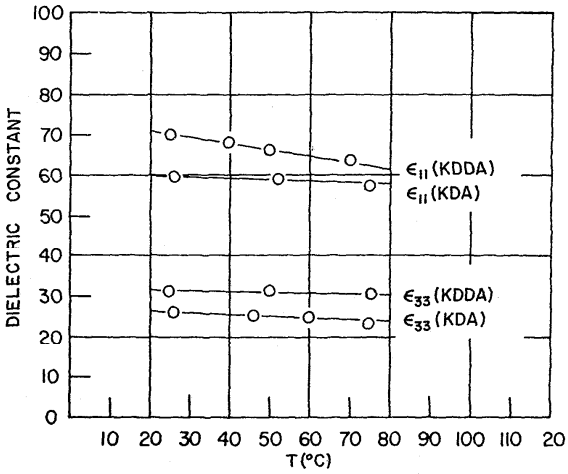

FIGURE 18. KD_2AsO_4 (KDDA). Temperature dependences of the dielectric constants ϵ_{11}, ϵ_{33} of KDDA measured by Adhav [1, 2].

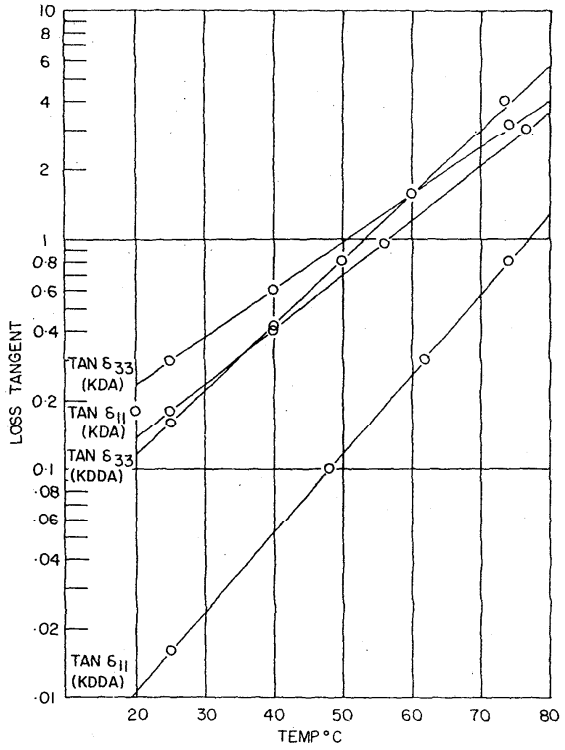

FIGURE 19. KD_2AsO_4 (KDDA). Temperature dependences of the dielectric loss tangents tan δ_{11}, tan δ_{33} of KDDA measured by Adhav [1, 2].

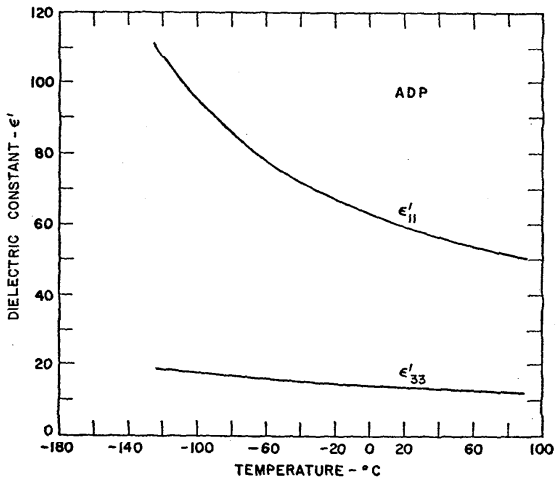

FIGURE 20. $NH_4H_2PO_4$ (ADP). Temperature dependences of the dielectric constants ϵ_{11}, ϵ_{33} for ADP reported by Kaminow [97].

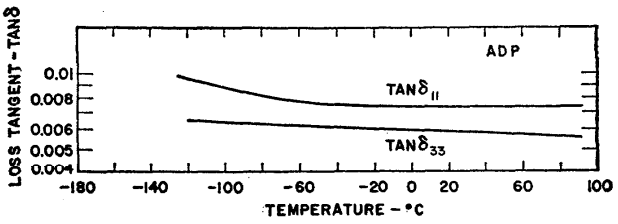

FIGURE 21. $NH_4H_2PO_4$ (ADP). Temperature dependences of the dielectric loss tangents tan δ_{11}, tan δ_{33} for ADP reported by Kaminow [97].

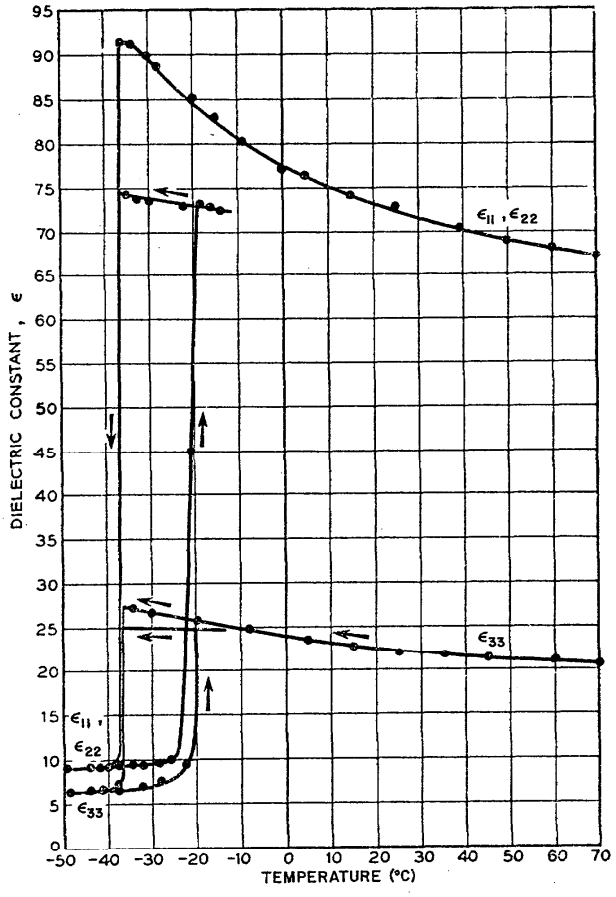

FIGURE 22. $ND_4D_2PO_4$ (ADDP). Temperature dependences of the dielectric constants ϵ_{11}, ϵ_{22}, ϵ_{33} of ADDP measured by Mason [125].

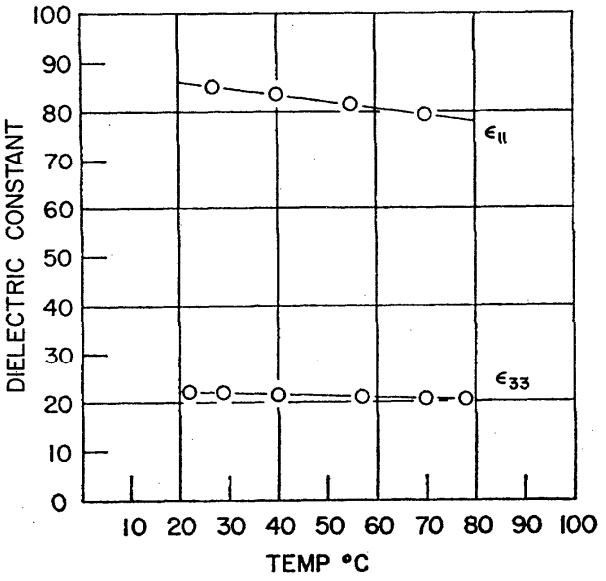

FIGURE 23. $NH_4H_2AsO_4$ (ADA). Temperature dependences of the dielectric constants ϵ_{11}, ϵ_{33} of ADA measured by Adhav [1, 2].

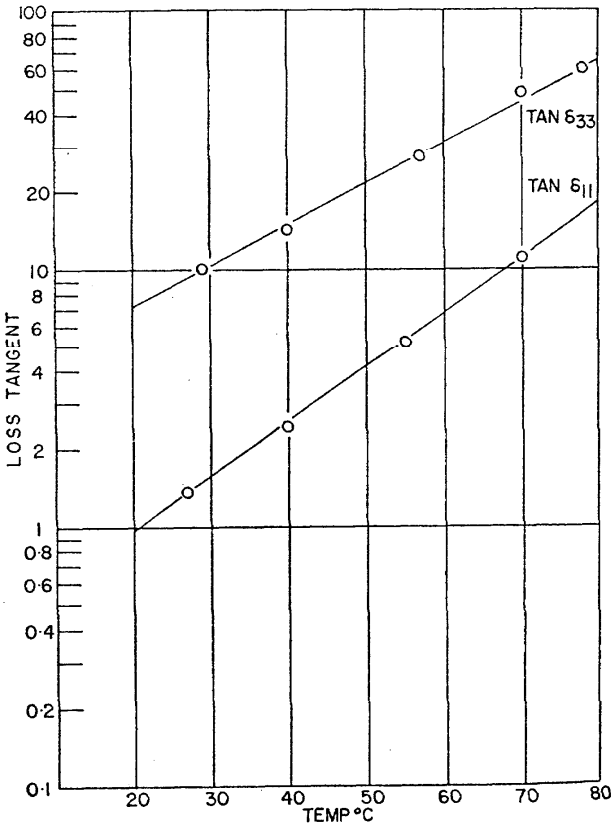

FIGURE 24. $NH_4H_2AsO_4$ (ADA). Temperature dependences of the dielectric loss tangents tan δ_{11}, tan δ_{33} of ADA measured by Adhav [1, 2].

3.4. Perovskites

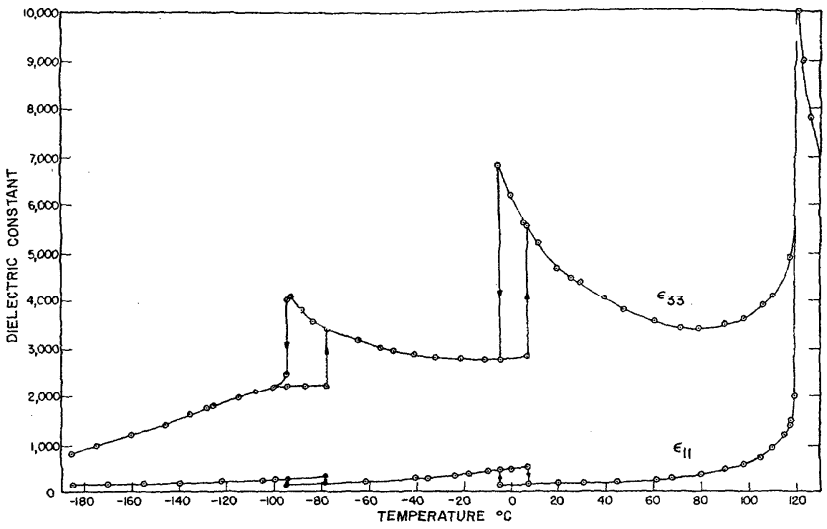

FIGURE 25. $BaTiO_3$. Temperature dependences of the dielectric constants ϵ_{11}, ϵ_{33} of flux grown $BaTiO_3$ measured by Merz [138].

The literature contains a considerable number of publications concerning the dielectric behavior of $BaTiO_3$ since the discovery of ferroelectricity in this material in 1943. Yet it was only recently (1968) that accurate measurements on melt grown crystals showed the true Curie temperature to be 406 ± 2 K rather than 393 K. The lower transition temperature measured on flux grown crystals appeared to be due to trace impurities (Wemple, et al. [203]).

Other phase transitions occur at 278 and 193 K.

Figure 25 shows ϵ_{11} and ϵ_{33} for *flux grown* crystals. The dielectric behavior of *melt* grown crystals between room temperature and 133 °C is shown in figure 26.

Above the upper Curie temperature ϵ is represented by $\epsilon = C/(T - 115)$, where $C = 1.5 \times 10^5$.

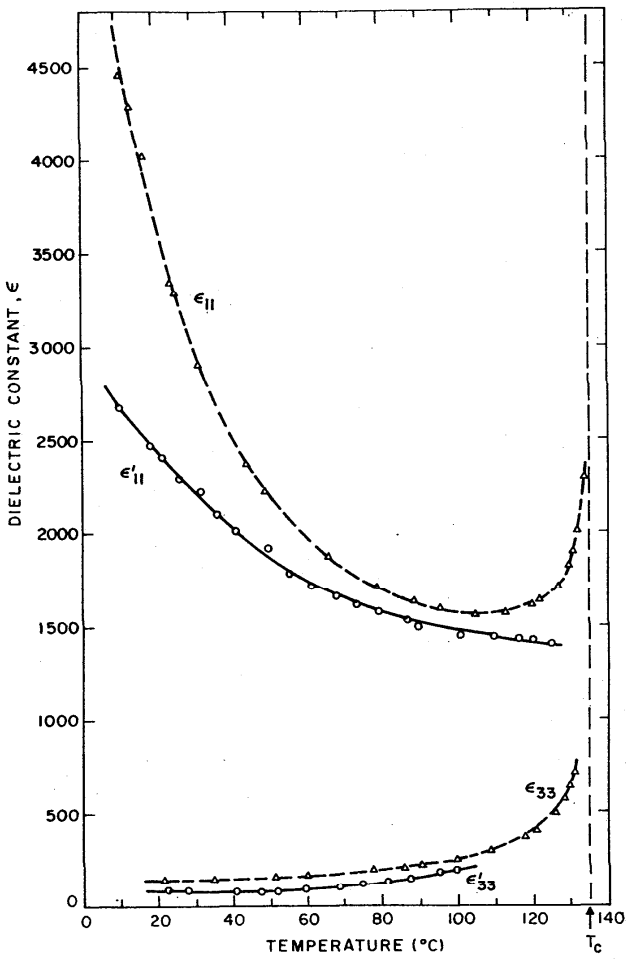

FIGURE 26. $BaTiO_3$. Temperature dependences of the dielectric constants ϵ_{11}, ϵ_{33} (unclamped values at 100 kHz) and ϵ'_{11}, ϵ'_{33} (unclamped values at 250 MHz) for melt-grown single domain $BaTiO_3$ measured by Wemple, et al. [203].

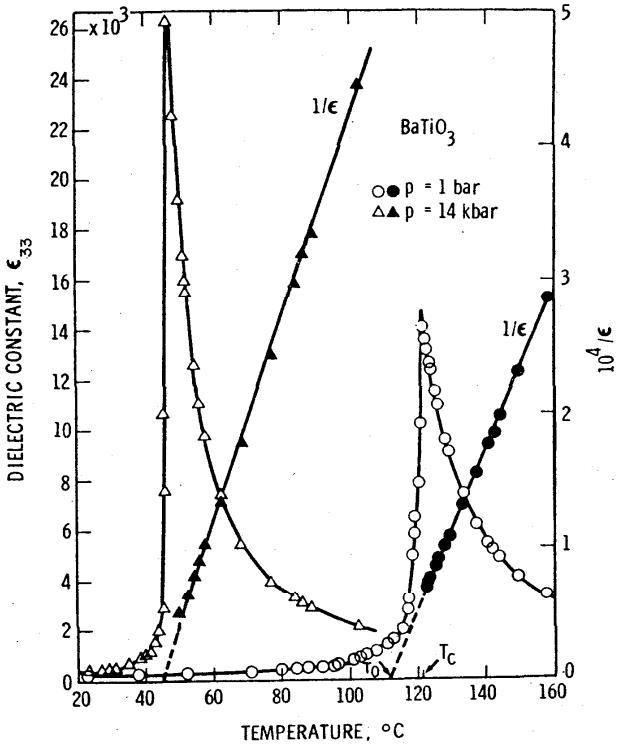

FIGURE 26a. $BaTiO_3$. Temperature dependences of the dielectric constant ϵ_{33} and its reciprocal $1/\epsilon_{33}$ for $BaTiO_3$. Data measured by Samara [164a] at 1 bar and 14 k bar are shown.

Both the ferroelectric–paraelectric transition temperature, T_c, and the extrapolated Curie temperature, T_o, decrease linearly with pressure.

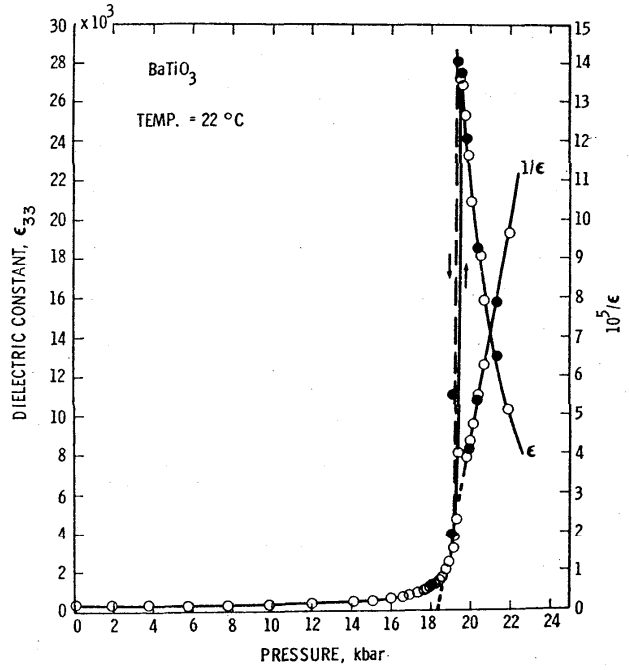

FIGURE 26b. $BaTiO_3$. Pressure dependence of the dielectric constant ϵ_{33} and its reciprocal $1/\epsilon_{33}$ at room temperature for $BaTiO_3$ measured by Samara [164a].

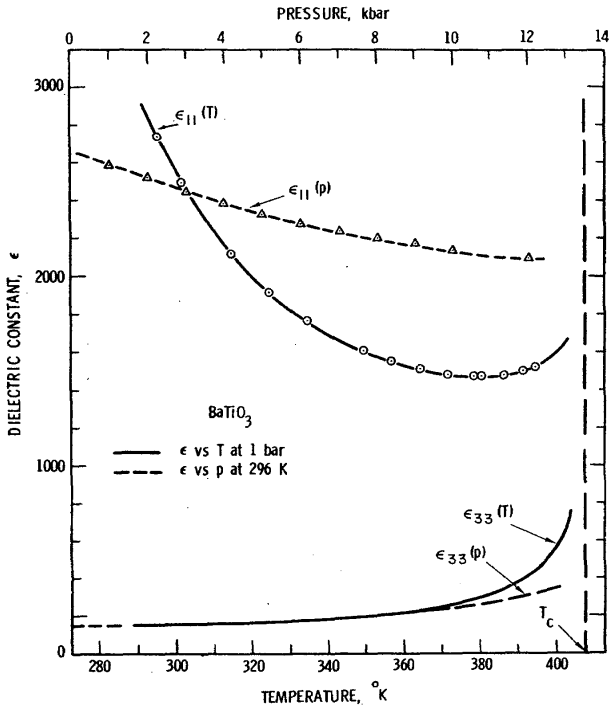

FIGURE 26c. $BaTiO_3$. Temperature and pressure dependences of the dielectric constants ϵ_{11}, ϵ_{33} of $BaTiO_3$ in the tetragonal phase measured by Samara [164b].

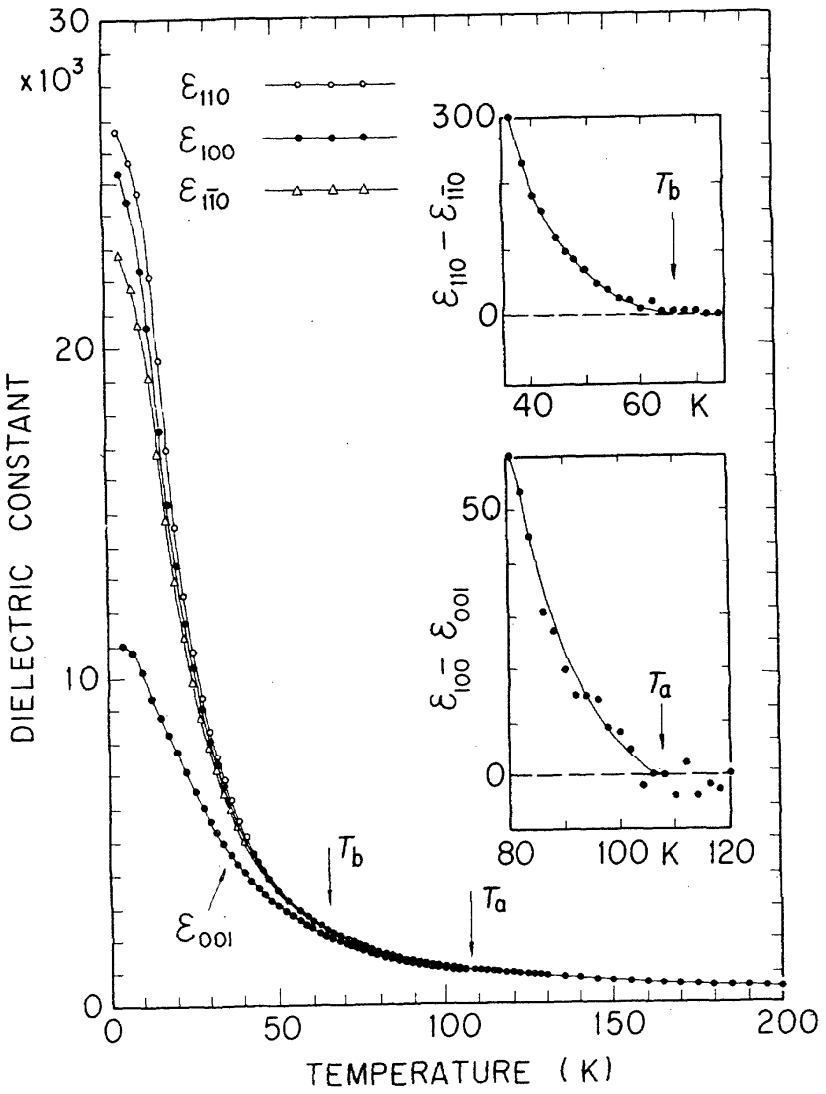

FIGURE 27. $SrTiO_3$. Temperature dependence of the dielectric constants ϵ_{110}, ϵ_{010} of $SrTiO_3$ measured by Sakudo, et al. [159].

This titanate has an extremely subtle phase-transition from the cubic to the tetragonal structure at about $T_a = 110$ K. The dielectric constant rises monotonically to very high values at liquid helium temperatures (see fig. 27). The second transition temperature T_b has not been confirmed by any other experimental technique. The compound is not ferroelectric at any temperature above absolute zero. The pressure dependences of the dielectric constant has been measured by Samara, et al. [161] as shown in fig. 28.

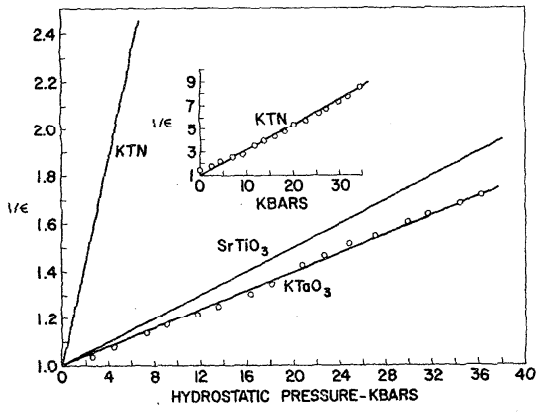

FIGURE 28. $KTa_{0.65}Nb_{0.35}O_3$ (KTN), $SrTiO_3$, $KTaO_3$. Pressure dependences of the dielectric constants of KTN, $SrTiO_3$, and $KTaO_3$ measured by Wemple, et al. [203].

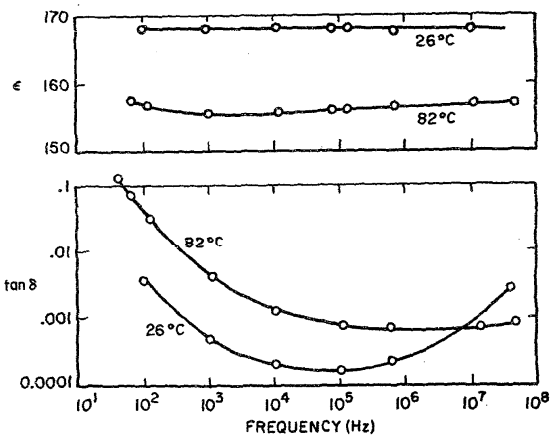

FIGURE 29. $CaTiO_3$. Frequency dependences of the dielectric constant, ϵ, and dielectric loss tangent, $\tan\delta$, for $CaTiO_3$ at two different temperatures after Martin [122].

Remarks—This material is not ferroelectric.

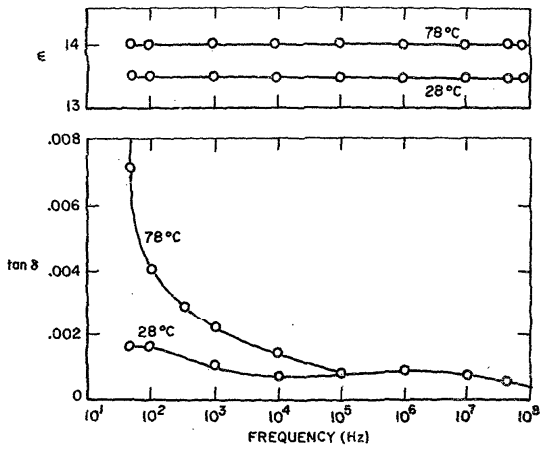

FIGURE 30. $MgTiO_3$. Frequency dependences of the dielectric constant, ϵ, and dielectric loss tangent, $\tan\delta$, for $MgTiO_3$ at two different temperatures after Martin [122].

Remarks—This material is not ferroelectric.

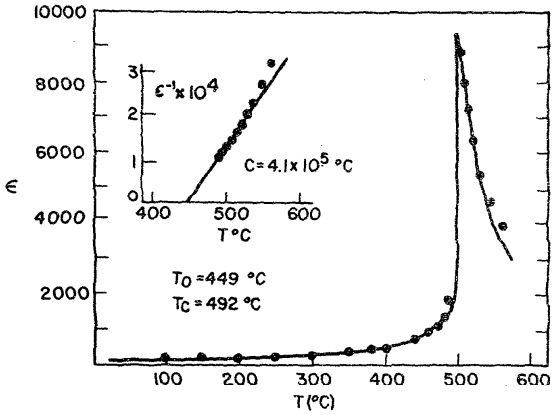

FIGURE 31. $PbTiO_3$. Temperature dependence of the dielectric constant of $PbTiO_3$ measured by Remeika, et al. [151].

Remarks—$T_c = 765$ K
$\epsilon = C/(T - T_0)$
where $C = 4.1 \times 10^5$
$T_0 = 722$ K

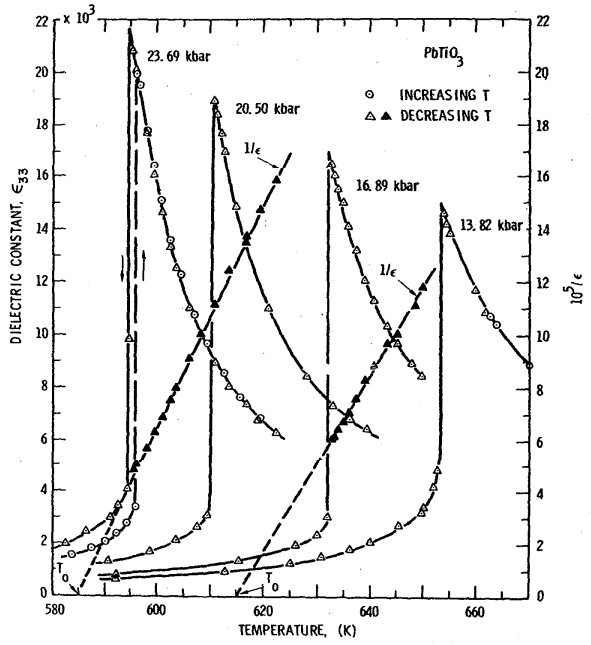

FIGURE 31a. $PbTiO_3$. Isobars of the temperature dependence of the dielectric constant, ϵ_{33}, of $PbTiO_3$ measured by Samara [164b].

The linear variation of $1/\epsilon$ vs T in the cubic phase is illustrated for two of the isobars.

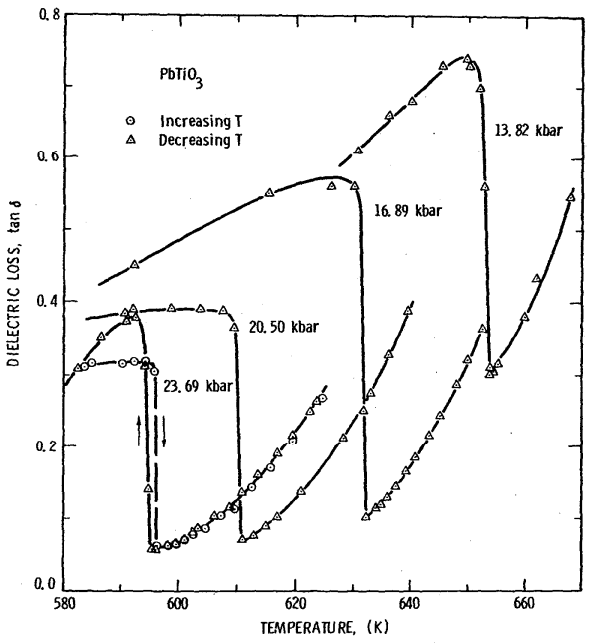

FIGURE 31b. $PbTiO_3$. Isobars of the temperature dependence of the dielectric loss of $PbTiO_3$ measured by Samara [164b].

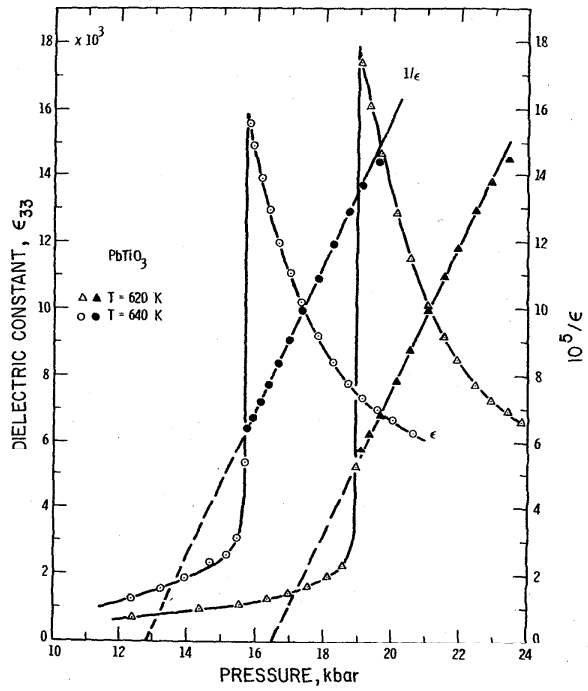

FIGURE 31c. $PbTiO_3$. Isotherms of the pressure dependence of the dielectric constant, ϵ_{33}, and its reciprocal, $1/\epsilon_{33}$, of $PbTiO_3$ measured by Samara [164b].

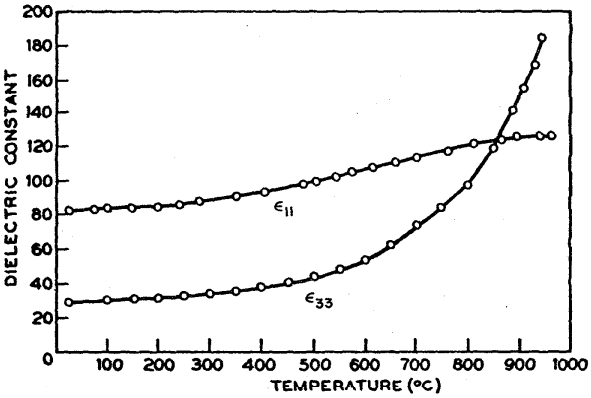

FIGURE 32. $LiNbO_3$. Temperature dependences of the dielectric constants ϵ_{11}, ϵ_{33} of $LiNbO_3$ measured at 10^5 Hz by Nassau, et al. [131].

Remarks—The Curie temperature of $LiNbO_3$ (1483 K) lies only 50 K below its melting point.

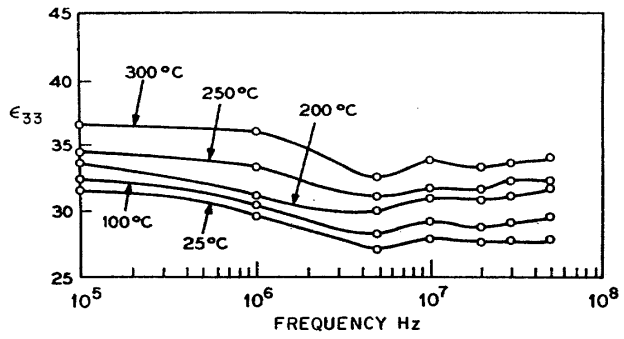

FIGURE 33. $LiNbO_3$. Frequency dependences of the dielectric constant, ϵ_{33}, of $LiNbO_3$ measured at various temperatures by Nassau [131].

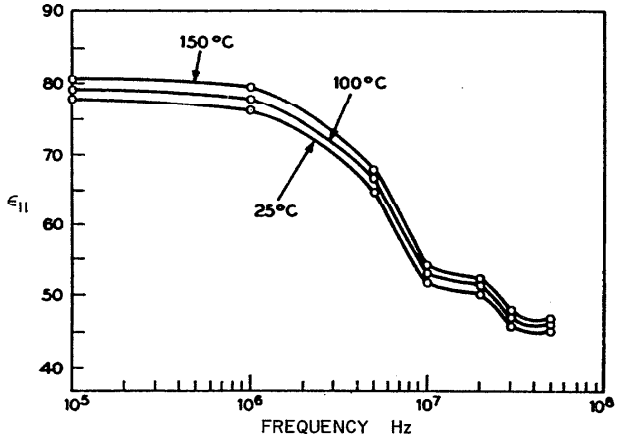

FIGURE 34. $LiNbO_3$. Frequency dependence of the dielectric constant ϵ_{11} of $LiNbO_3$ at different temperatures measured by Nassau, et al. [131].

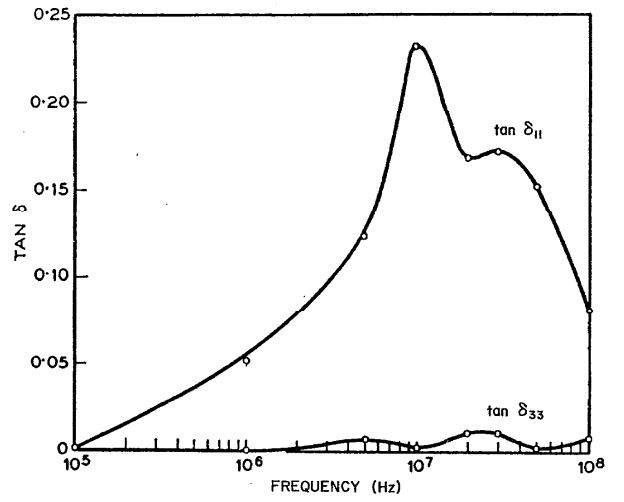

FIGURE 35. $LiNbO_3$. Frequency dependences of the dielectric loss tangents tan δ_{11} and tan δ_{33} of $LiNbO_3$ measured by Nassau, et al. [131].

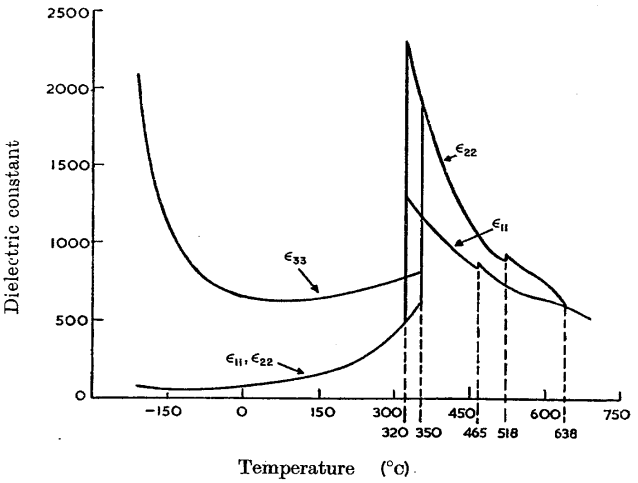

FIGURE 36. $NaNbO_3$. Temperature dependences of the dielectric constants ϵ_{11}, ϵ_{22}, ϵ_{33} of $NaNbO_3$ as measured by Cross, et al. [44].

Remarks—This crystal exhibits paraelectric, antiferroelectric, and ferroelectric phases.

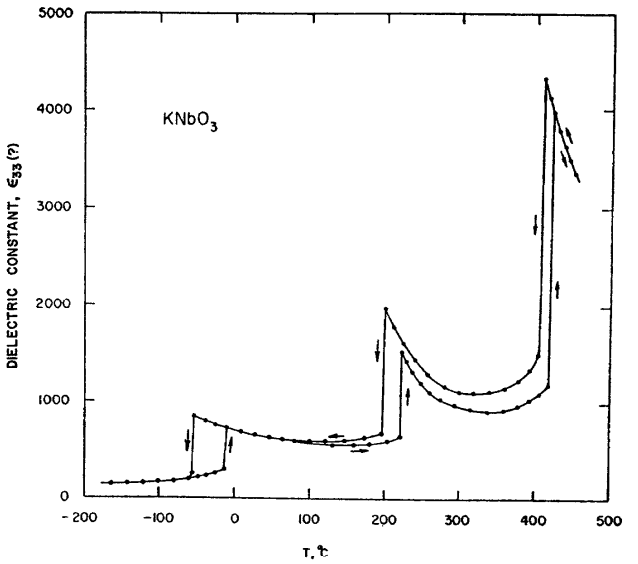

FIGURE 37. $KNbO_3$. Temperature dependence of the dielectric constant ϵ_{33} of $KNbO_3$ measured by Shirane, et al. [174]. ($\nu = 10$ kHz.)

Remarks—The dielectric behavior is similar to that of $BaTiO_3$. There are three transformations at 691 K, ~ 483 K, and ~ 240 K as measured on cooling; considerable hysteresis has been observed.

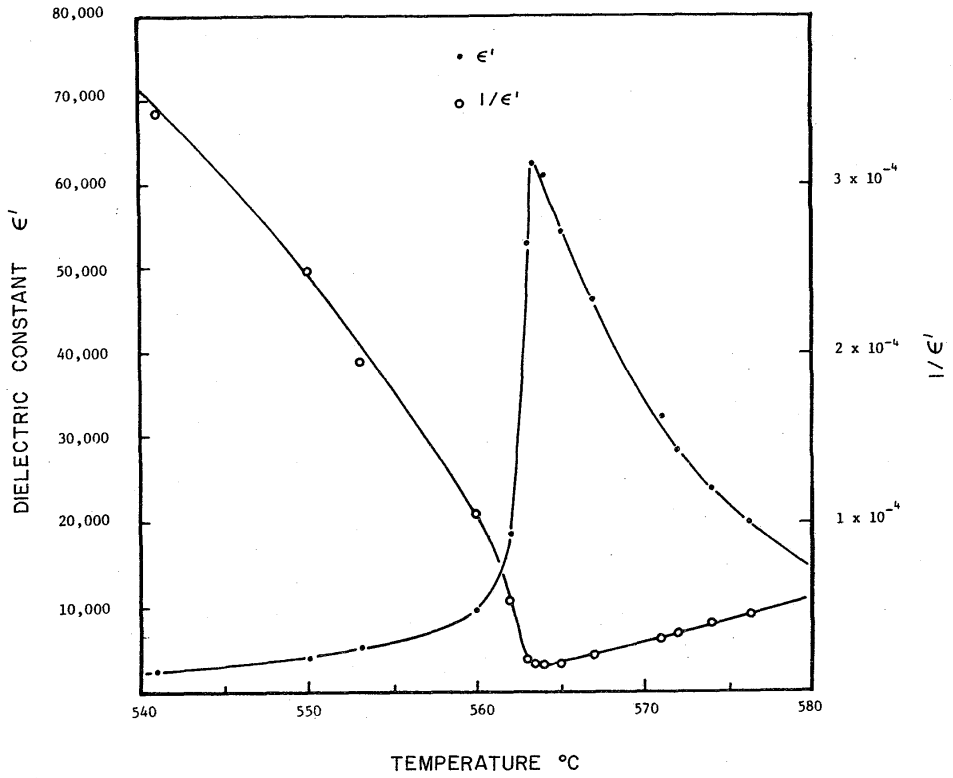

FIGURE 38. $Ba_2NaNb_5O_{15}$ ("bananas"). Temperature dependence of the dielectric constant of $Ba_2NaNb_5O_{15}$ measured by Rice, et al. [153].

Remarks—The measured Curie temperature $T_c = 833$ K.

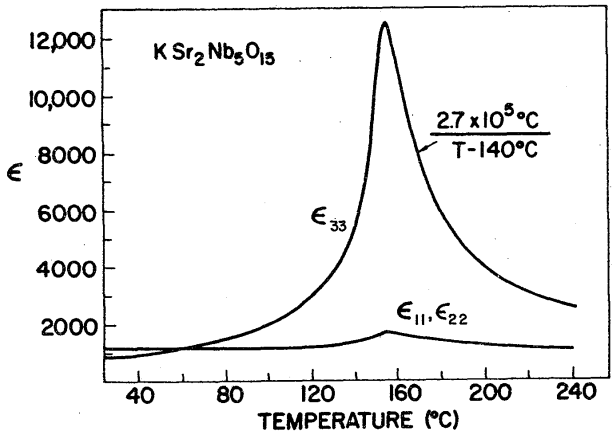

FIGURE 39. $Sr_2KNb_5O_{15}$. Temperature dependences of the dielectric constants ϵ_{11}, ϵ_{33} of $Sr_2KNb_5O_{15}$ measured by Giess [65].

Remarks—This material follows a Curie-Weiss law $\epsilon = C/(T - T_0)$ where $C = 2.7 \times 10^5$ and $T_0 = 140$ K.

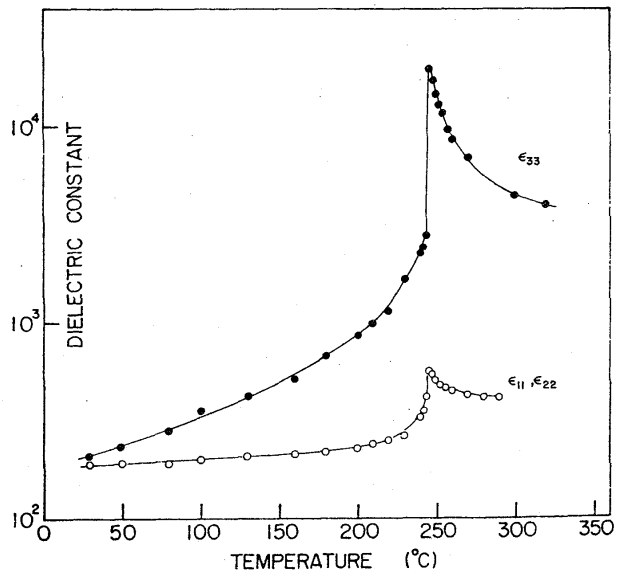

FIGURE 40. $Ba_6Ti_2Nb_8O_{30}$. Temperature dependences of the dielectric constants ϵ_{11}, ϵ_{33} of $Ba_6Ti_2Nb_8O_{30}$ as measured by Itoh [88].

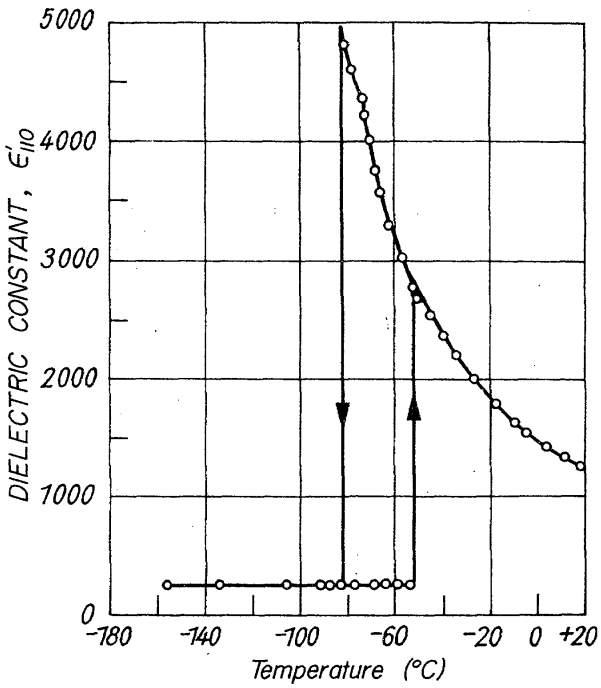

FIGURE 41. $Cd_2Nb_2O_7$. Temperature dependence of the dielectric constant of $Cd_2Nb_2O_7$ as measured by Shirane, et al. [174].

Remarks—The Curie temperature $T_c = 185$ K, and $\epsilon = C/(T - T_0)$ where $C = 4.6 \times 10^4$ and $T_0 = 150$ K.

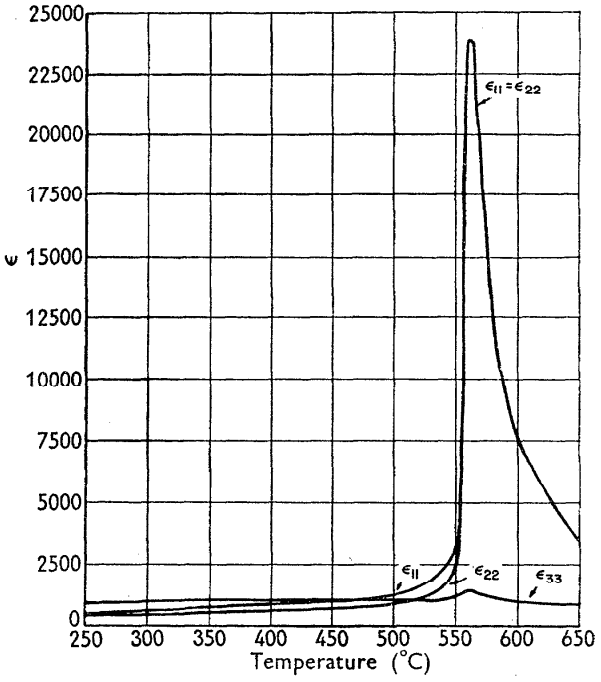

FIGURE 42. $PbNb_2O_6$. Temperature dependences of the dielectric constants ϵ_{11}, ϵ_{22}, ϵ_{33} of $PbNb_2O_6$ as measured by Francombe, et al. [59].

Remarks—The Curie temperature T_c is 843 K and $\epsilon = C/(T - T_0)$ where $C = 3 \times 10^5$ and $T_0 = 530$ K.

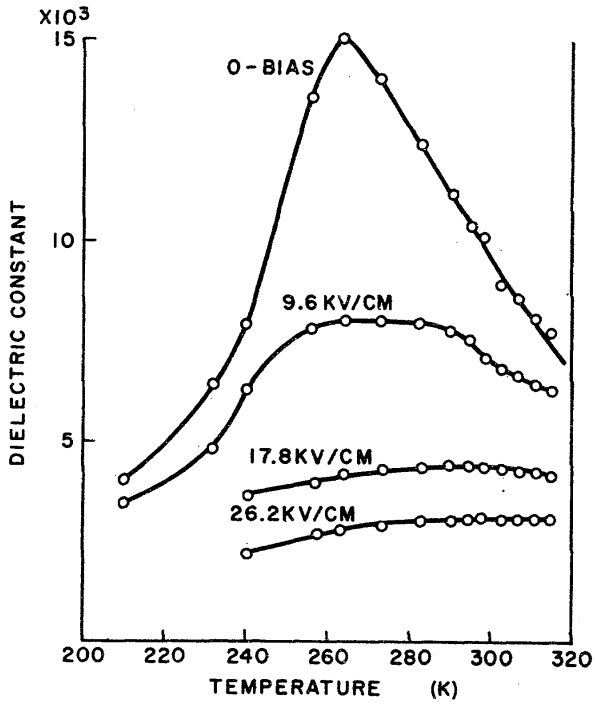

FIGURE 43. $Pb_3MgNb_2O_9$. Temperature dependence of the dielectric constant of $Pb_3MgNb_2O_9$ measured by Bonner, et al. [25].

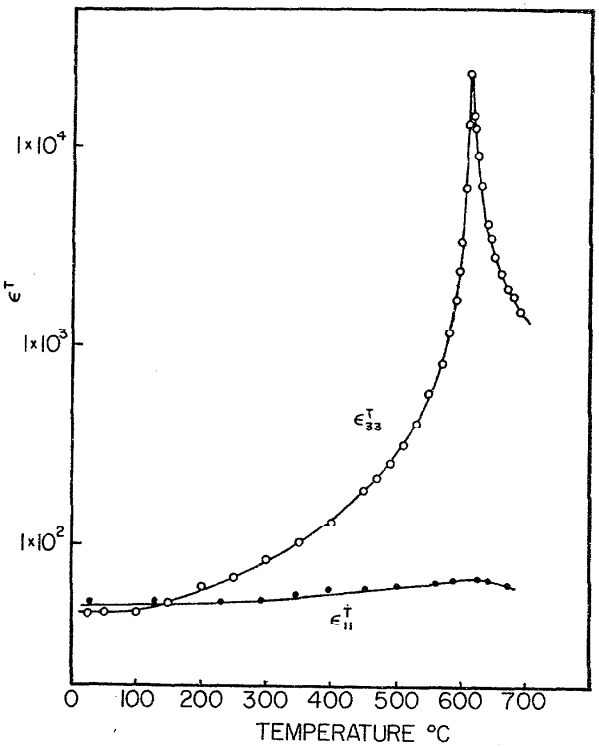

FIGURE 44. $LiTaO_3$. Temperature dependences of the dielectric constants ϵ_{11}, ϵ_{33} of $LiTaO_3$ measured by Yamada [209].

Remarks—The Curie temperature $T_c = 833$ K to 891 K.

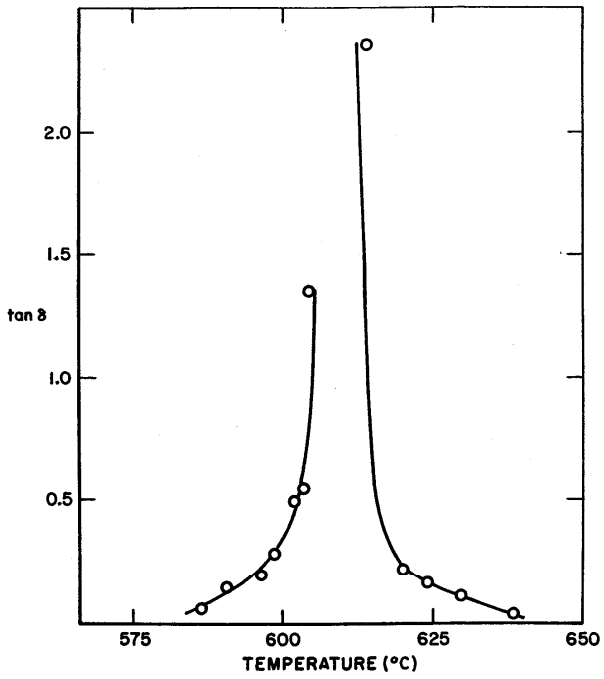

FIGURE 45. $LiTaO_3$. Temperature dependence of the dielectric loss tangent of $LiTaO_3$ measured by Yamada, et al. [209].

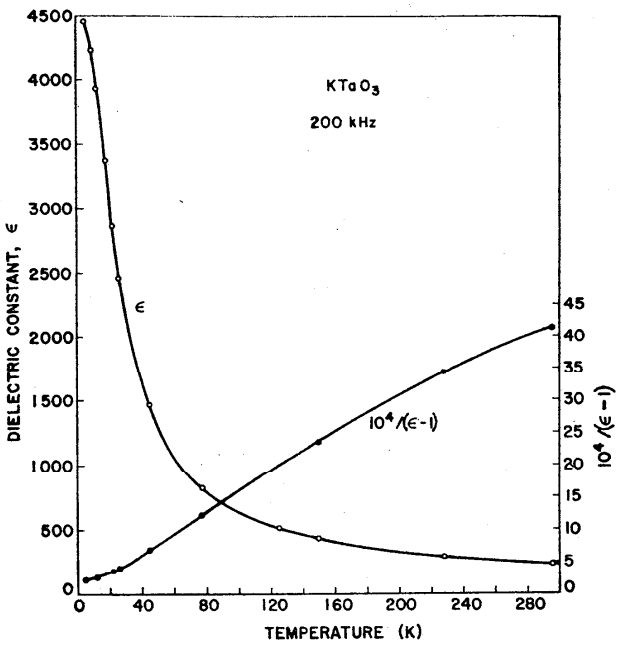

FIGURE 46. $KTaO_3$. Temperature dependence of the dielectric constant of $KTaO_3$ measured at 200 kHz by Wemple [201].

Remarks—This compound, like $SrTiO_3$, is not ferroelectric at any temperature. No phase transitions have been observed for this material. The pressure dependence is shown in fig. 28. $\epsilon = 48 + C/(T-4)$ where $C = 5.7 \times 10^4$.

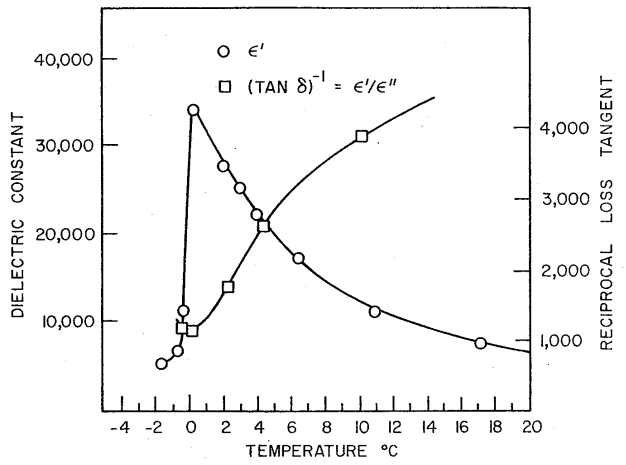

FIGURE 47. $KTa_{0.66}Nb_{0.34}O_3$ (KTN). Temperature dependence of the dielectric constant and the reciprocal of the dielectric loss tangent of KTN measured at 10 kHz by Chen [38].

Remarks—The most useful composition of $KTa_xNb_{1-x}O_3$ (KTN) for electro-optical purposes is $x = 0.66$. This compound has a Curie temperature $T_c \sim 271$ K. Two other transitions occur at ~ 220 K and ~ 170 K. For the pressure dependence of the dielectric constant see fig. 28. $\epsilon = C/(T-271)$ where $C = 1.45 \times 10^5$.

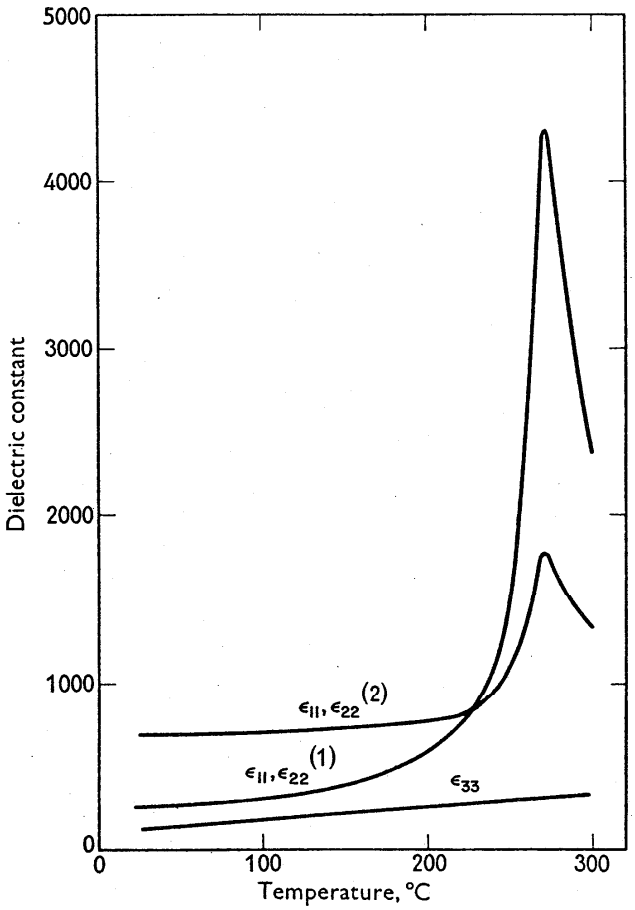

FIGURE 48. $PbTa_2O_6$. Temperature dependences of the dielectric constants ϵ_{11}, ϵ_{33} of $PbTa_2O_6$ measured by Subbarao [182].

Remarks—This material follows a Curie-Weiss law $\epsilon = C/(T-T_0)$ where $C = 1.5 \times 10^5$ and $T_0 = 533$ K.

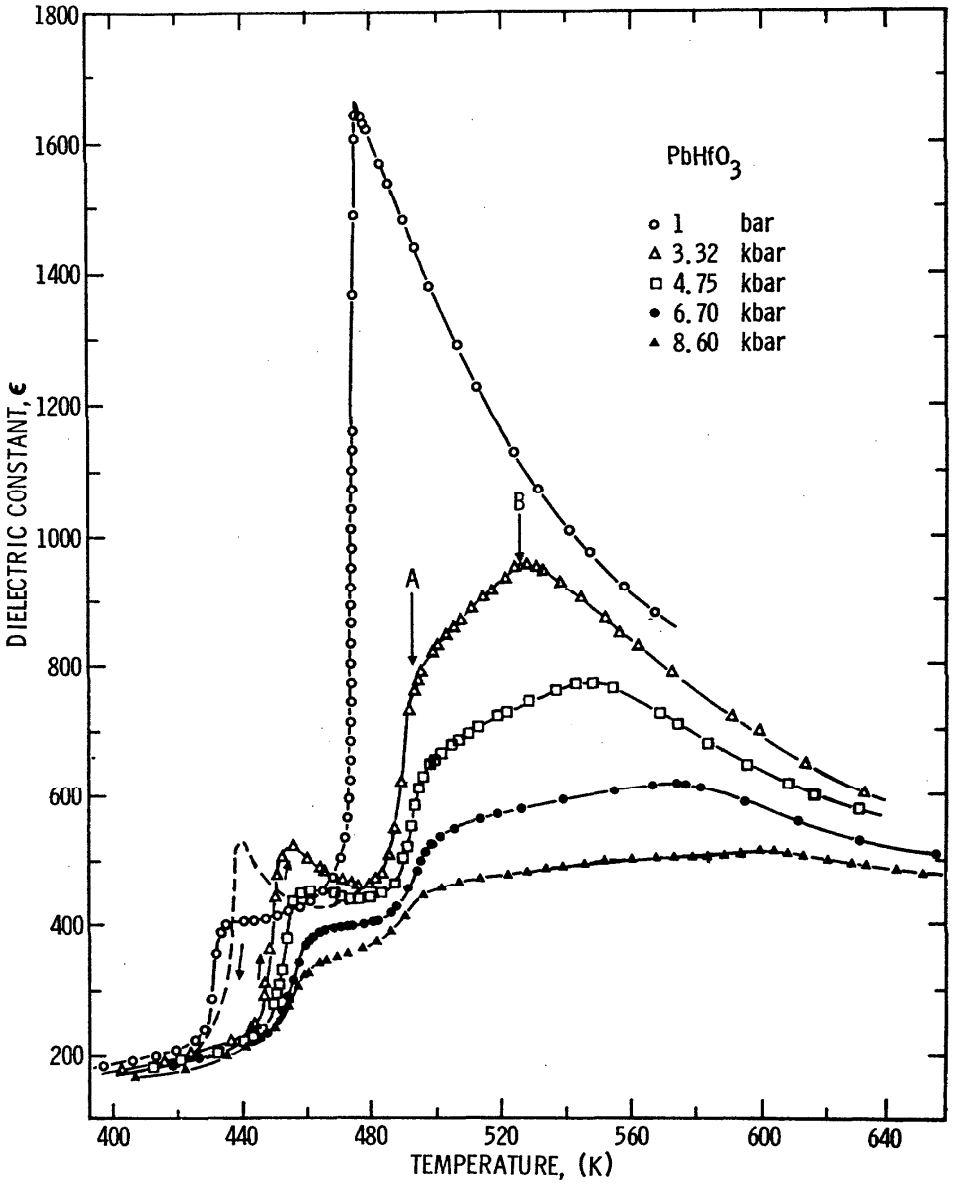

FIGURE 49. $PbHfO_3$. Temperature dependence of the dielectric constants of $PbHfO_3$ measured at different pressures by Samara [164].

Remarks—$PbHfO_3$ follows a Curie-Weiss $\epsilon = C/(T - T_0)$ law above 476 K where $C = 1.65 \times 10^5$ K and $T_0 = 378$ K according to Samara [164].

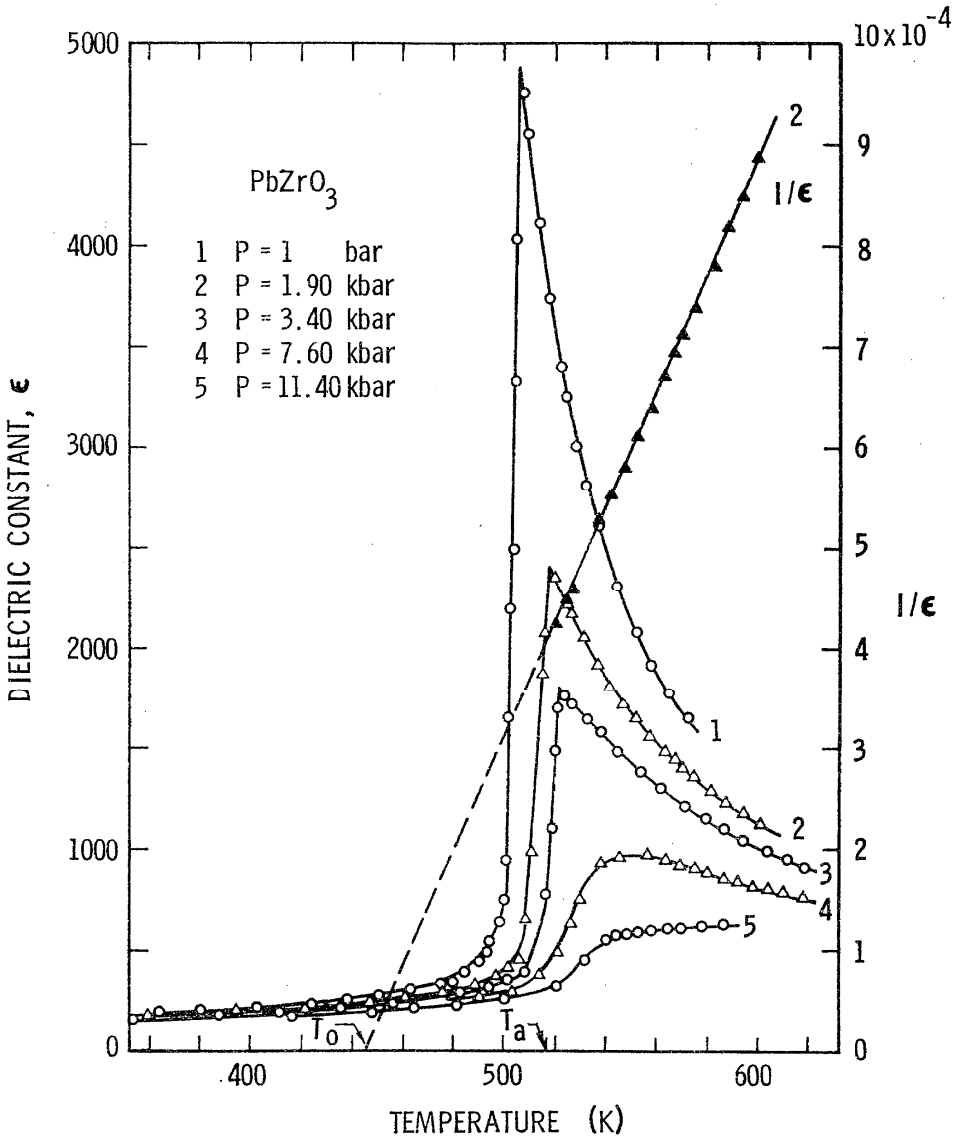

FIGURE 50. $PbZrO_3$. Temperature dependence of the dielectric constant of $PbZrO_3$ at different pressures measured by Samara [164].

Remarks—$PbZrO_3$ is antiferroelectric with $T_c = 503$ K and a Curie-Weiss law $\epsilon = C/(T - T_0$ where $C = 1.60 \times 10^5$ and $T_0 = 475$ K according to Samara [164].

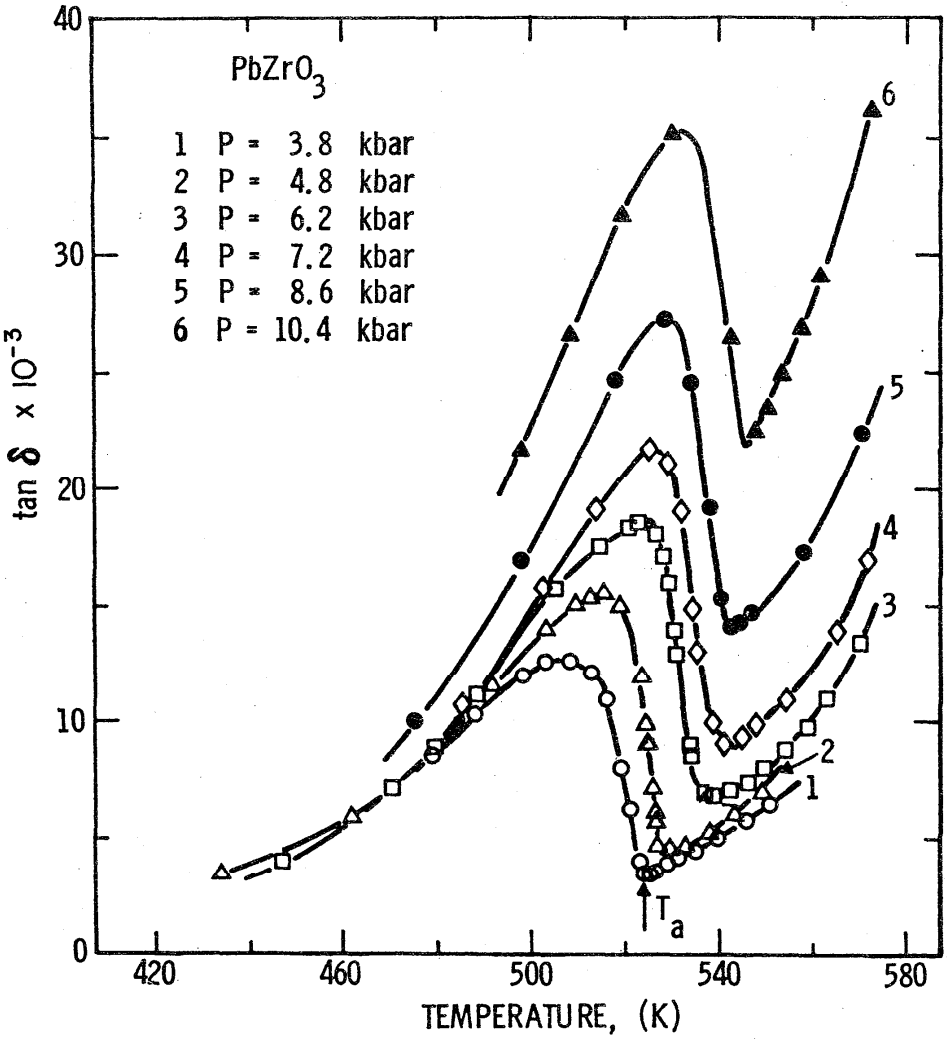

FIGURE 51. $PbZrO_3$. Temperature dependence of the dielectric loss tangent of $PbZrO_3$ at different pressures measured by Samara [164].

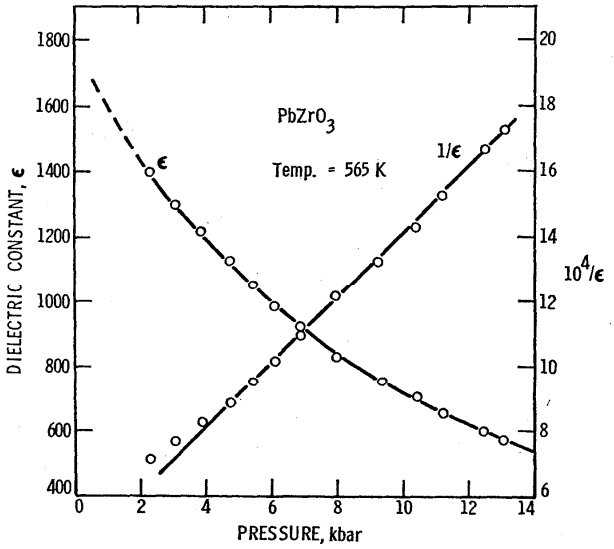

FIGURE 52. $PbZrO_3$. Pressure dependence of the dielectric constant of $PbZrO_3$ measured at 565 K by Samara [164].

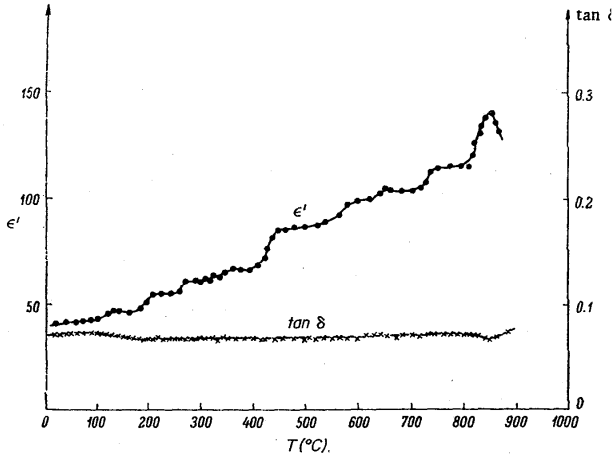

FIGURE 53. $BiFeO_3$. Temperature dependences of the dielectric constant, ϵ', and the dielectric loss tangent, tan δ, of $BiFeO_3$ measured at 9.4×10^9 Hz by Krainik [108].

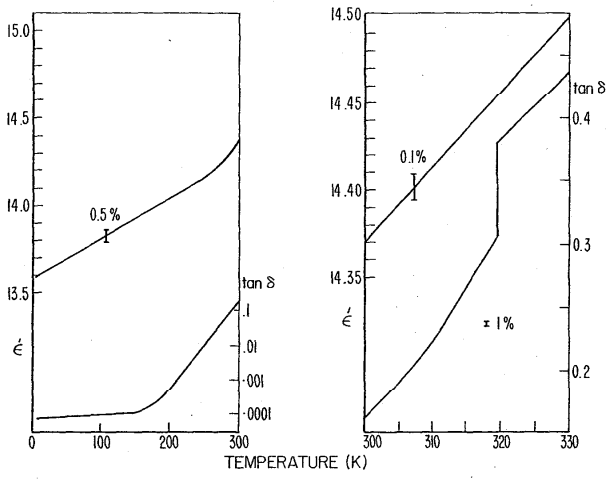

FIGURES 54 and 55. $CsPbCl_3$. Temperature dependences of the dielectric constant ϵ' and the dielectric loss tangent, tan δ, measured by Cohen, et al. [40].

3.5. Nitrates and Nitrites

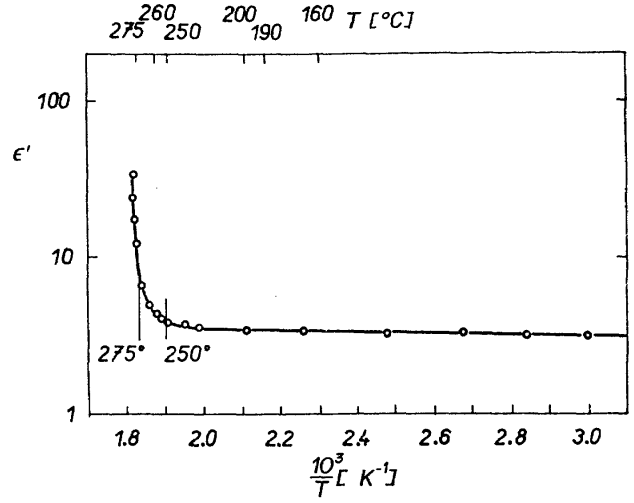

FIGURE 56. $NaNO_3$. Reciprocal temperature dependence of the dielectric constant of $NaNO_3$ measured by Mariani, et al. [121].

Remarks—The Curie temperature $T_c = 548$ K.

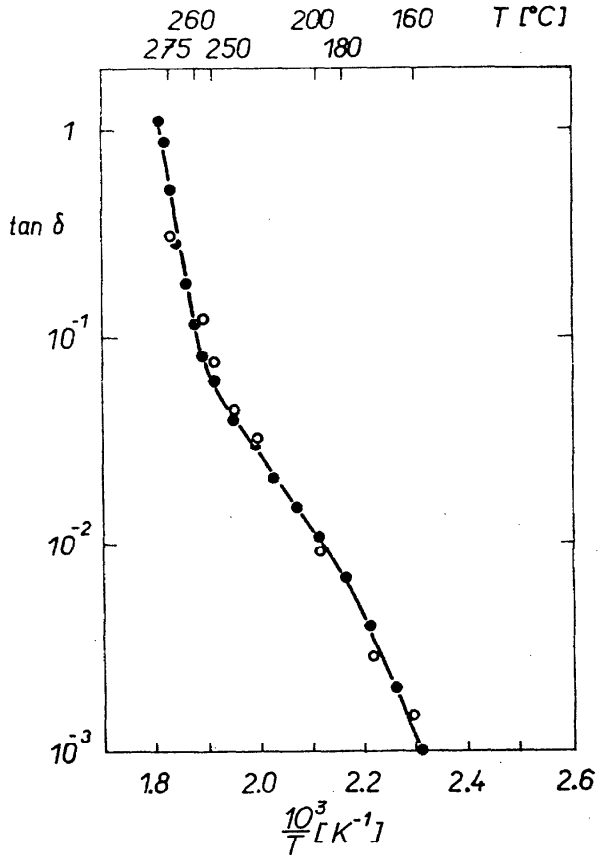

FIGURE 57. $NaNO_3$. Reciprocal temperature dependence of the dielectric loss tangent of $NaNO_3$ measured by Mariani, et al. [121].

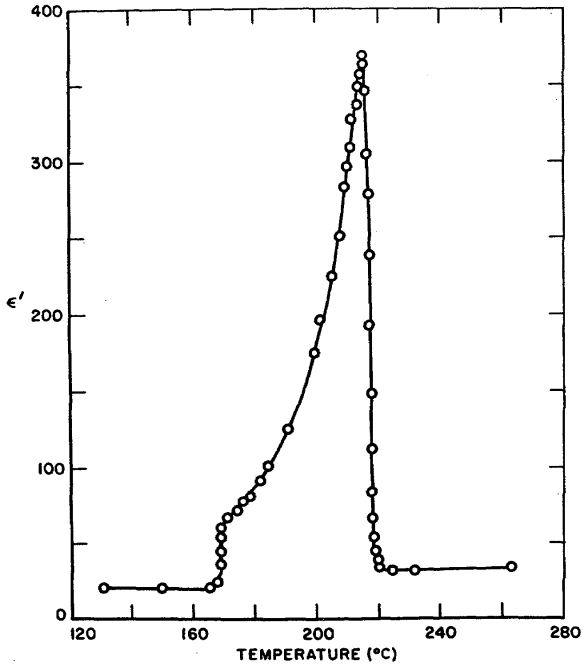

FIGURE 58. $RbNO_3$. Temperature dependence of the dielectric constant of $RbNO_3$ measured at 10^6 Hz by Dantsiger, et al. [46].

Remarks—$RbNO_3$ has two transformations, one at $T_{t1} = 487$ K and the other at $T_{t2} = 437$ K.

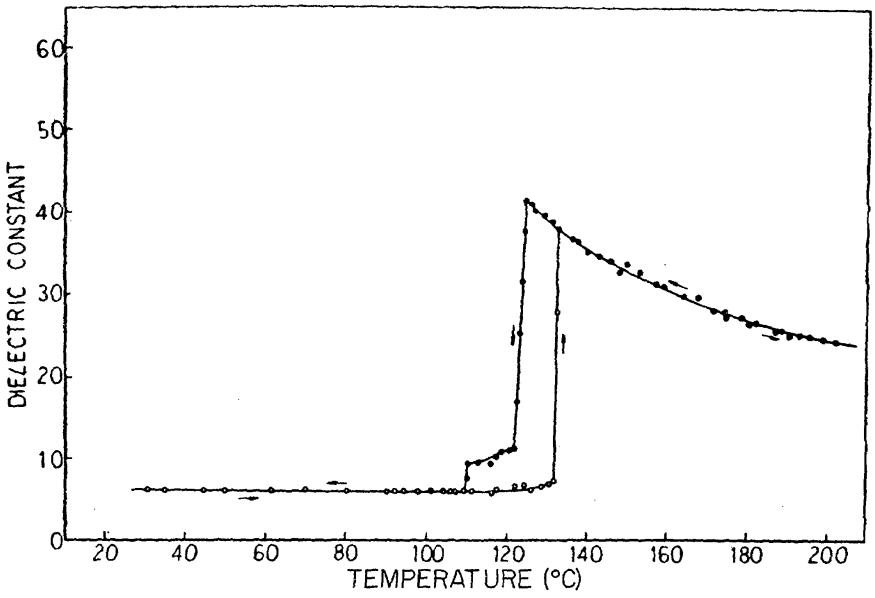

FIGURE 59. KNO_3. Temperature dependence of the dielectric constant of KNO_3 measured at 1043 Hz by Sawada, et al. [166].

Remarks—KNO_3 has a Curie temperature $T_c = 397$ K and follows a Curie-Weiss law $\epsilon = C/(T - T_0)$ where $C = 4.3 \times 10^3$ and $T_0 = 293$ K. The pressure dependence of the spontaneous polarization was measured by Midorikawa, et al. [126] up to 3 kbar at 403 K. The Curie temperature, T_c, shifts to higher temperatures according to T_c (K) = 396.3 K + 19.8 p, where p is expressed in kbars.

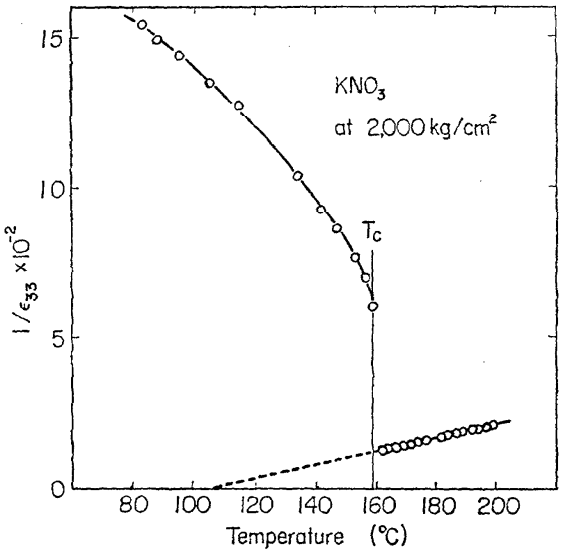

FIGURE 60. KNO_3. Temperature dependence of the dielectric constant of KNO_3 under hydrostatic pressure of 2 kbar measured by Midorikawa [126].

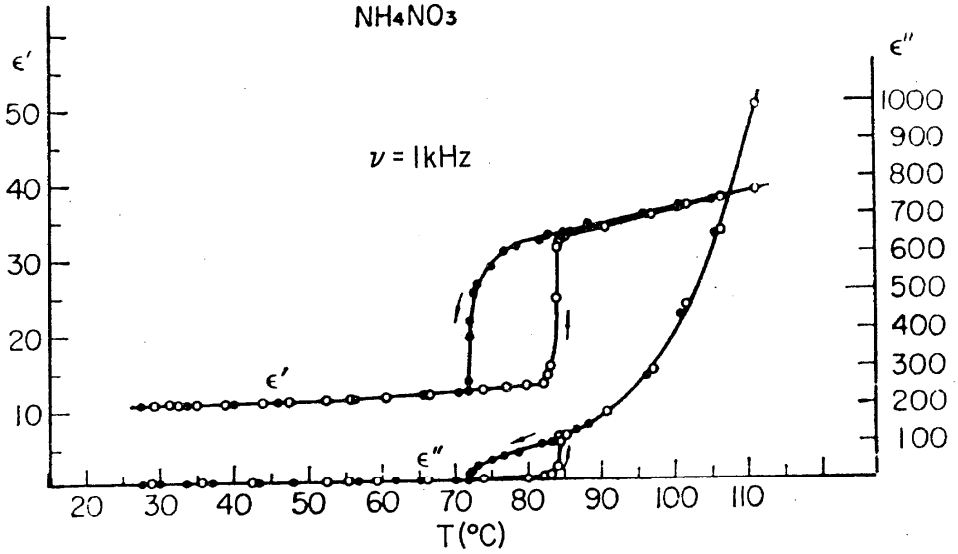

FIGURE 61. NH_4NO_3. Temperature dependences of the real and imaginary parts of the dielectric constant of NH_4NO_3 pressed powder sample measured by Yamashita, et al. [210].

Remarks—NH_4NO_3 undergoes four phase transformations:

Temperature	from	to
$T_{c_1} = 398.4$	cubic	tetragonal
$T_{c_2} = 357.4$	tetragonal	orthorhombic
$T_{c_3} = 305.5$	orthorhombic	orthorhombic
$T_{c_4} = 255.2$	orthorhombic	hexagonal

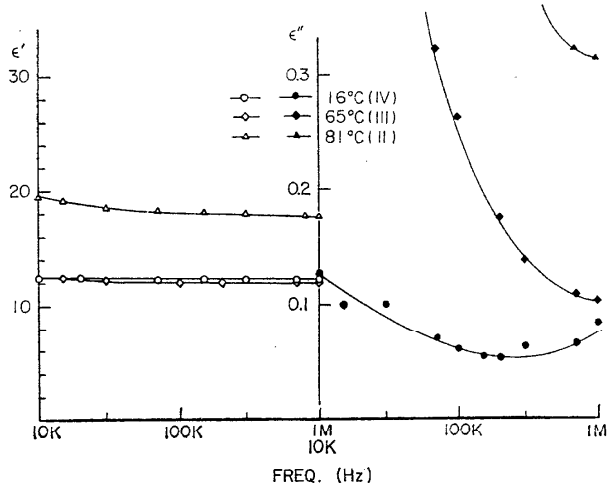

FIGURE 62. NH_4NO_3. Frequency dependences of the real and imaginary parts of the dielectric constant ϵ', ϵ'' of NH_4NO_3 pressed powder sample measured at different temperatures by Yamashita, et al. [210].

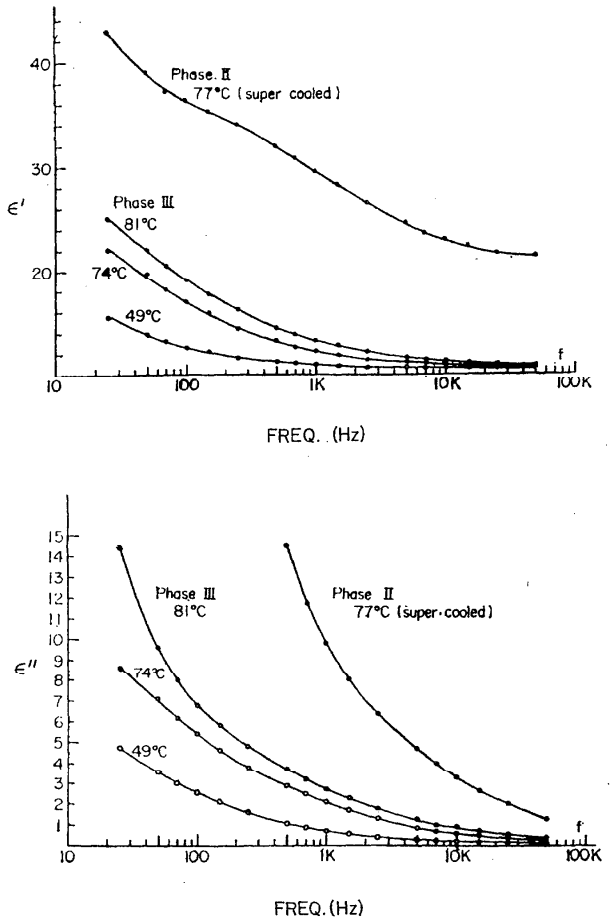

FIGURE 63. NH_4NO_3. Frequency dependences of the real and imaginary parts of the dielectric constant ϵ', ϵ'' of NH_4NO_3 pressed powder sample measured at different temperatures by Yamashita, et al. [210].

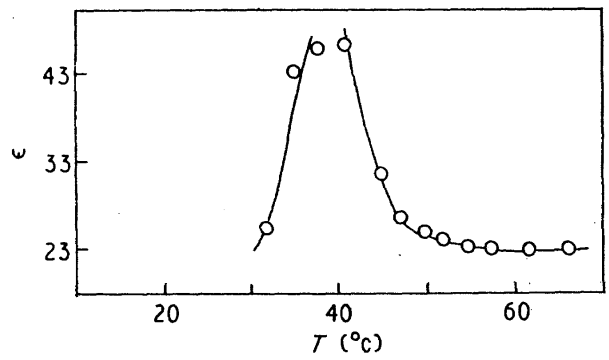

FIGURE 64. KNO_2. Temperature dependence of the dielectric constant of KNO_2 measured by Rao [149].

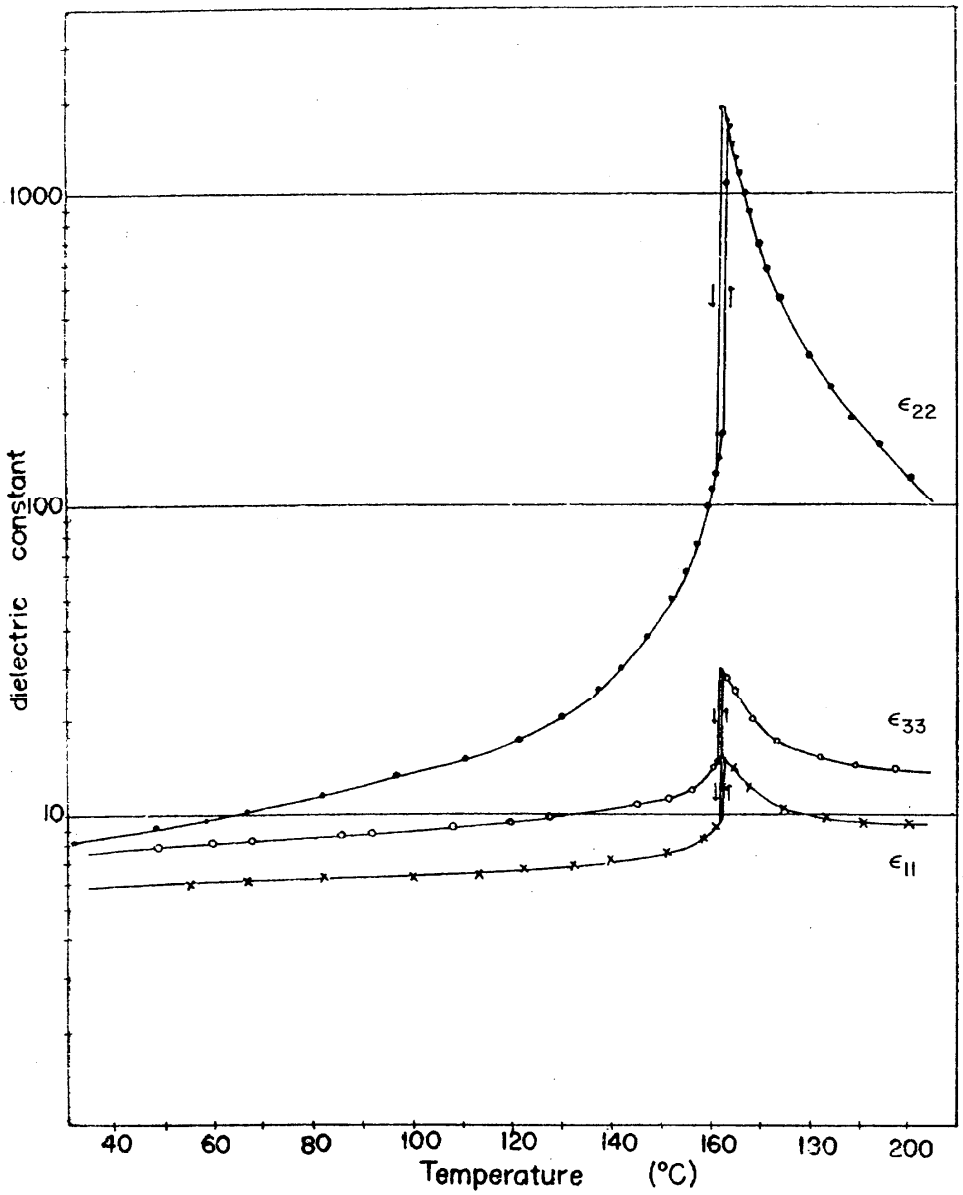

FIGURE 65. $NaNO_2$. Temperature dependences of the dielectric constants ϵ_{11}, ϵ_{22}, ϵ_{33} of $NaNO_2$ measured at 100 kHz by Nomura [134].

Remarks—$NaNO_2$ has a Curie temperature $T_c = 437.4$ K for temperatures greater than T_c, $\epsilon_{22} = C/(T - T_0)$ where $C = 5.13 \times 10^3$ and $T_0 = 437.4$ K.

3.6. Chlorates, Bromates, and Iodates

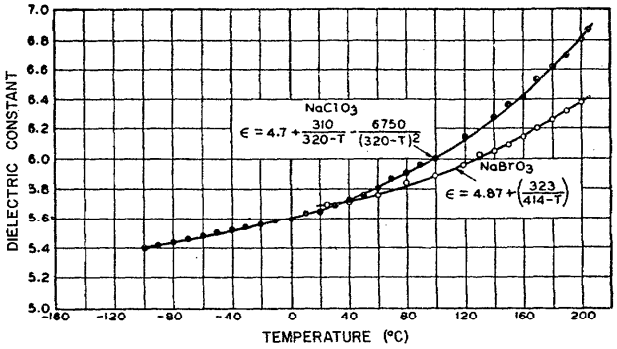

FIGURE 66. $NaBrO_3$, $NaClO_3$. Temperature dependences of the dielectric constants of $NaBrO_3$ and $NaClO_3$ measured by Mason [123].

Remarks—The temperature dependence of the dielectric constant of $NaBrO_3$ is $\epsilon = 4.87 + \frac{323}{414 - T}$ and for $NaClO_3$ is $\epsilon = 4.7 + \frac{310}{320 - T} - \frac{6750}{(32 - T)^2}$

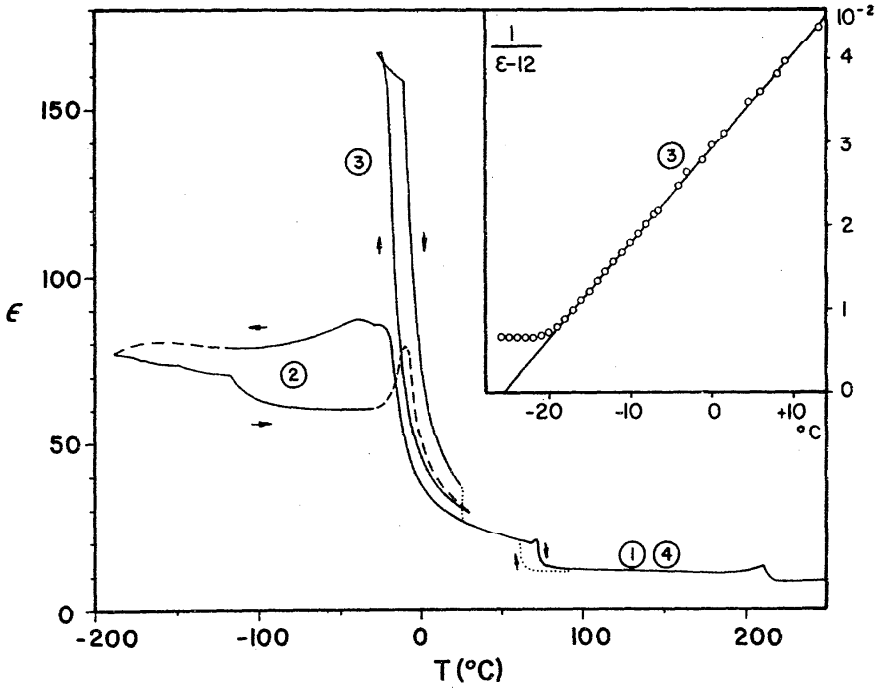

FIGURE 67. KIO_3. Temperature dependence of the dielectric constant of KIO_3 measured at 10 kHz by Herlach [79].

Curves 1 and 4 are repeatable while 2 and 3 are history dependent except that 3 always follows a Curie-Weiss law.

Remarks—This material has four transitions:

$T_{c_1} = 485$ K
$T_{c_2} = 343$ K
$T_{c_3} = 257$–263 K
$T_{c_4} = 83$ K

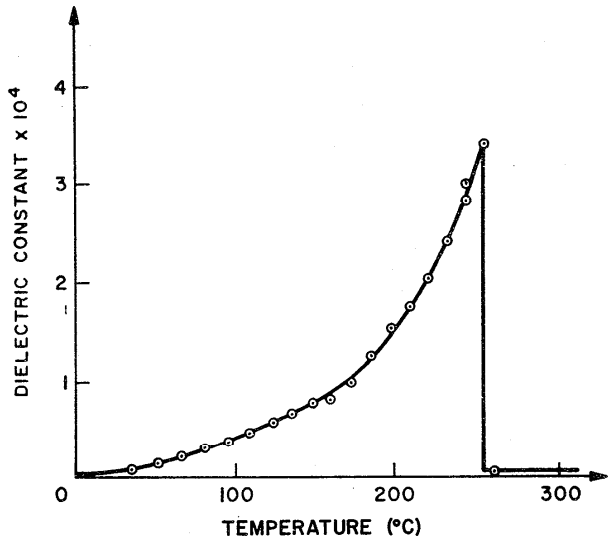

FIGURE 68. $LiIO_3$. Temperature dependence of the dielectric constant of $LiIO_3$ measured by Nash [130].

Remarks—The Curie temperature $T_c = 529$ K for $LiIO_3$.

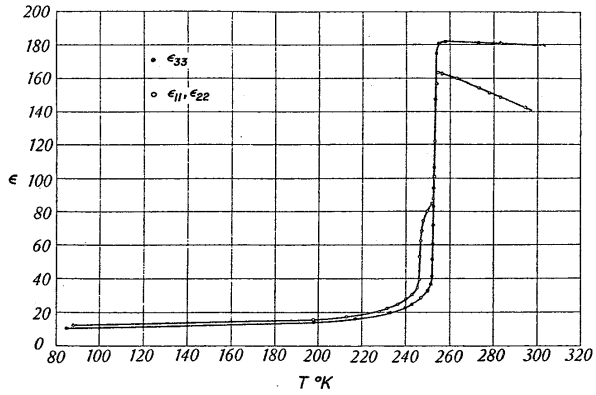

FIGURE 69. $(NH_4)_2H_3IO_6$. Temperature dependence of the dielectric constant of $(NH_4)_2H_3IO_6$ measured by Bärtschi [16].

3.7. Sulfates, Selenates, Beryllates and Selenites.

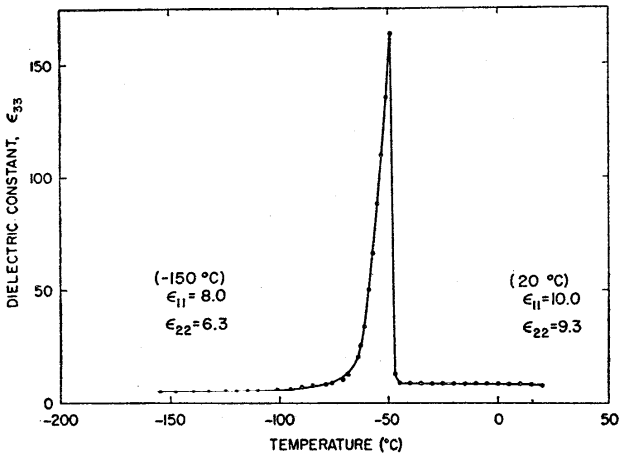

FIGURE 70. $(NH_4)_2SO_4$. Temperature dependence of the dielectric constant ϵ_{33} of $(NH_4)_2SO_4$ measured by Hoshino, et al. [84].

Remarks—The measured Curie temperature is 224 K.

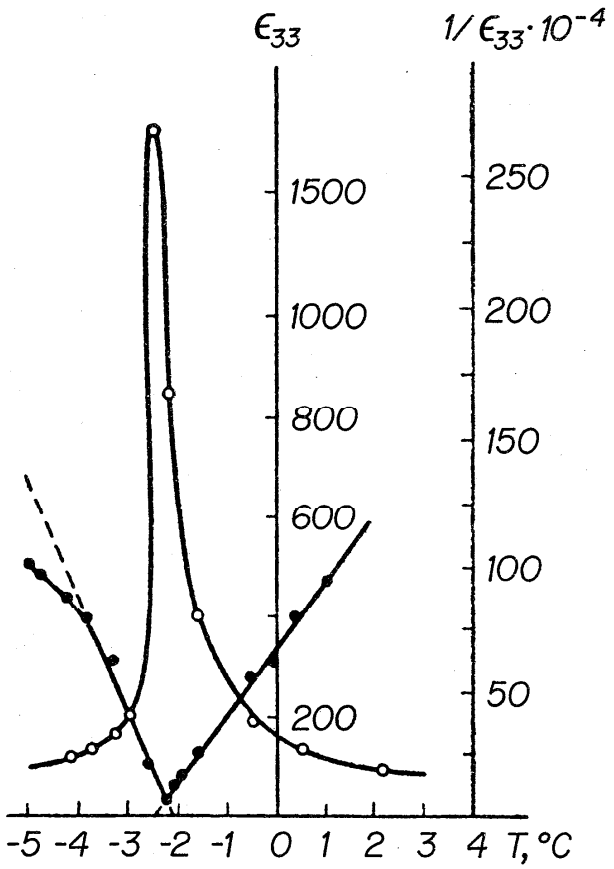

FIGURE 71. NH_4HSO_4. Temperature dependence of the dielectric constant of NH_4HSO_4 measured by Strukov, et al. [181].

Remarks—The measured Curie temperature is 270.8 K.

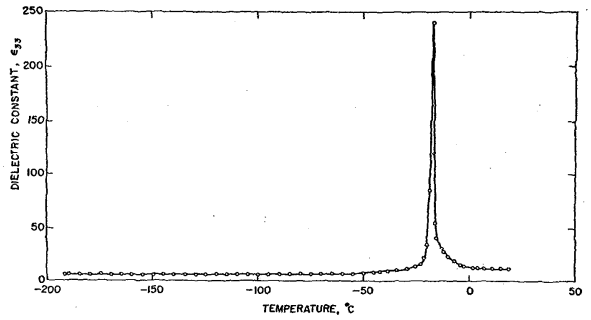

FIGURE 72. $RbHSO_4$. Temperature dependence of the dielectric constant of $RbHSO_4$ measured by Pepinsky [145].

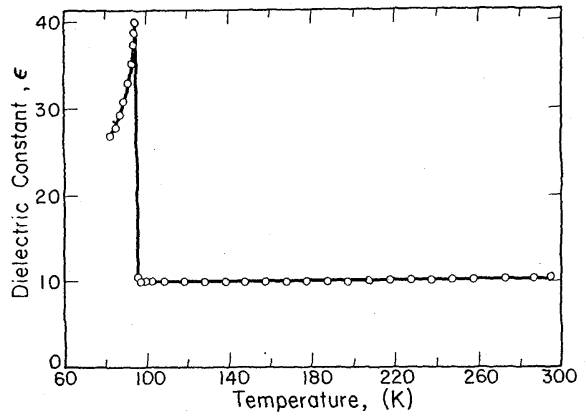

FIGURE 73. $(NH_4)_2Cd_2(SO_4)_3$. Temperature dependence of the dielectric constant of $(NH_4)_2Cd_2(SO_4)_3$ measured by Eastman, et al. [50].

Remarks—The Curie temperature is 95 K.

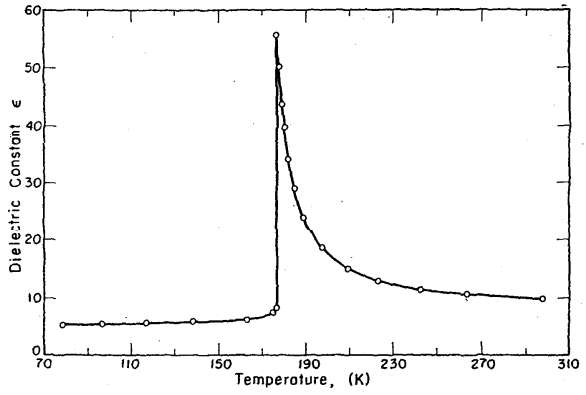

FIGURE 74. $CH_3NH_3Al(SO_4)\cdot 12H_2O$, (MASD). Temperature dependence of the dielectric constant of MASD measured by Pepinsky, et al. [144].

Remarks—The Curie temperature of methylamine aluminum alum (MASD), $CH_3NH_3Al(SO_4)_2\cdot 12H_2O$, is 177 K.

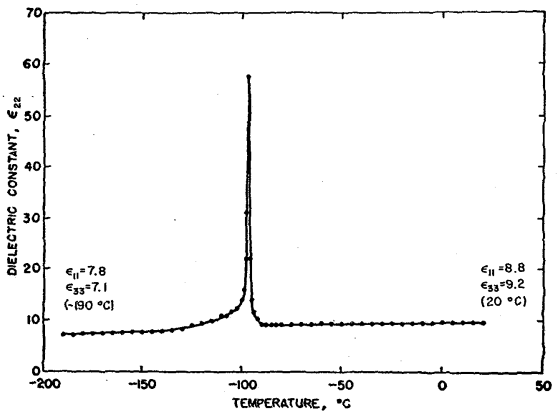

FIGURE 75. $(NH_4)_2BeF_4$. The temperature dependence of the dielectric constant of $(NH_4)_2BeF_4$ measured by Hoshino, et al. [95].

Remarks—The Curie temperature of $(NH_4)_2BeF_4$ is 176 K.

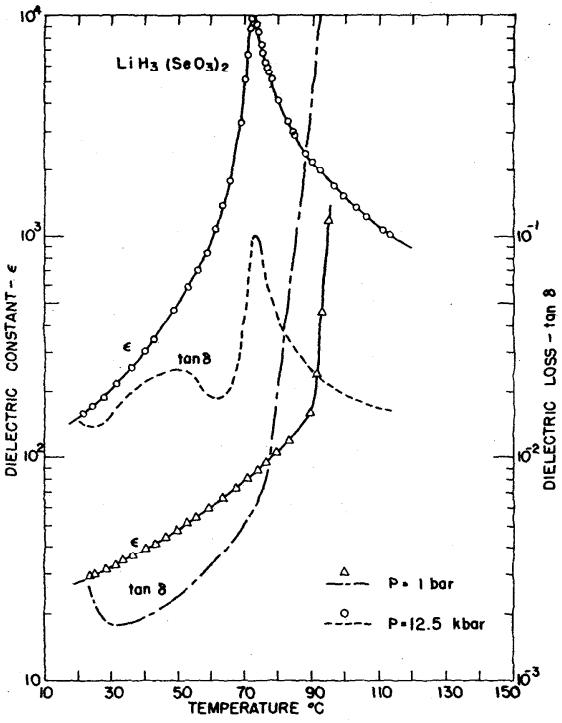

FIGURE 76. $LiH_3(SeO_3)_2$. Temperature dependence of the dielectric constant and dielectric loss tangent for $LiH_3(SeO_3)_2$ measured at atmospheric pressure and at 12.5 kbar by Samara [161].

Remarks—Both $LiH_3(SeO_3)_2$ and $LiD_3(SeO_3)_2$ remain ferroelectric up to their melting points. Under hydrostatic pressure of 12.5 kbar the ferroelectric transition occurs at 342.5 K in both compounds according to Samara [161].

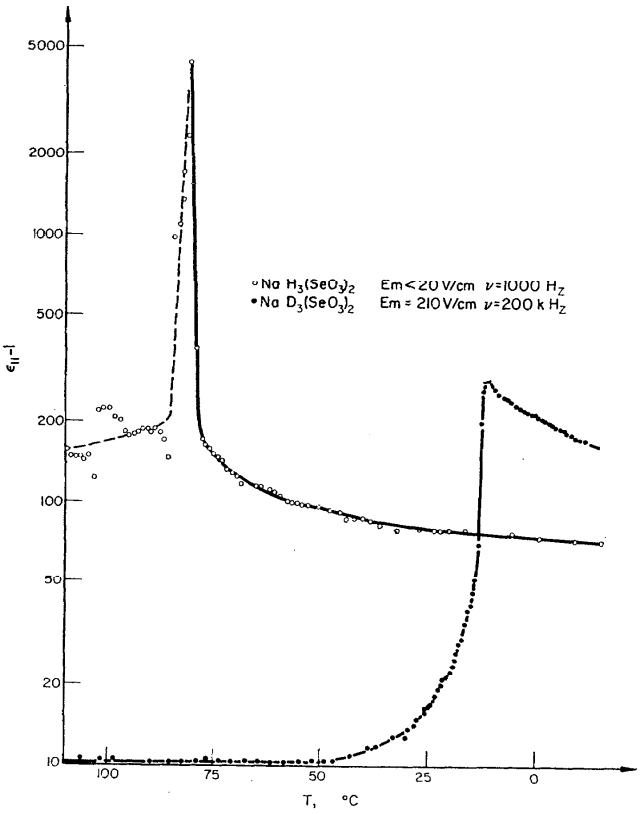

FIGURE 77. $NaH_3(SeO_3)_2$, $NaD_3(SeO_3)_2$. Temperature dependence of the dielectric constant, ϵ_{11}, of $NaH_3(SeO_3)_2$ and $NaD_3(SeO_3)_2$ measured by Blinc [22].

Remarks—Sodium trihydrogen selenite has a Curie temperature $T_c = 193 \pm 2$ K and follows a Curie-Weiss law $\epsilon = C/(T - T_0)$ where $C = (4.6 \pm 0.5) \times 10^2$, $T_0 = 192 \pm 2$ K reported by Pepinsky, et al. [144].

Sodium trideuterium selenite has a $T_c = 270.65 \pm 1$ K with $\epsilon = C/(T - T_0)$ where $C = (7 \pm 1) \times 10^3$ and $T_0 = 245 \pm 5$ K measured by Blinc [22].

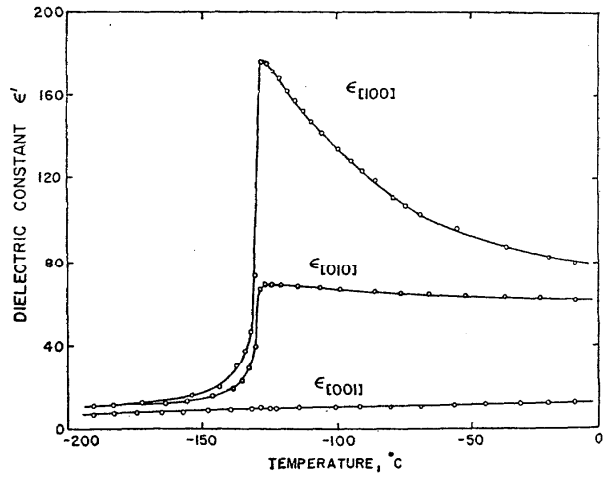

FIGURE 78. $CsH_3(SeO_3)_2$. Temperature dependences of the dielectric constants, ϵ_{100}, ϵ_{010}, ϵ_{001}, of $CsH_3(SeO_3)_2$ measured by Makita [119].

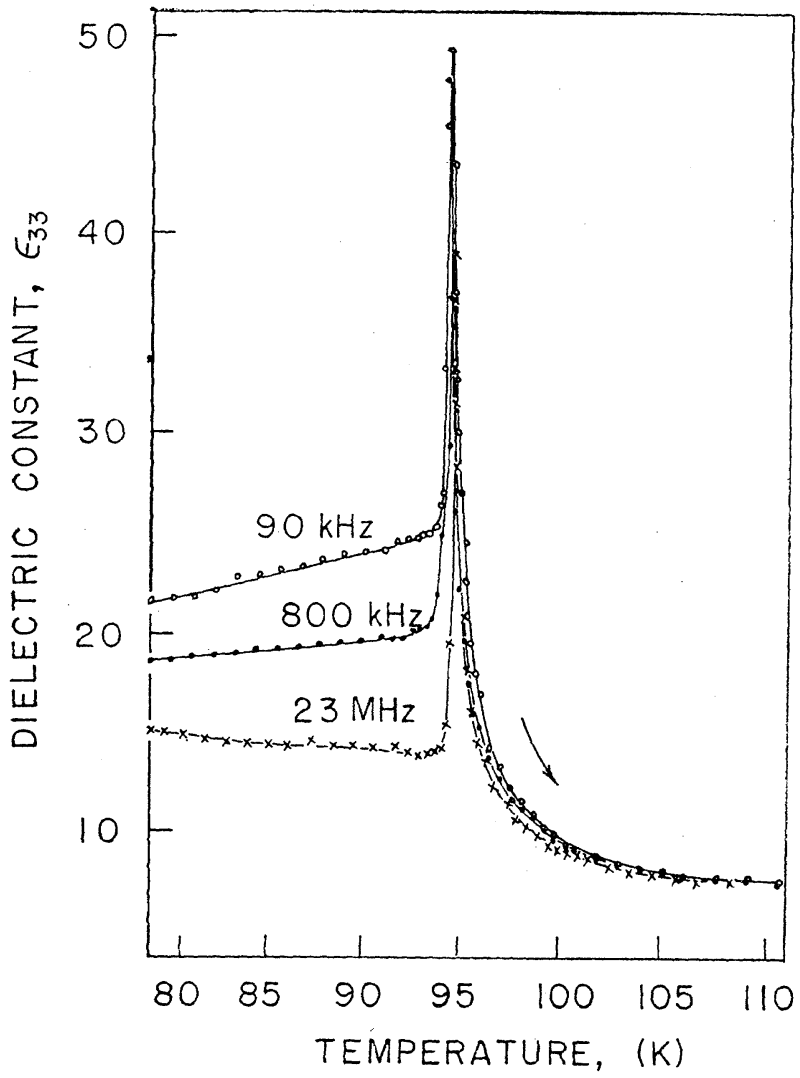

FIGURE 79. K_2SeO_4. Temperature dependence of the dielectric constant of K_2SeO_4 at different frequencies measured by Aiki [4].

Remarks—This material follows a Curie-Weiss law $\epsilon = \epsilon' + C/(T - T_c)$ above $T_c = 93.0$ K for warming and $T_c = 92.3$ K for cooling; where $\epsilon' = 6.14$, and $C = 27$ K for warming and 30 K for cooling.

3.8. Miscellaneous Ferroelectrics and Piezoelectrics

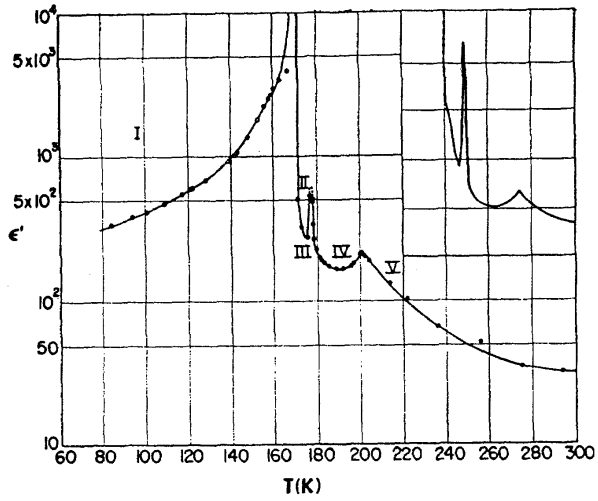

FIGURE 80. $SC(NH_2)_2$(Thiourea). Temperature dependence of the dielectric constant of $SC(NH_2)_2$ measured by Goldsmith, et al. [66]. The inset shows the detail of the temperature range 160 K to 220 K.

Remarks—Thiourea, $SC(NH_2)_2$ undergoes ferroelectric transitions at 169 K, 176 K, 180 K, 202 K. The dielectric constant perpendicular to the ferroelectric axis is temperature independent and approximately equal to 3.

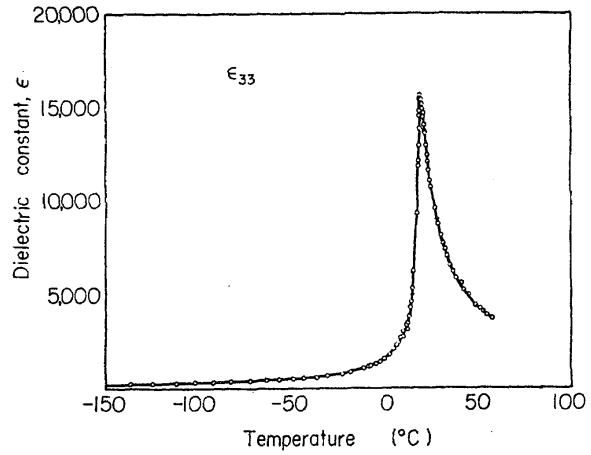

FIGURE 81. SbSI. Temperature dependence of the dielectric constant of SbSI measured by Hamano, et al. [74].

Remarks—The Curie temperature is 294 K for SbSI.

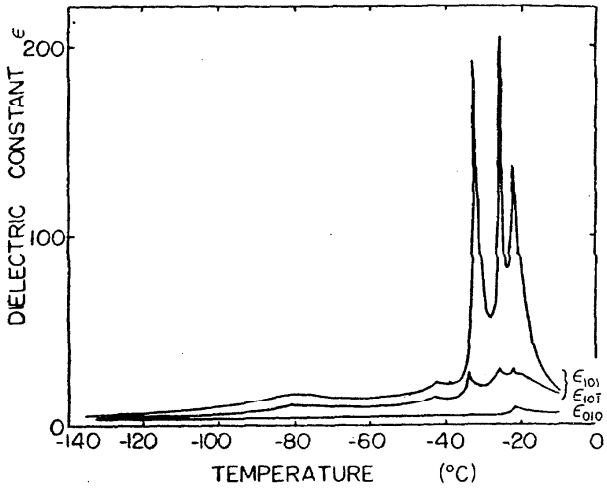

FIGURE 82. $K_4Fe(CN)_6 \cdot 3H_2O$ (potassium ferrocyanide). Temperature dependence of the dielectric constant of potassium ferrocyanide measured by Waku, et al. [193].

Remarks—This crystal is monoclinic (pseudotetragonal). It has several phase transformations which are shown as anomalies in the dielectric constant in fig. 82. A Curie temperature $T_c = 248.5$ K was measured by Waku, et al. [193] and $T_c = 251$ K was reported by Jona, et al. [92].

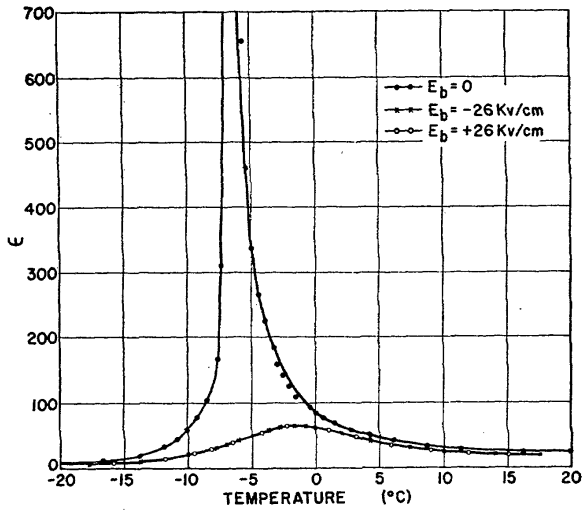

FIGURE 83. $CaB_3O_4(OH)_3 \cdot H_2O$ (colemanite). Temperature dependence of the dielectric constant of colemanite measured by Wieder, et al. [204].

Remarks—The Curie temperature of colemanite, $CaB_3O_4(OH)_3 \cdot H_2O$ is 266 K.

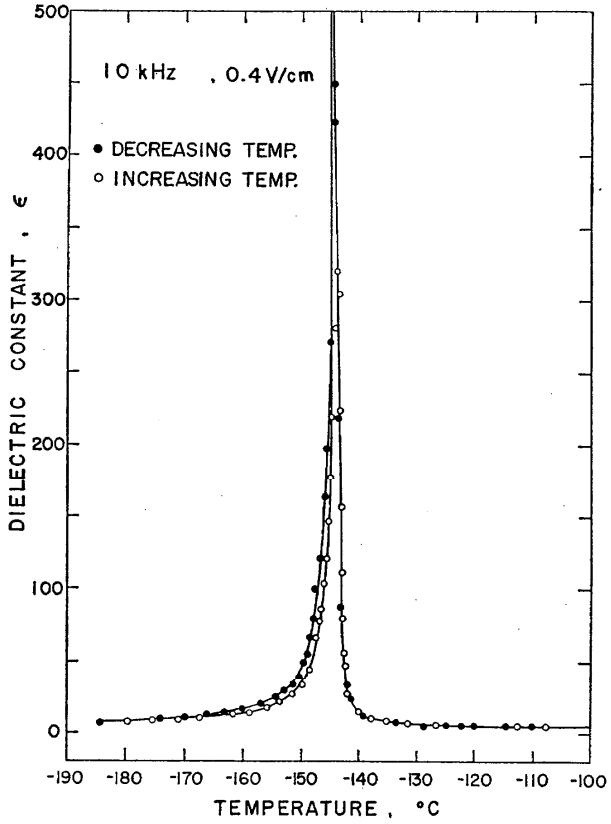

FIGURE 84. $HNH_4(ClCH_2COO)_2$. Temperature dependence of the dielectric constant of $HNH_4(ClCH_2COO)_2$ measured along the [102] axis by Ichikawa, et al. [87].

Remarks—The Curie temperature is 128 K.

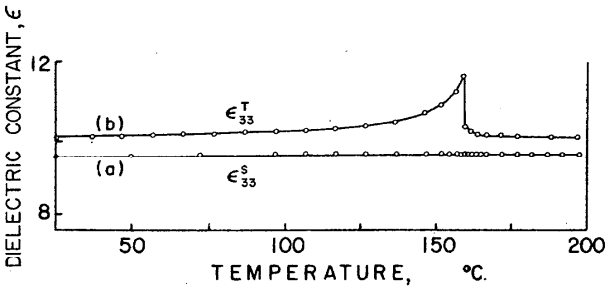

FIGURE 87. $Gd_2(MoO_4)_3$. Temperature dependence of the dielectric constant ϵ_{33} of $Gd_2(MoO_4)_3$ measured by Cross [44] in the clamped condition, ϵ^T, and in the free condition, ϵ^S.

Remarks—The Curie temperature is 432 K.

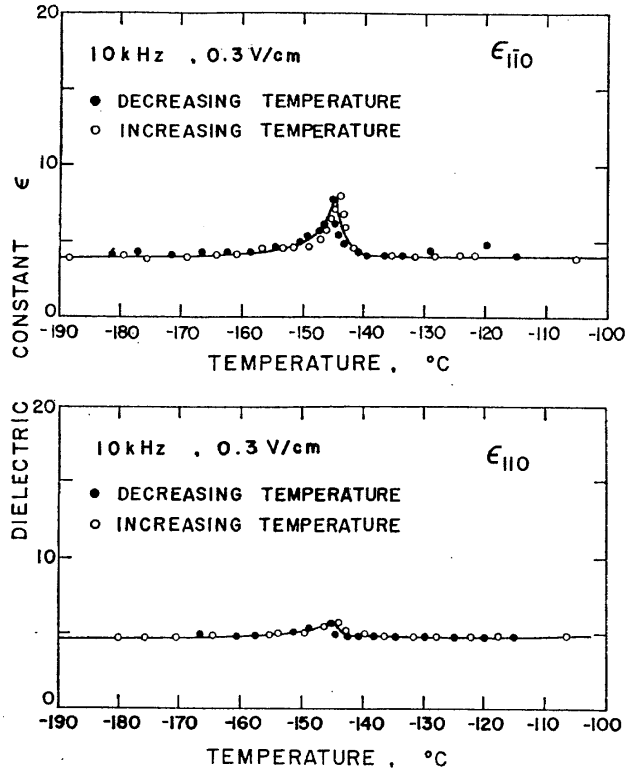

FIGURES 85 and 86. $HNH_4(ClCH_2COO)_2$. Temperature dependence of the dielectric constant of $HNH_4(ClCH_2COO)_2$ along the $[1\bar{1}0]$ axis measured by Ichikawa, et al. [87].

$HNH_4(ClCH_2COO)_2$. Temperature dependence of the dielectric constant of $HNH_4(ClCH_2COO)_2$ along the [110] axis measured by Ichikawa, et al. [87].

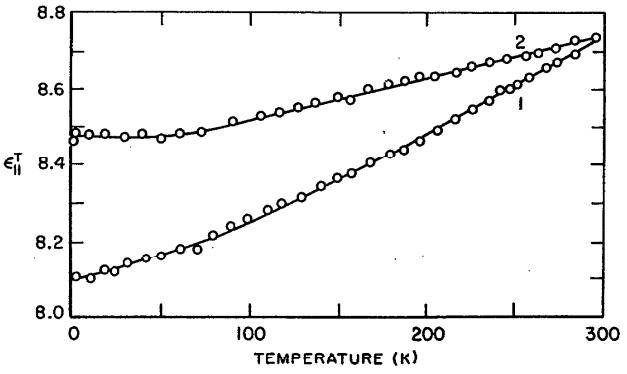

FIGURE 88. ZnS. Temperature dependence of the dielectric constants ϵ_{11} and ϵ_{33} for ZnS measured by Kobayashi, et al. [107].

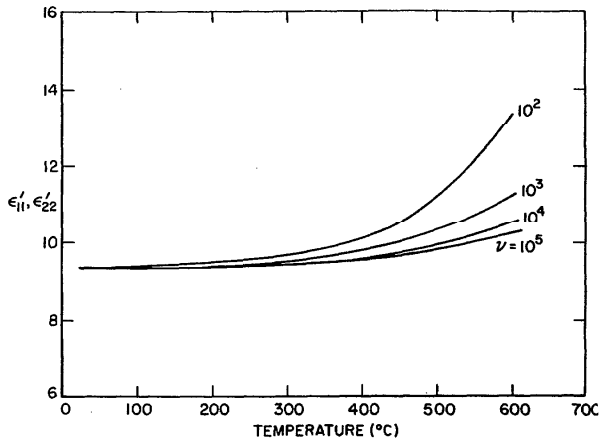

FIGURE 89. Al_2O_3. Temperature dependence of the dielectric constants ϵ'_{11}, ϵ'_{22}, for Al_2O_3 measured by von Hippel, et al. [191].

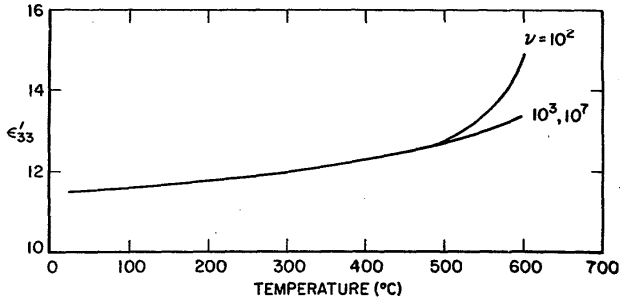

FIGURE 90. Al_2O_3. Temperature dependence of the dielectric constant, ϵ'_{33} for Al_2O_3 measured by von Hippel, et al. [191].

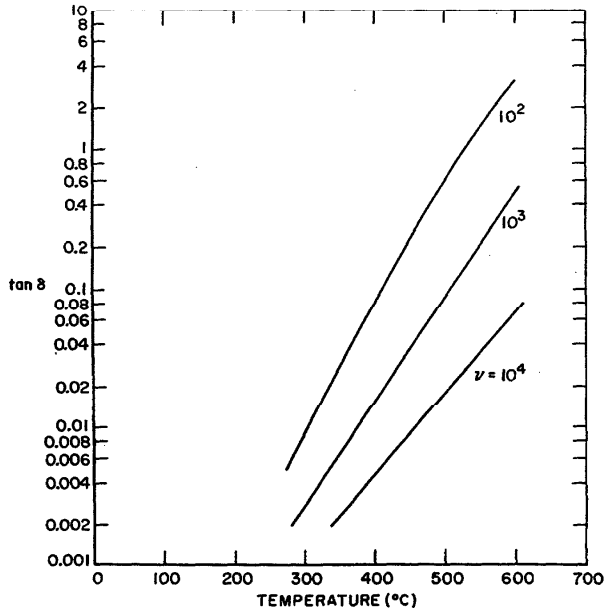

FIGURE 91. Al_2O_3. Temperature dependence of the dielectric loss tangent tan δ_{11} for Al_2O_3 measured by von Hippel, et al. [191] at several frequencies.

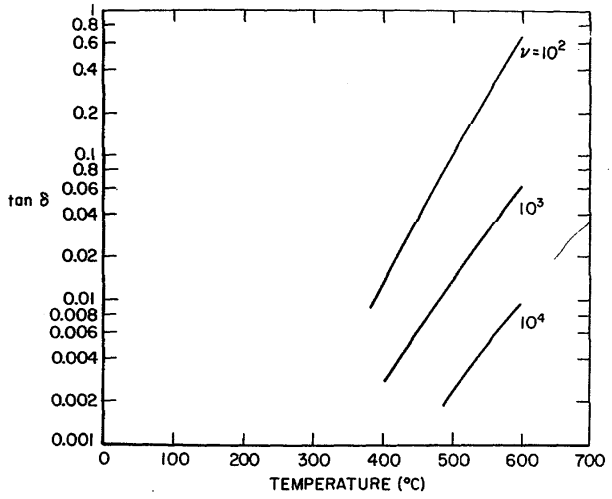

FIGURE 92. Al_2O_3. Temperature dependence of the dielectric loss tangent tan δ_{33} for Al_2O_3 measured by von Hippel, et al. [191] at several frequencies.

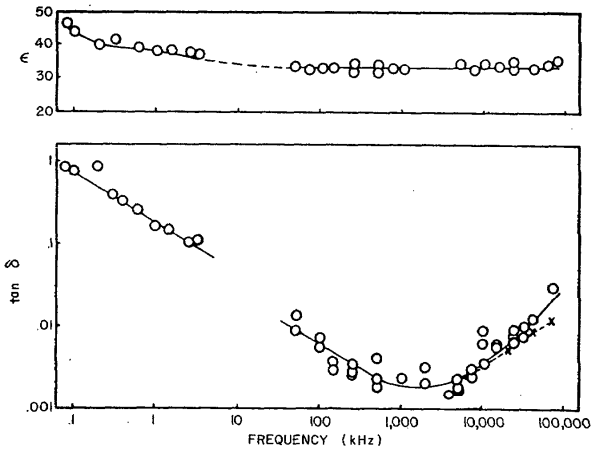

FIGURE 93. BaO (baria). Frequency dependence of dielectric constant and dielectric loss tangent of BaO measured by Bever, et al. [21].

Remarks—Measurements at 248 K, 296 K, and 333 K over the frequency range 60 Hz—3 kHz did not show any temperature dependence of dielectric constant or dielectric loss tangent.

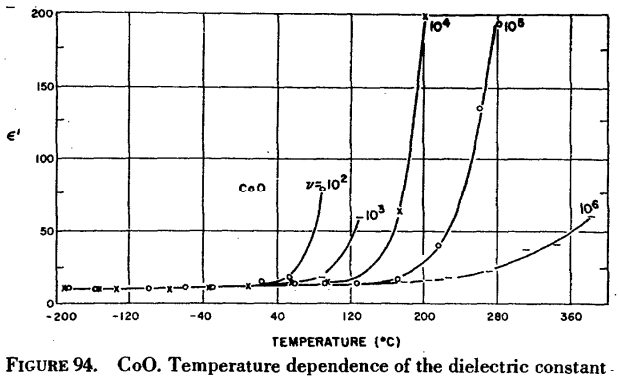

FIGURE 94. CoO. Temperature dependence of the dielectric constant of CoO measured by Rao, et al. [149].

Remarks—Plotting the conductivity (as deduced from the dielectric loss $\epsilon'' : \sigma = \omega\epsilon''\epsilon'$) versus $\frac{1}{T}$ one finds the activation energy for intrinsic conduction to be 0.73 eV for CoO.

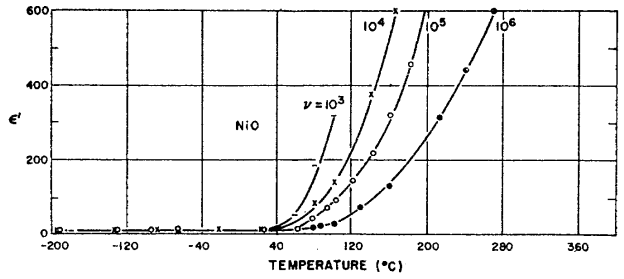

FIGURE 95. NiO. Temperature dependence of the dielectric constant of NiO measured by Rao, et al. [149].

Remarks—Plotting the conductivity (as deduced from the dielectric loss ϵ'' : $\sigma=\omega\epsilon''\epsilon'$) versus $\frac{1}{T}$ one finds the activation energy for intrinsic conduction to be 0.66 eV for NiO.

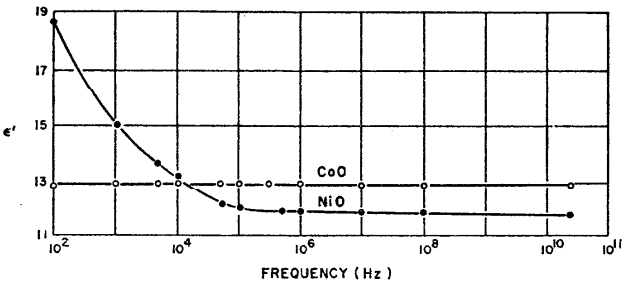

FIGURE 96. CoO, NiO. Frequency dependence of dielectric constant ϵ' of CoO and NiO at 298 K measured by Rao, et al. [149].

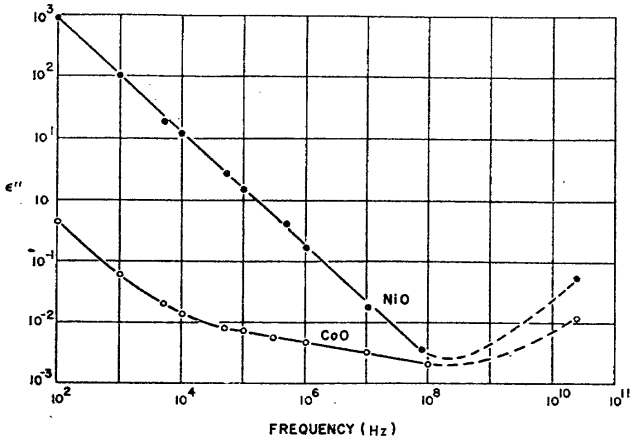

FIGURE 97. CoO. NiO. Frequency dependence of the dielectric loss ϵ'' of CoO and NiO at 298 K measured by Rao, et al. [149].

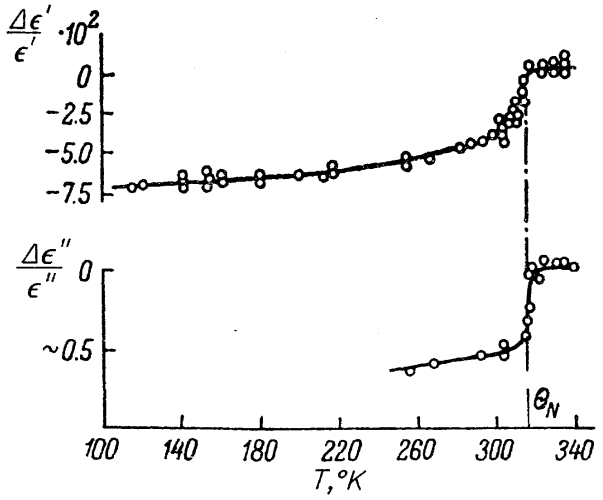

FIGURE 98. Cr_2O_3. Temperature dependence of the percentage change in dielectric constant ϵ and dielectric loss ϵ'' relative to their values at the Néel temperature, θ_N, of Cr_2O_3 measured by Samokhvalov, et al. [165].

Remarks—The absolute value of the dielectric constant at the Néel temperature (θ_N) is 8. The value of the dielectric loss is 0.03–0.05 at θ_N measured at 9.5 GHz.

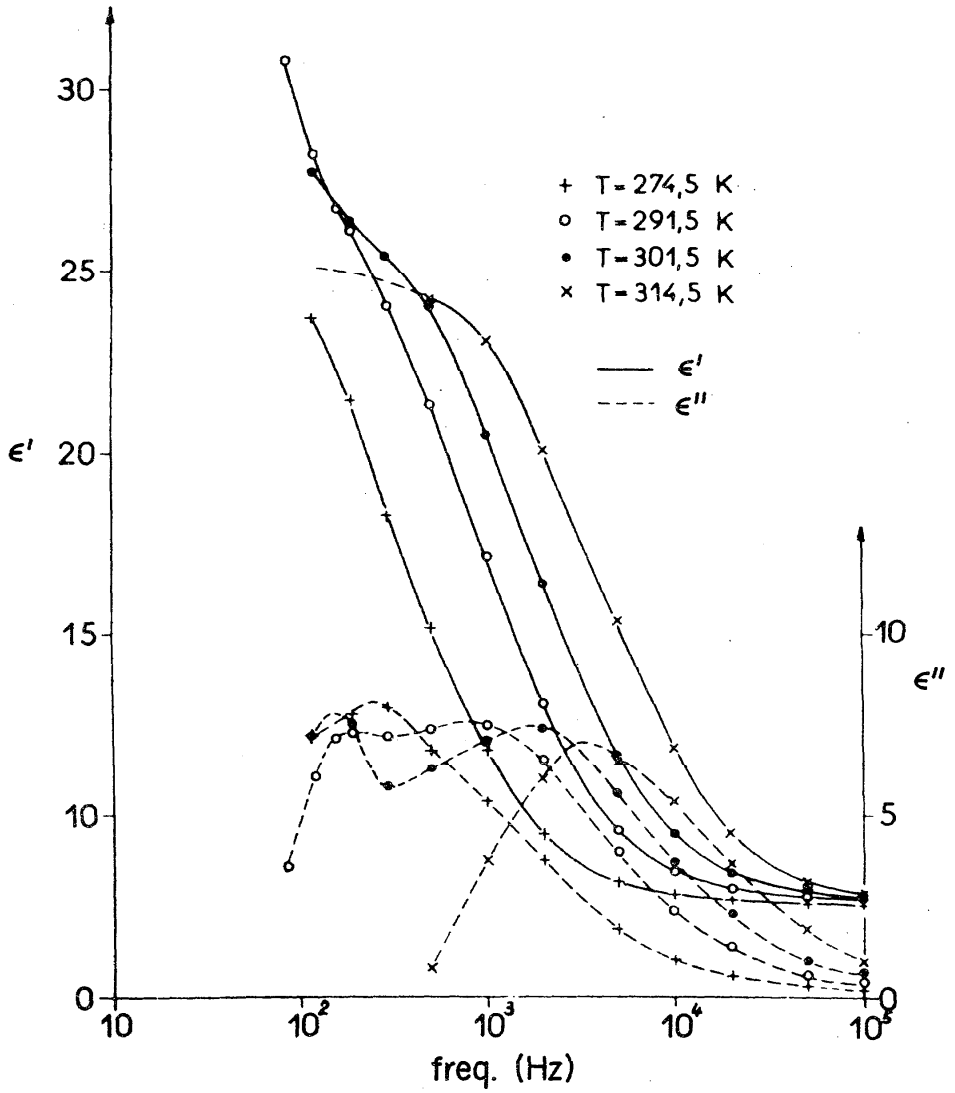

FIGURE 99. Cu_2O (cuprite). Frequency dependence of the real and imaginary parts of the dielectric constant, ϵ' and ϵ'', of Cu_2O measured at four different temperatures by Noguet [133].

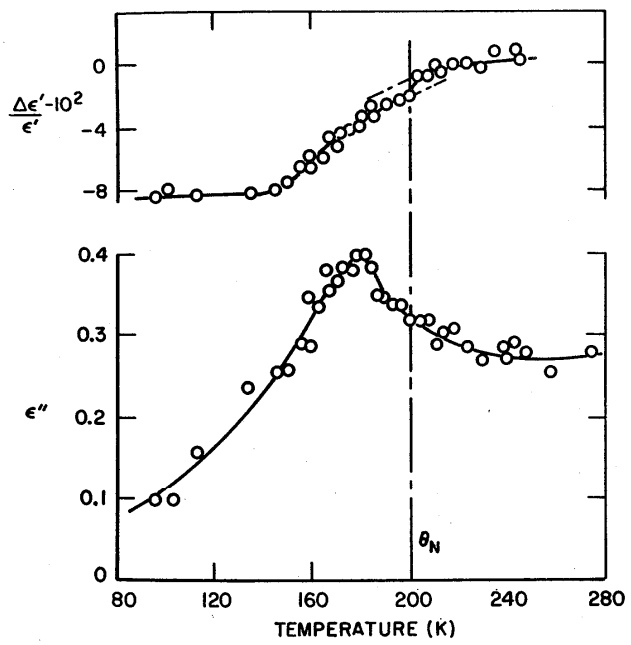

FIGURE 100. FeO. Temperature dependence of the percentage change of dielectric constant ϵ' and dielectric loss ϵ'' relative to their values at 240 K for FeO measured by Samokhvalov, et al. [165].

Remarks—The dielectric constant of FeO at its Néel temperature of 240 K is measured at 9.5 GHz by Samokhvalov, et al. [165].

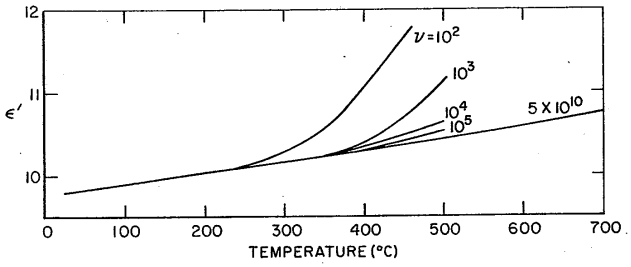

FIGURE 101. MgO (periclase). Temperature dependence of the dielectric constant ϵ of MgO for various frequencies (f) measured by von Hippel, et al. [191].

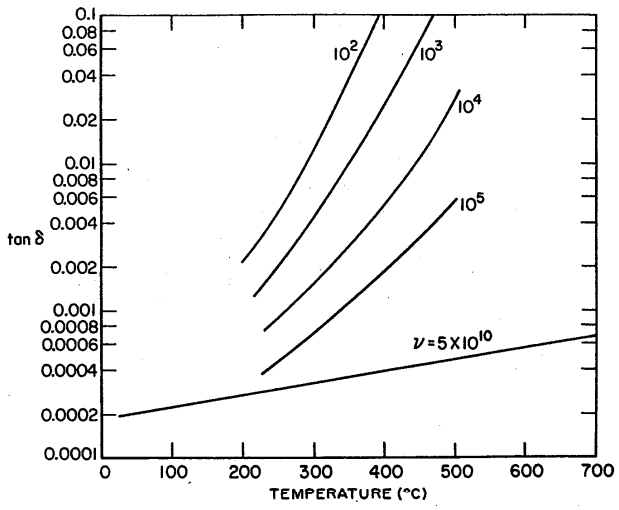

FIGURE 102. MgO (periclase). Temperature dependence of the dielectric loss tangent of MgO for various frequencies measured by von Hippel, et al. [191].

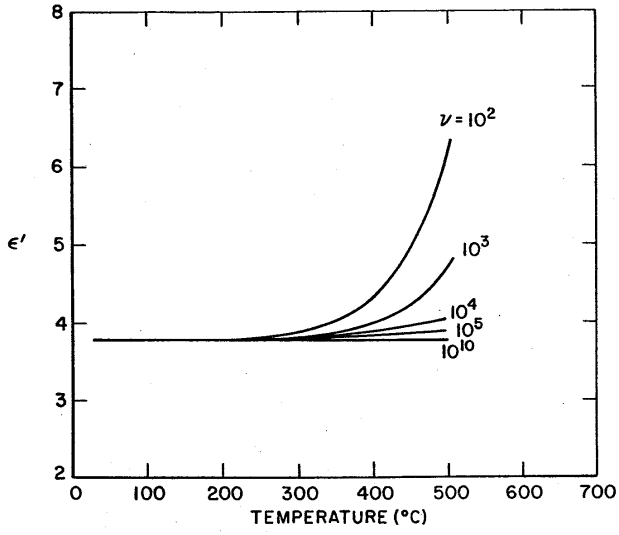

FIGURE 103. SiO_2 (quartz). Temperature dependence of dielectric constant of Corning 915 C fused silica, SiO_2, measured by von Hippel, et al. [191].

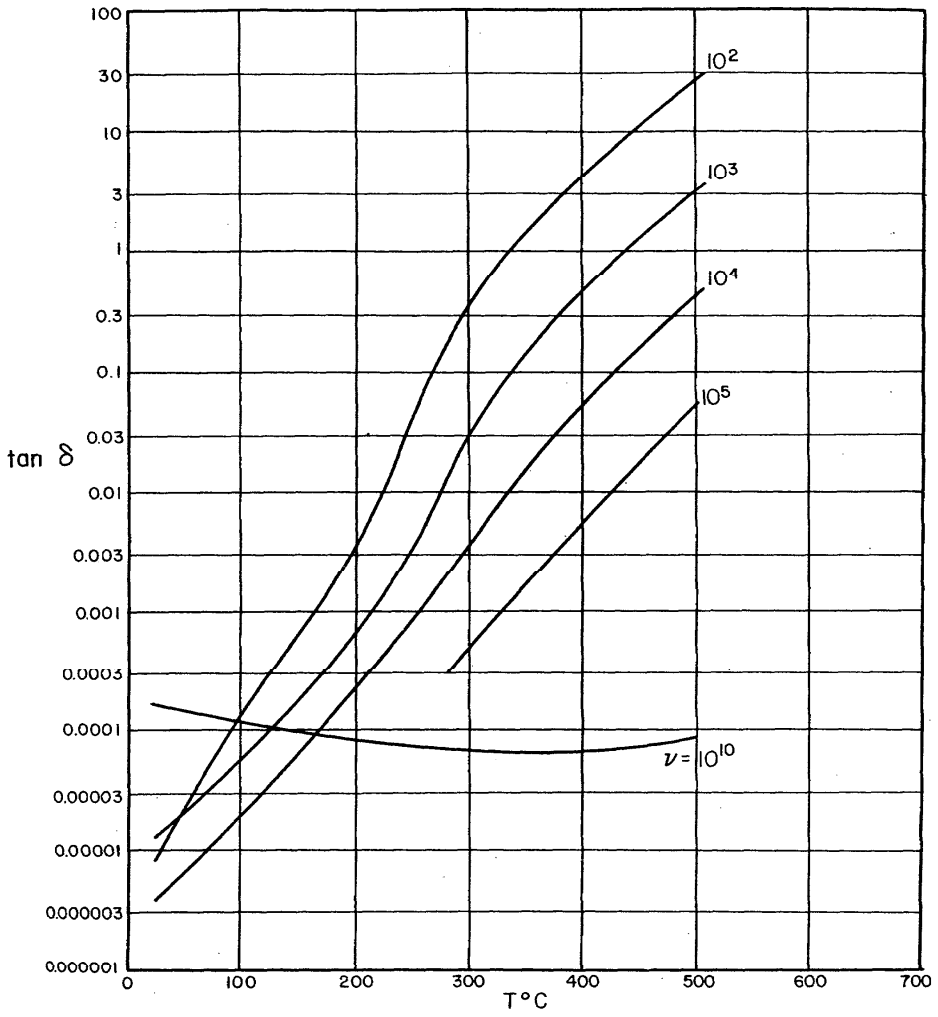

FIGURE 104. SiO_2 (quartz). Temperature dependence of dielectric loss tangent of 915 C fused silica, SiO_2, measured by von Hippel, et al. [191].

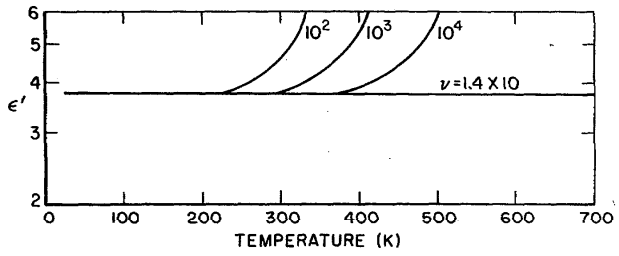

FIGURE 105. SiO_2 (quartz). Temperature dependence of the dielectric constant of General Electric fused quartz, SiO_2, measured by von Hippel, et al. [191].

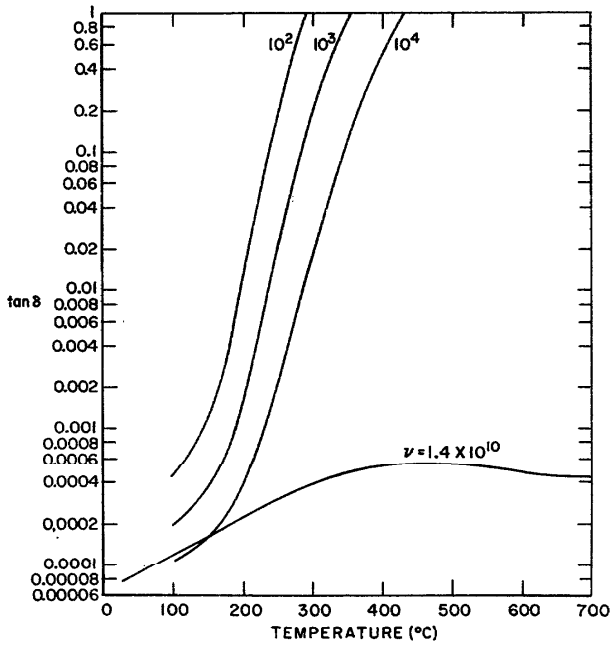

FIGURE 106. SiO_2 (quartz). Temperature dependence of the dielectric loss tangent of General Electric fused quartz, SiO_2, measured by von Hippel, et al. [191].

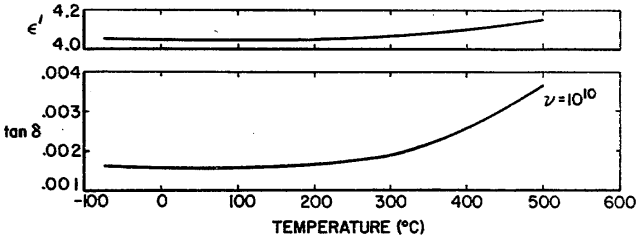

FIGURE 107. Glass, borosilicate. Temperature dependence of the dielectric constant and dielectric loss tangent for borosilicate glass of composition 73.2 percent SiO_2 − 24.8 percent B_2O_3 measured by von Hippel, et al. [191].

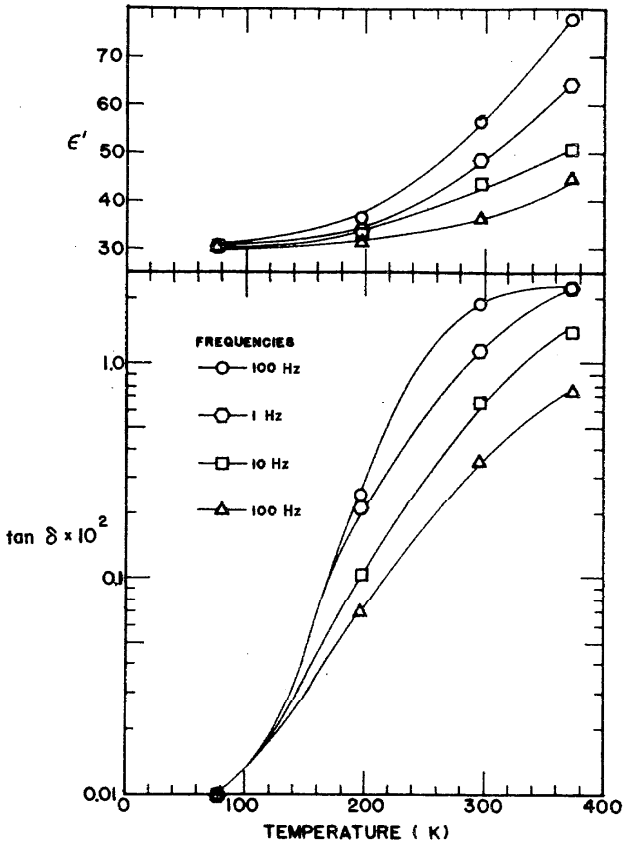

FIGURE 108. Ta_2O_5 (tantala). The temperature dependence of the dielectric constant ϵ' and of the dielectric loss tangent tan δ of the Ta_2O_5 measured parallel to the cleavage plane at 10^2, 10^3, 10^4, and 10^5 Hz by Pavlovic [143].

Remarks—The dielectric constants for ceramic Ta_2O_5 measured by Pavlovic [143] are:

$\epsilon' = 24$ (at room temperature),
$\epsilon' = 21.5$ (at 77 K).

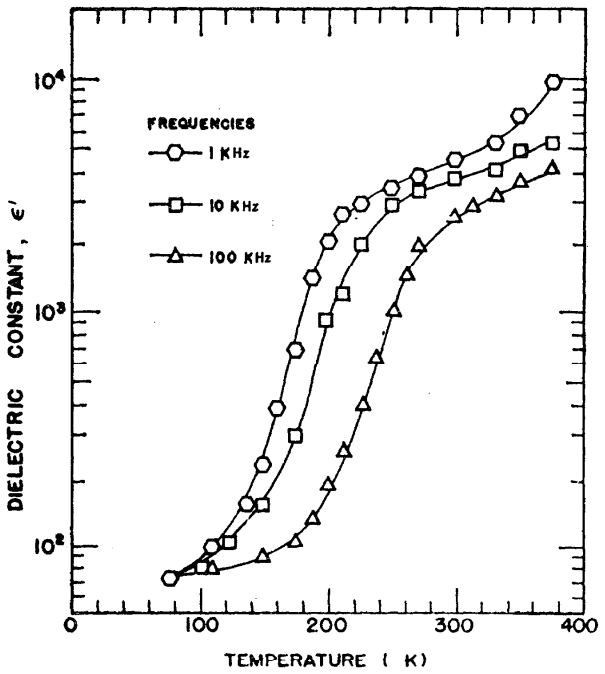

FIGURE 109. Ta_2O_5 (tantala). The temperature dependence of the dielectric constant of Ta_2O_5 measured perpendicular to the cleavage plane at 10^3, 10^4, and 10^5 Hz by Pavlovic[143].

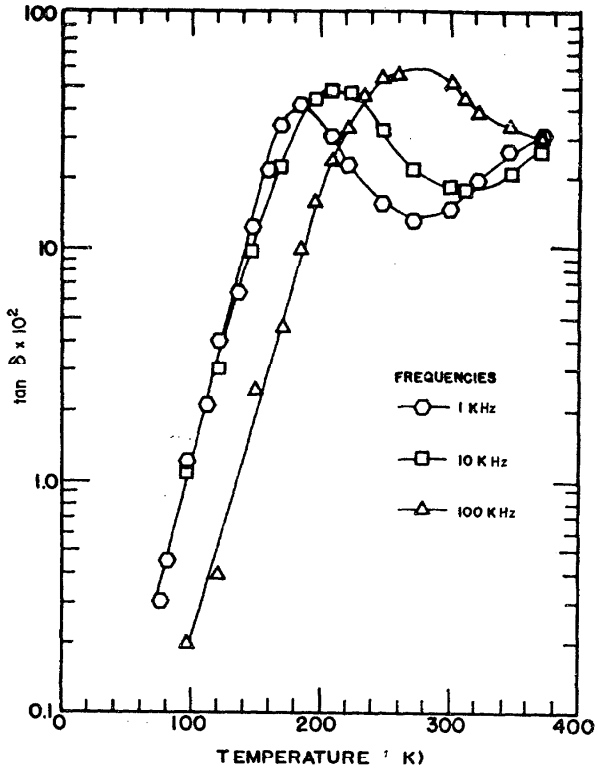

FIGURE 110. Ta_2O_5 (tantala). Temperature dependence of the dielectric loss tangent, tan δ, of the Ta_2O_5 measured perpendicular to the cleavage plane at 10^3, 10^4, and 10^5 Hz by Pavlovic [143].

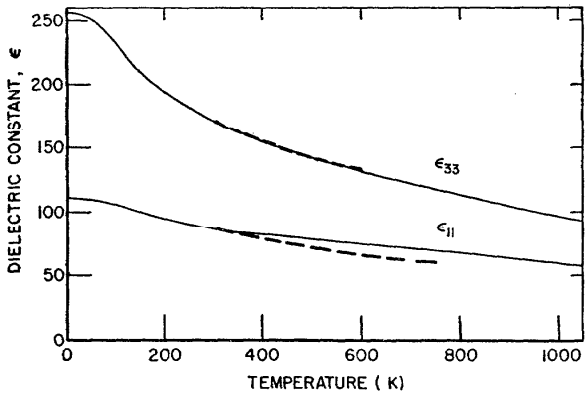

FIGURE 111. TiO_2 (rutile). Temperature dependence of the dielectric constants ϵ_{11}, ϵ_{33} of TiO_2 measured by Parker [140].

Remarks—The experiments on rutile referred to here were made on extremely pure and well-oxidized samples. The measured dielectric constant was not a function of frequency over the range $100-3\times10^6$ Hz, ac field (0.1 − 30 V/cm) or dc bias (0 − 4000 V/cm).

3.10. Ice

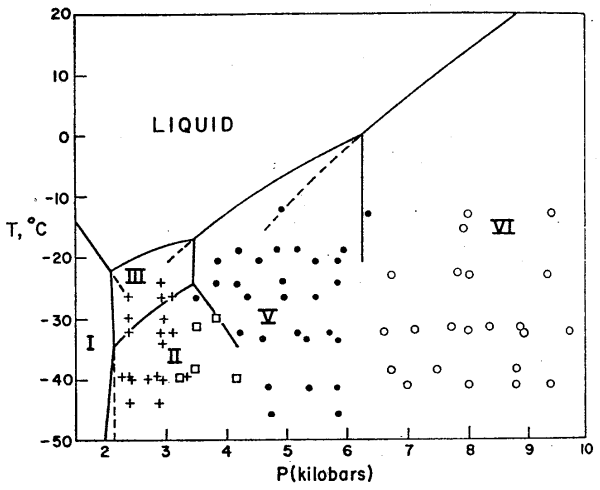

FIGURE 112. H_2O (ice). A portion of the phase diagram of H_2O under pressure after Wilson, et al. [228].

Remarks—H_2O forms several solid phases that are stable only under pressure, namely Ices II, III, V, VI, VIII, as well as a number of metastable phases.

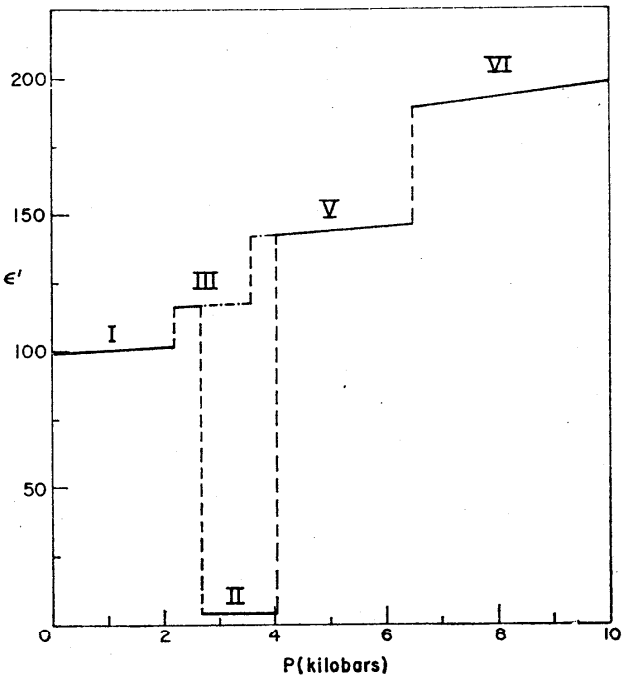

FIGURE 113. H_2O (ice). Pressure dependence of the dielectric constant of various phases of ice (H_2O) at 243 K measured by Wilson, et al. [207].

Remarks—Measurements of ϵ' and ϵ'' were made over the frequency range 45 Hz–300 Hz and limiting values of ϵ were derived from Cole-Cole plots of ϵ'' versus ϵ'.

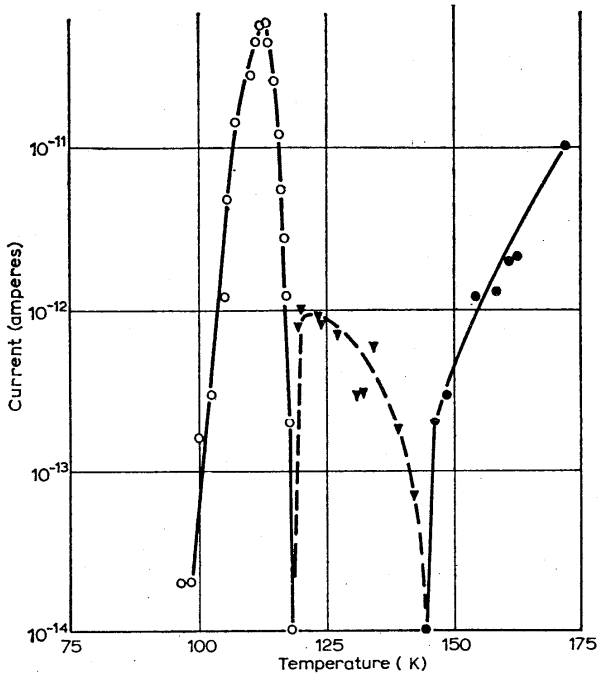

FIGURE 114. H_2O (ice). Charging currents in ice I as a function of temperature measured by Onsager, et al. [138].

Remarks—Measurements of charging currents and dielectric properties below 150 K indicate a possible ferroelectric transition in ice I near 100 K.

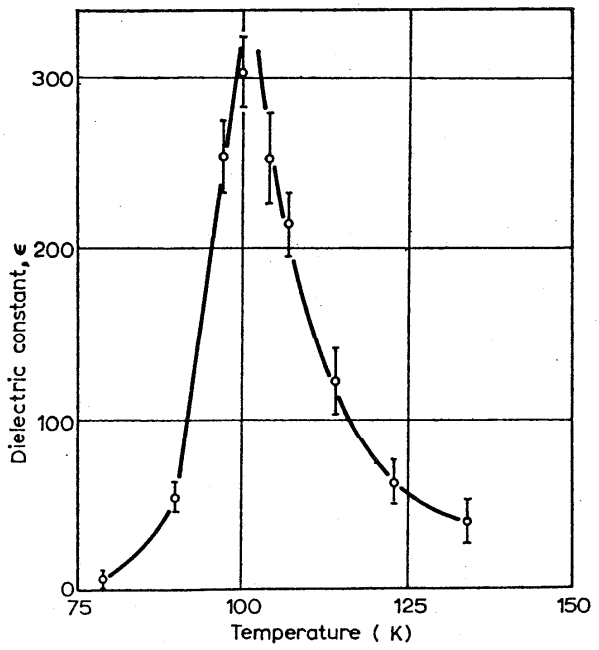

FIGURE 115. H_2O (ice). Temperature dependence of the dielectric constant of ice I reported by Onsager, et al. [138].

3.11. Binary Halides

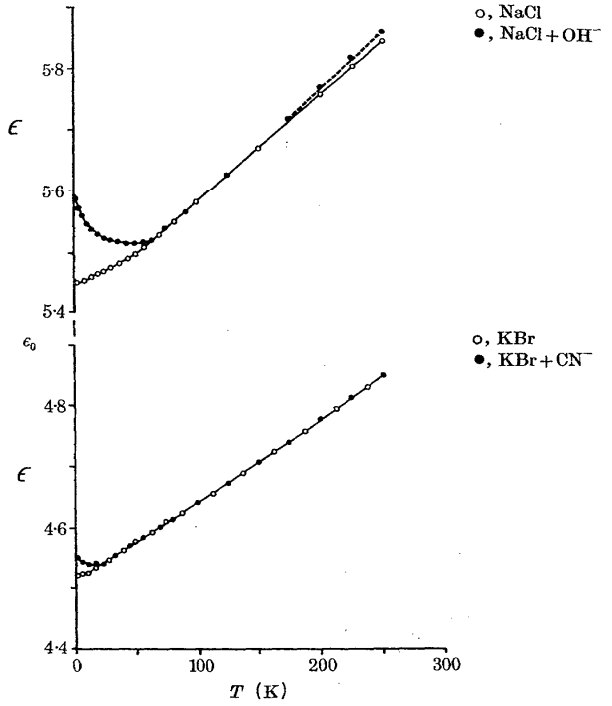

FIGURES 116 and 117. NaCl. Temperature dependences of the dielectric constants of NaCl and NaCl plus the ionic impurity OH^- (one part in 10^5) measured at 1.6 kHz by Lowndes, et al. [118a].

KBr. Temperature dependences of the dielectric constants of KBr and KBr plus the ionic impurity CN^- (one part in 10^6) measured at 1.6 kHz by Lowndes, et al. [118a].

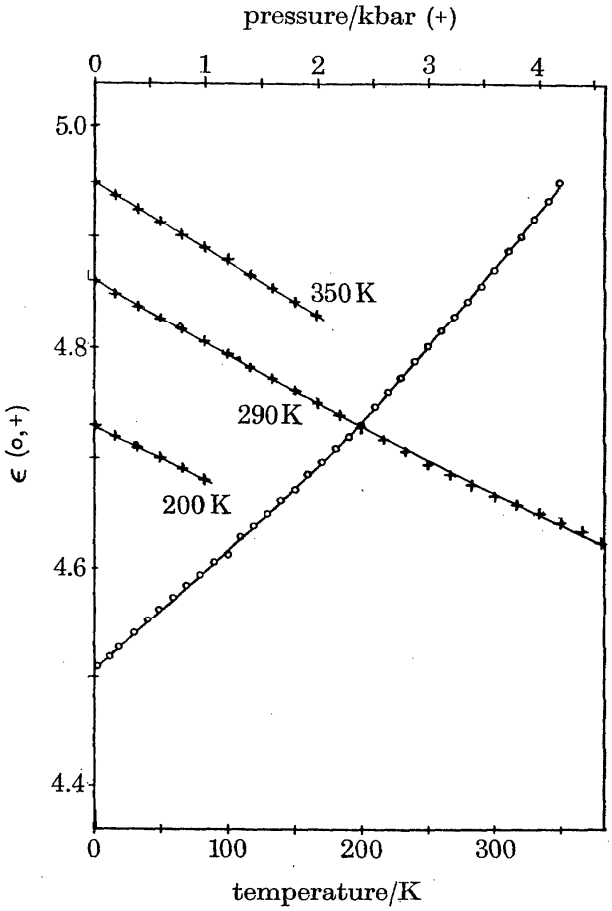

FIGURE 118. RbBr. Temperature (○) and pressure (+) dependences of the dielectric constant of RbBr measured by Lowndes, et al. [118b].

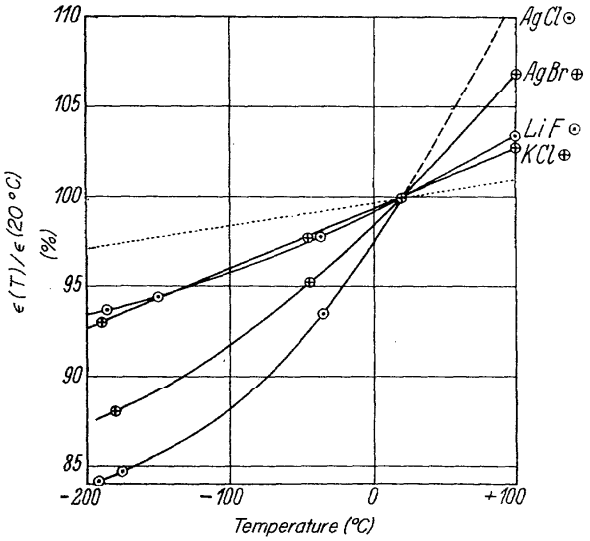

FIGURE 119. AgCl, AgBr. Temperature dependence of the dielectric constant of AgCl and AgBr normalized to their values at room temperature measured by Eucken, et al. [52].

Remarks—The room temperature values of dielectric constant are 11.15 for AgCl and 12.50 for AgBr.

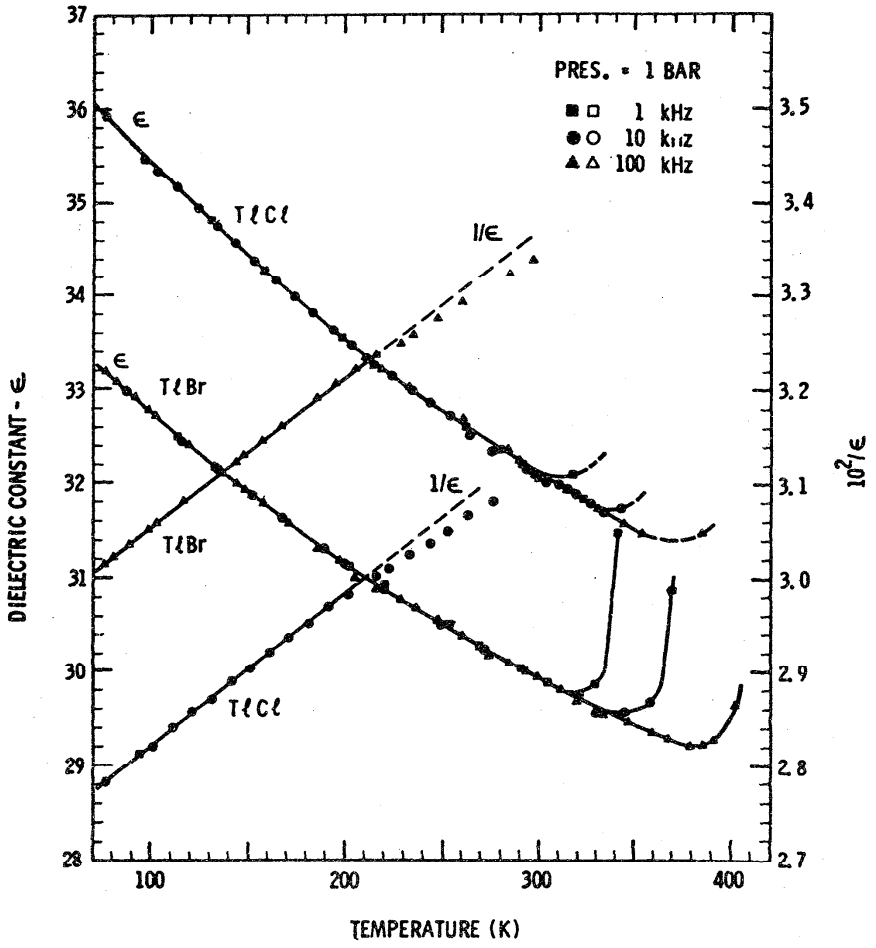

FIGURE 120. TlCl, TlBr. Temperature dependences of the dielectric constants and their reciprocals for TlCl and TlBr measured at 10^3, 10^4, and 10^5 Hz in the [100] direction by Samara [162].

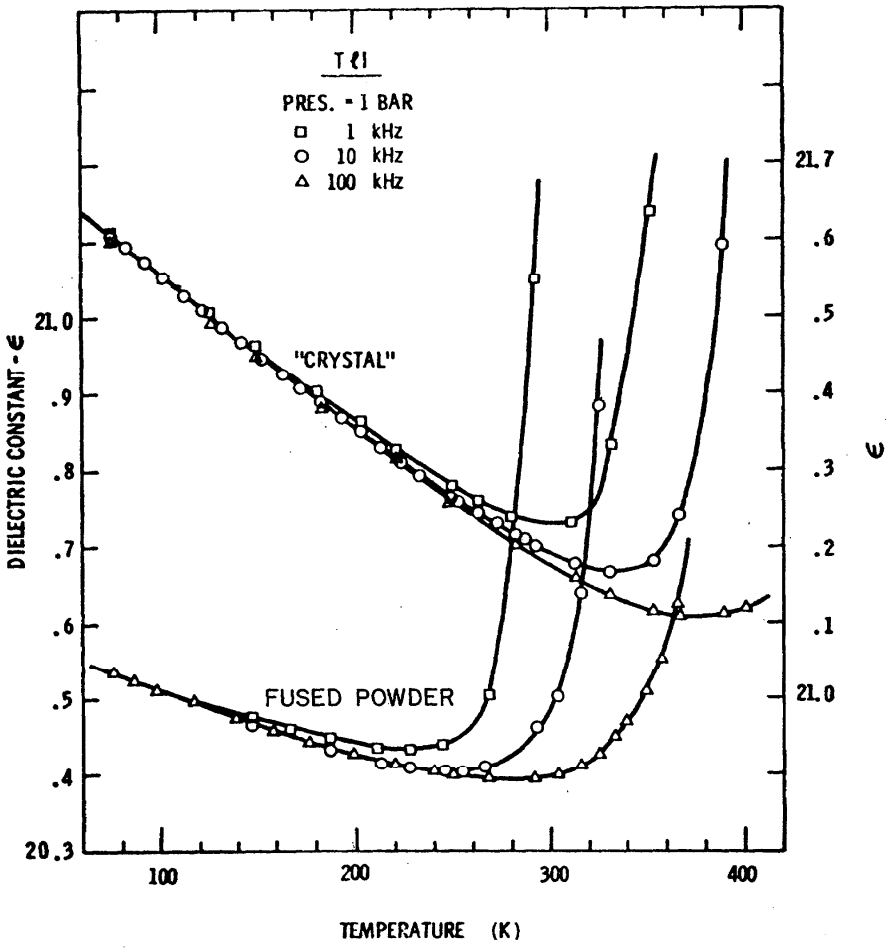

FIGURE 121. TlI. Temperature dependence of the dielectric constant of the best "crystals" of TlI measured at 10^3, 10^4, and 10^5 Hz in the [100] direction by Samara [162].

Remarks—TlCl and TlBr (both cubic structure) can be produced as single crystal. So far the quality of TlI "crystals" (double layered orthorhombic structure) has been very poor. From fig. 112 the activation energy for ionic conduction in TlBr is: $E_t = 0.85$ eV ($E_t = 0.84$ eV for TlCl) according to Samara [162].

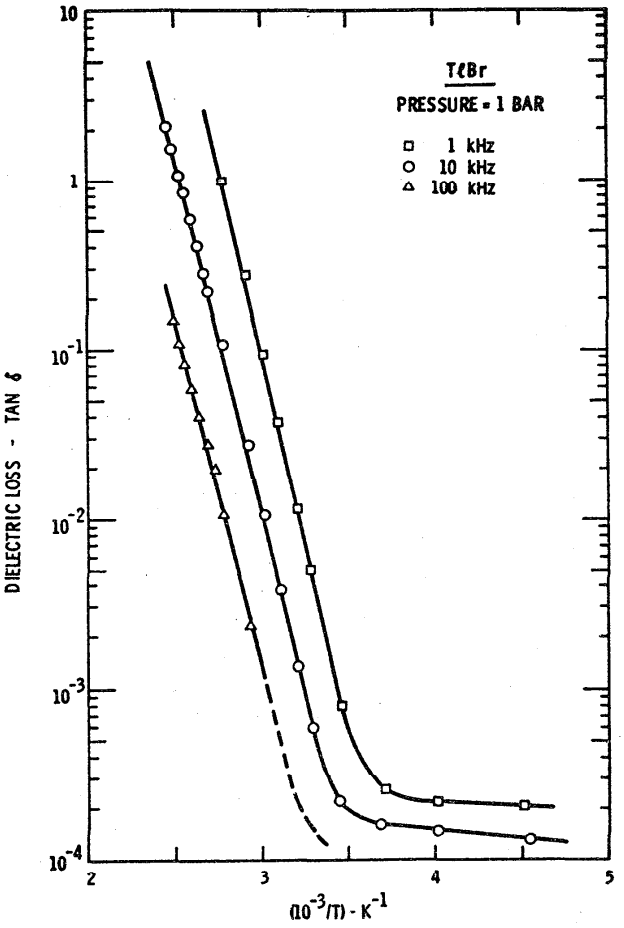

FIGURE 122. TlBr. Temperature dependence of the dielectric loss tangent, tan δ, of TlBr measured at 10^3, 10^4, and 10^5 Hz in the [100] direction by Samara [162].

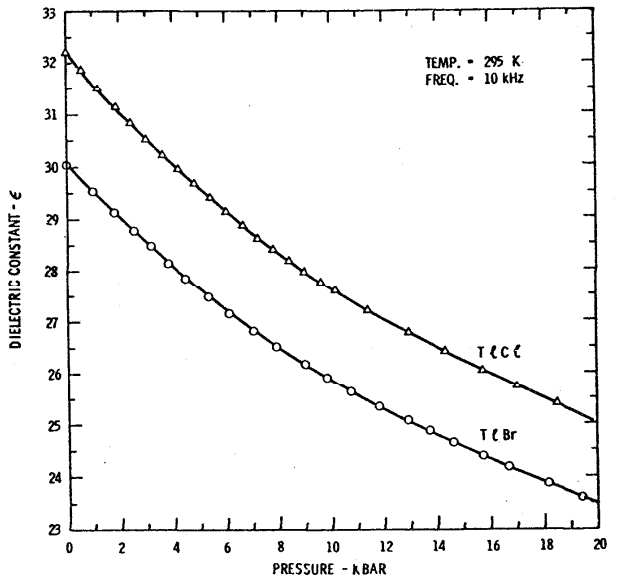

FIGURE 123. TlCl, TlBr. Pressure dependence of the dielectric constant of TlCl and TlBr measured at 295 K and 10^5 Hz by Samara [162].

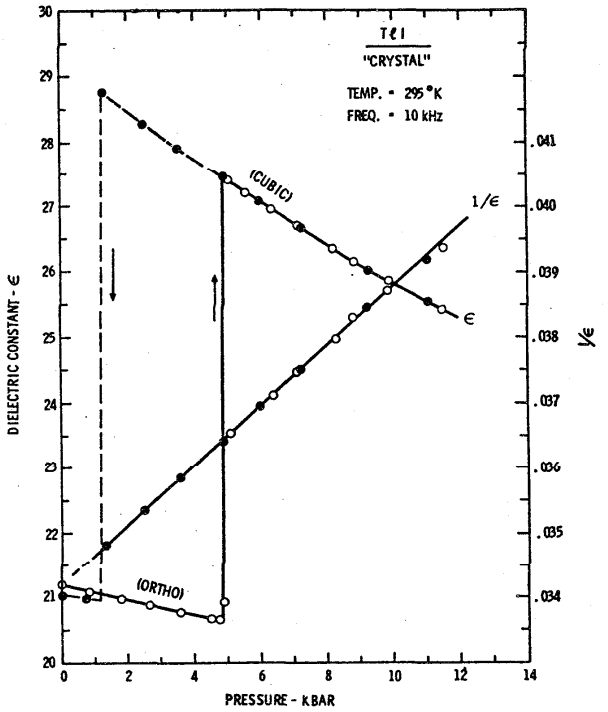

FIGURE 124. TlI. Pressure dependence of the dielectric constant and its reciprocal of TlI "crystal" measured at 295 K and 10^5 Hz by Samara [162] showing the discontinuity at the orthorhombic-cubic transition and the hysteresis effect.

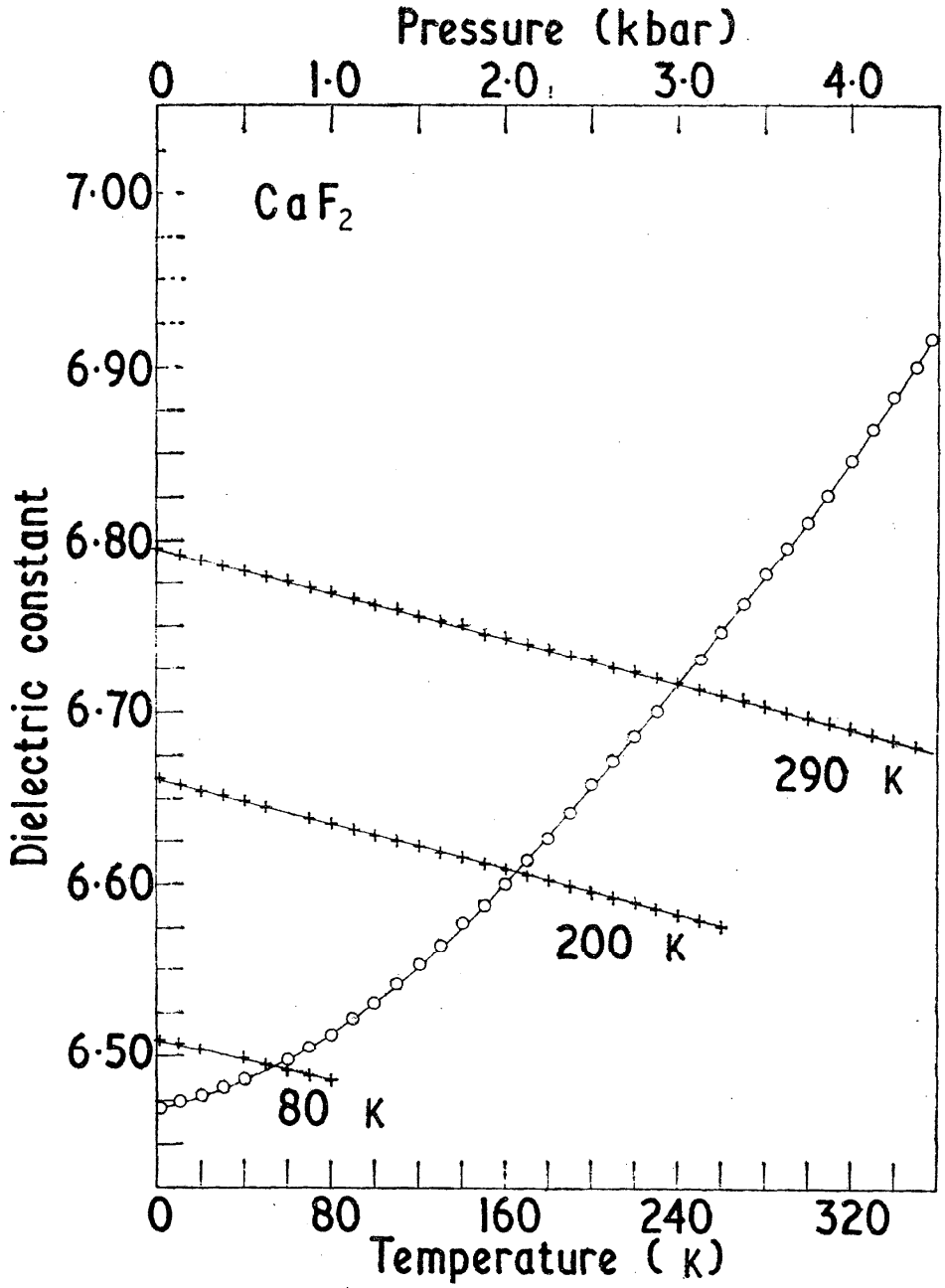

FIGURE 125. CaF_2. Temperature (O) and pressure (+) dependence of the static dielectric constant of CaF_2 measured by Lowndes, et al. [118].

Remarks—The dielectric constant at 300 K is 6.81.

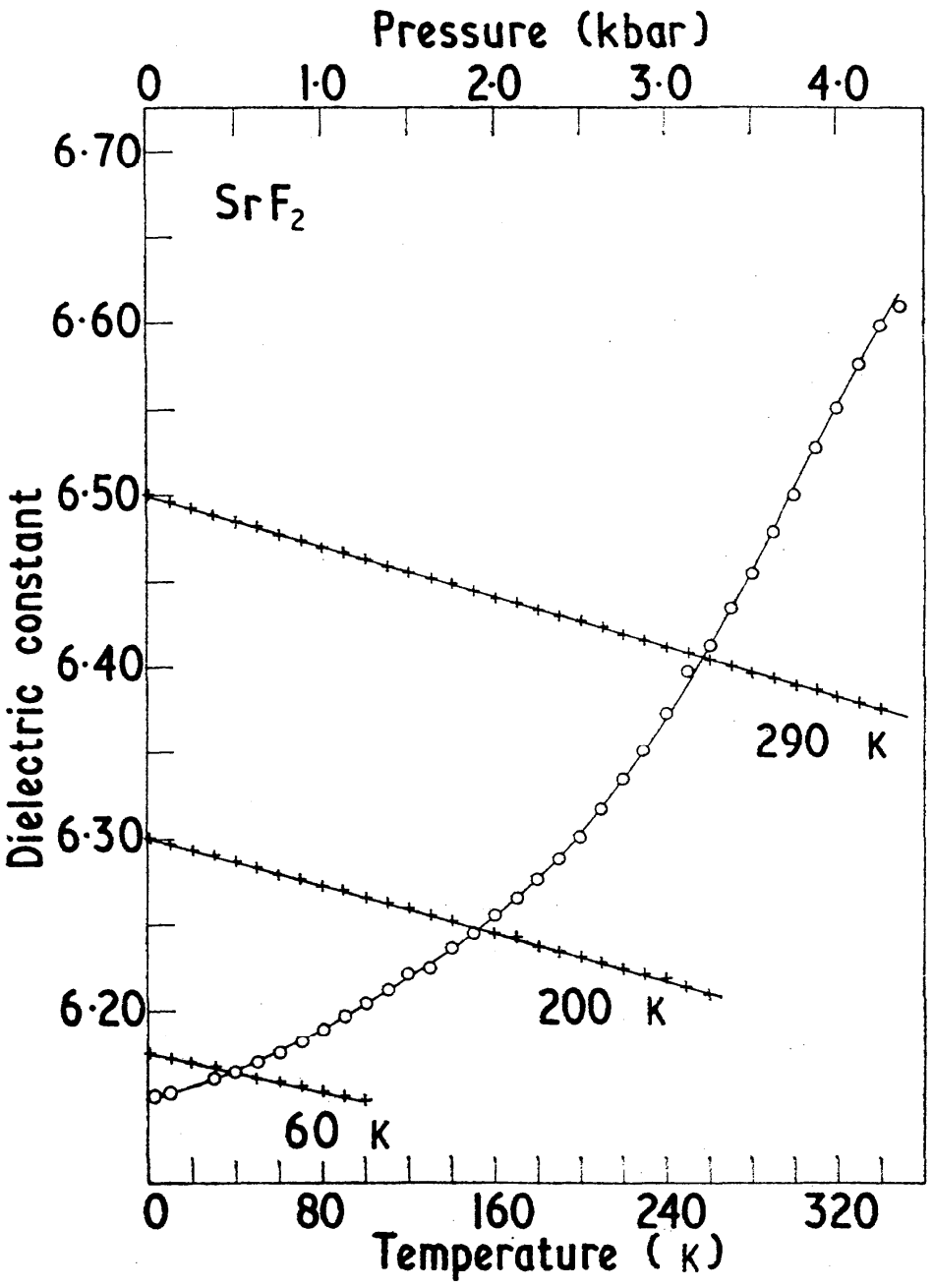

FIGURE 126. SrF_2. Temperature (○) and pressure (+) dependence of the dielectric constant of SrF_2 measured by Lowndes, et al. [118].

Remarks—The dielectric constant at 300 K is 6.50.

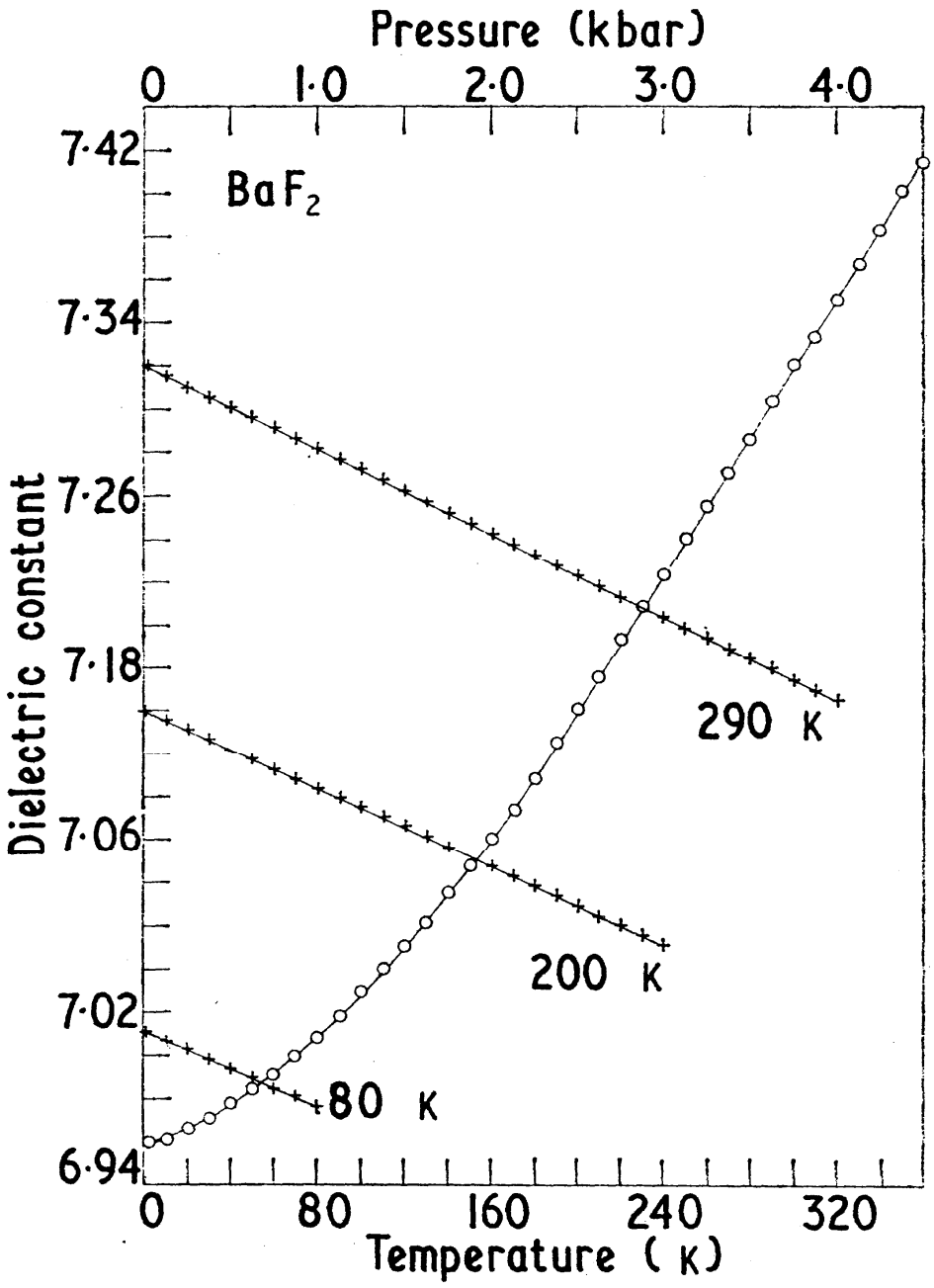

FIGURE 127. Temperature (○) and pressure (+) dependence of the dielectric constant of BaF_2 measured by Lowndes, et al. [118].

Remarks—The dielectric constant at 300 K is 7.32.

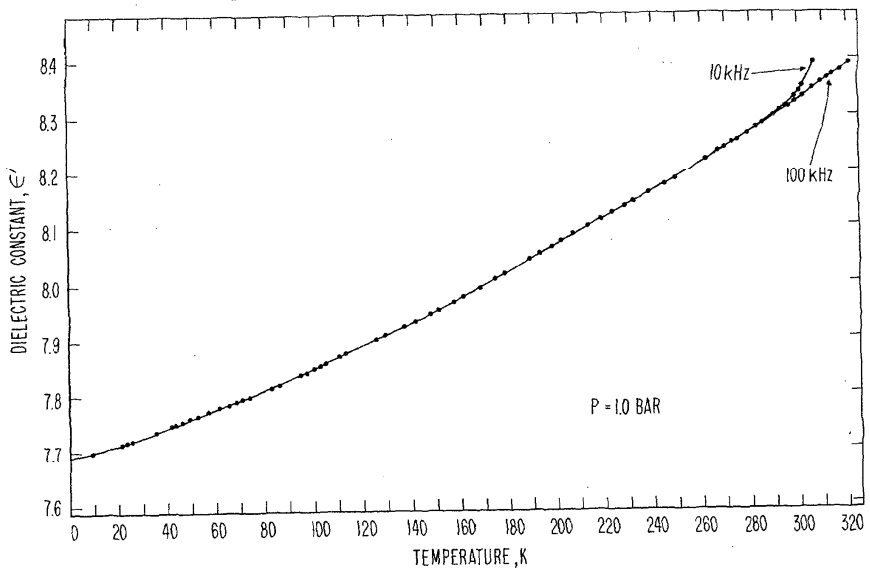

FIGURE 128. CdF_2. Temperature dependence of the dielectric constant of CdF_2 measured by Young, et al. [212].

Remarks—The dielectric constant at 300 K is 8.33 measured by Young, et al. [212].

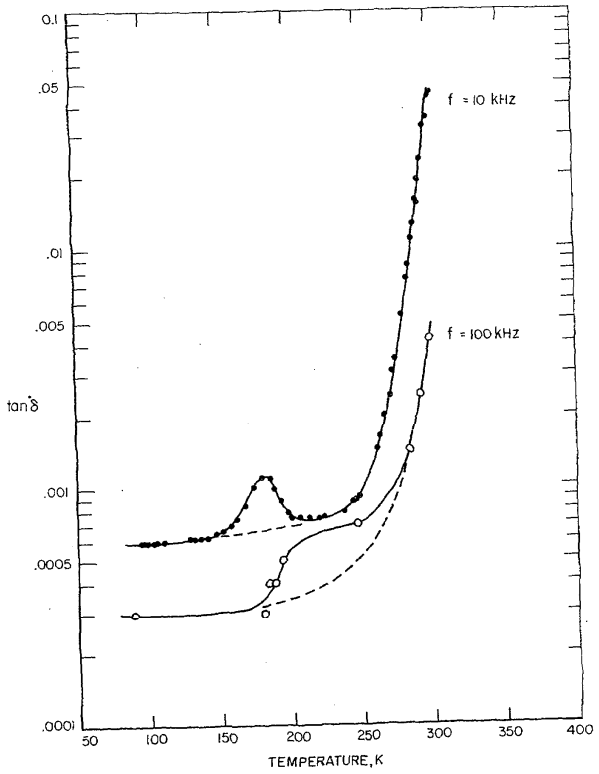

FIGURE 129. CdF_2. Pressure dependence of the dielectric constant of CdF_2 measured by Young, et al. [212].

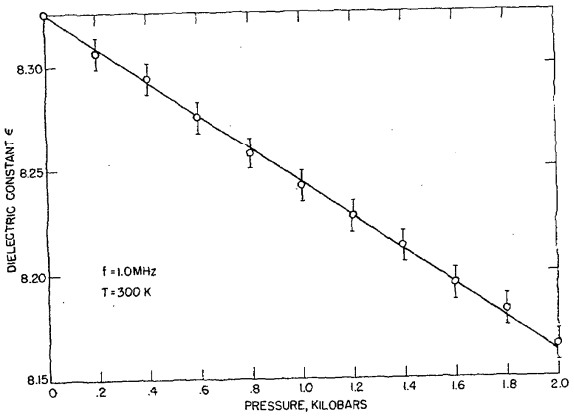

FIGURE 130. CdF_2. Temperature dependence of dielectric loss tangent of CdF_2 measured by Young, et al. [212].

4. Acknowledgments

The authors want to thank Dr. A. D. Franklin for a critical reading of the manuscript. Discussions with Dr. A. H. Kahn concerning the correct definitions of the major dielectric quantities were very helpful.

5. Bibliographic References

[1] Adhav, R. S., J. Appl. Phys. **39,** 4095 (1968).
[2] Adhav, R. S., J. Acoust. Soc. Am. **43,** 835 (1968).
[3] Aigrain, P., and Balkanski, M., Ergeb. Exakt. Naturw. **48,** 41 (1969).
[4] Aiki, K., Hukuda, K., Koga, H., and Kobayashi, T., J. Phys. Soc. Japan **28,** 389 (1970).
[5] Andeen, C., Fontanella, J., and Schuele, D., J. Appl. Phys. **42,** 2216 (1971).
[6] Ascher, E., Rieder, H., Schmid, H., and Stössel, H., J. Appl. Phys. **37,** 1404 (1966).
[7] Aven, M., and Segall, B., Phys. Rev. **130,** 81 (1963).
[8] Aven, M., and Marple, D. T. F., and Segall, B., J. Appl. Phys. **32,** 2261 (1961).
[9] Axe, J. D., Gaglianello, J. W., and Scardefield, J. E., Phys. Rev. **139,** A1211 (1965).
[10] Axe, J. D., and Pettit, G. D., Phys. Rev. **151,** 676 (1966).
[11] Axe, J. D., and Pettit, G. D., J. Phys. Chem. Solids **27,** 621 (1966).
[12] Ballman, A. A., J. Am. Ceramic Soc. **48,** 112 (1965).
[13] Ballman, A. A., J. Crystal Growth **1,** 37 (1967).
[14] Barker, A. S., Jr., Phys. Rev. **165,** 917 (1968).
[15] Barker, A. S., Jr., and Summers, C. J., J. Appl. Phys. **41,** 3552 (1970).
[16] Bärtschi, P., Helv. Phys. Acta **18,** 267 (1945).
[17] Belyaev, L. M., Belikova, G. S., Dobrzhanskii, G. F., Netesov, G. B., and Shaldin, Yu. V., Sov. Phys.-Solid State **6,** 2007 (1965).
[18] Bergstein, A., Czech. J. Phys. **6,** 164 (1956).
[19] Berlincourt, D., Cook, W. R., Jr., and Rander, M. E., Acta Cryst. **16,** 163 (1963).
[20] Berlincourt, D., Jaffe, H., and Shiozawa, L. R., Phys. Rev. **129,** 1009 (1963).
[21] Bever, R. S., and Sproull, R. L., Phys. Rev. **83,** 801 (1951).
[22] Blinc, R., Jovanovic, A., Levstik, A., and Prelesnik, A., J. Phys. Chem. Solids **26,** 1359 (1965).
[23] Bokov, V. A., Smolenskii, S. A., Kizhaev, S. A., Mylinikova, I. E., Sov. Phys.-Solid State **5,** 2646 (1964).
[24] Bokov, V. A., Kizhaev, S. A., Mylinikova, I. E., Tutor, A. G., Sov. Phys.-Solid State **6,** 1359 (1965).
[25] Bonner, W. A., Dearborn, E. F., Geusic, J. E., Marcos, H. M., and Van Uitert, L. G., Appl. Phys. Letters, **10,** 163 (1967).
[26] Borchardt, H. J., and Bierstedt, P. E., in Optical Properties of Ions in Crystals, edited by H. M. Crosswhite and H. W. Moos (Interscience Publishers, New York, 1967), p. 344.
[27] Bosman, A. J., and Havingo, E. E., Phys. Rev. **129,** 1593 (1963).
[28] Brodsky, M. H., and Burstein, E., J. Phys. Chem. Solids **28,** 1655 (1967).
[29] Brower, W. S., Jr., and Fang, P. H., J. Appl. Phys. **40,** 4988 (1969).
[30] Brown, R. D., and Koenig, S. H., Phys. Letters **2,** 309 (1962).
[31] Bruce, J. H., Trans. Faraday Soc. **35,** 206 (1939).
[32] Bube, R. H., and Lind, E. L., Phys. Rev. **115,** 1159 (1959).
[33] Burstein, E., Perkowitz, S., and Brodsky, M. H., J. Phys. Radium **29,** C4-78 (1968).
[34] Busch, Georg, Helv. Phys. Acta **11,** 269 (1938).
[35] Cady, W. G., Piezoelectricity (McGraw-Hill Book Company, Inc., New York, 1946).
[36] Campbell, T. G., and Lawson, A. W., J. Phys. Chem. Solids **30,** 775 (1969).
[37] Champlin, K. S., Erlandson, R. J., Glover, G. H., Hauge, P. S., and Lu, T., Appl. Phys. Letters **11,** 348 (1967).
[38] Chen, F. S., Geusic, J. E., Kurtz, S. K., Skinner, J. G., and Wemple, S. H., J. Appl. Phys. **37,** 388 (1966).
[39] Cochran, W., Ferroelectricity, Proceedings of Symposium on Ferroelectricity, General Motors Research Laboratory, 1966, edited by Weller, E. F. (Elsevier Publishing Co., New York, 1967), p. 68.
[40] Cohen, M. I., Young, K. F., Chang, T., and Brower, W. S., Jr., J. Appl. Phys. **42,** 5267 (1971).
[41] Collins, R. J., and Kleinman, D. A., J. Phys. Chem. Solids **11,** 190 (1959).
[42] Crevecoeur, C., private communication.
[43] Cross, L. E., Nicholson, B. J., Phil. Mag. **46,** 453 (1955).
[44] Cross, L. E., Fouskova, A., and Cummins, S. E., Phys. Rev. Letters **21,** 812 (1968).
[45] D'Altroy, F. A., and Fan, H. Y., Phys. Rev. **103,** 1671 (1956).
[46] Dantsiger, A. Y., and Fesenko, E. G., Sov. Phys.-Crystallogr. **10,** 272 (1965).
[47] Demau C., J. Phys. Radium **24,** 284 (1963).
[48] Di Giura, V., and Spinolo, G., Nuovo Cimento **B,** 192 (1968).
[49] Dunlap, W. C., Jr., and Watters, R. L., Phys. Rev. **92,** 1396 (1953).
[50] Eastman, D., see p. 339 in ref. [92].
[51] Emmenegger, F. P., and Roetschi, H., J. Phys. Chem. Solids **32,** 787 (1971).
[52] Eucken, A., and Büchner, A., Z. Physik. Chem. **27B,** 321 (1934).
[53] Ezuchevskaya, V. M., Syrkin, Ya., K., and Deichman, E. N., Zh. Neorg. Khim. **9,** 1495 (1964).
[54] Ezuchevskaya, V. M., Syrkin, Ya., K., and Shchelokov, R. N., Zh. Neorg. Khim. **9,** 1758 (1964).
[55] Fang, P. H., and Brower, W. S., Jr., Phys. Rev. **129,** 1561 (1963).
[56] Fatuzzo, E., Nitsche, R., Roetschi, H., and Zingg, S., Phys. Rev. **125,** 514 (1962).
[57] Fatuzzo, E., Harbeke, G., Merz, W. J., Nitsche, R., Roetschi, H., and Ruppel, W., Phys. Rev. **127,** 2036 (1962).
[58] Feldman, C., and Hacskaylo, M., Rev. Sci. Instr. **33,** 1459 (1962).
[59] Francombe, M. H., and Lewis, B., Acta Cryst. **11,** 696 (1958).
[60] Geick, R., Schroder, U., and Stuke, J., Phys. Status Solidi **24,** 99 (1967).
[61] Gesi, K., J. Phys. Soc. Japan **28,** 395 (1970).
[62] Gesi, K., and Tateno, J., Japan J. Appl. Phys. **8,** 1358 (1969).
[63] Gibbs, D. F., and Hill, G. J., Phil. Mag. **9,** 367 (1964).
[64] Gibson, A. F., Granville, J. W., and Paige, E. G. S., J. Phys. Chem. Solids **19,** 198 (1961).
[65] Giess, E. A., Burns, G., O'Kane, D. F., Smith, A. W., Appl. Phys. Letters **11,** 233 (1967).
[66] Goldsmith, G. J., and White, J. G., J. Chem. Phys. **31,** 1175 (1959).
[67] Grandjean, D., Claudel, J., Bréhat, F., Hadni, A., Strimer, P., and Thomas, R., J. Phys. Radium **31,** 471 (1970).
[68] Gränicher, H., Helv. Phys. Acta **24,** 619 (1951).
[69] Grigas, I. P., Karpus, A. S., Sov. Phys.-Solid State **9,** 2265 (1968).
[70] Grigas, I. P., Karpus, A. S., Sov. Phys.-Solid State **9,** 2270 (1968).
[71] Guillien, R., Compt. Rend. **208,** 1561 (1939).
[72] Guntherschultze, A., and Keller, F., Z. Physik **75,** 78 (1932).
[73] Hablützel, J., Helv. Phys. Acta **12,** 489 (1939).
[74] Hamano, K., Nakamura, T., Ishibashi, Y., and Ooyane, T., J. Phys. Soc. Japan **20,** 1886 (1965).
[75] Hass, M., and Henvis, B. W., J. Phys. Chem. Solids **23,** 1099 (1962).
[76] Haussühl, S., Acustica **23,** 165 (1970).
[77] Havinga, E. E., and Bosman, A. J., Phys. Rev. **140,** A292 (1965).
[78] Helg, U., and Gränicher, H., J. Phys. Soc. Japan **28,** Supplement, 169 (1970).
[79] Herlach, F., Helv. Phys. Acta **34,** 305 (1961).
[80] Hodgson, J. N., J. Phys. Chem. Solids **23,** 1737 (1962).
[81] Hofman, D., Lely, J. A., and Volger, J., Physica **23,** 236 (1957).
[82] Højendahl, K., Kgl. Danske Videnskab. Selskab, Mat.-Fys. Medd. **16,** 1 (1938).
[83] Højendahl, K., Z. Physik. Chem. (Leipzig) **20B,** 54 (1933).
[84] Hoshino, S., Mitsui, T., Jona, F., and Pepinsky, R., Phys. Rev. **107,** 1255 (1957).
[85] Hoshino, S., Vedam, K., Okaya, Y., and Pepinsky, R., Phys. Rev. **112,** 405 (1958).
[86] Hutson, A. R., Phys. Rev. **108,** 222 (1957).

[87] Ichikawa, M., and Mitsui, T., Phys. Rev. **152**, 495 (1966).
[88] Itoh, Y. Miyazawa, S., Yamada, T., and Iwasaki, H., Japan J. Appl. Phys. **9**, 157 (1970).
[89] Jaeger, R., Ann. Physik **53**, 409 (1917).
[90] Jaffe, H., Proc. IEEE **53**, 1372 (1965).
[91] Jantzen, O., Naturwiss. **50**, 14 (1963).
[92] Jona, F., and Shirame, G., Ferroelectric Crystals, New York: The MacMillan Company, 1962.
[93] Jones, B. W., Phil. Mag. **16**, 1085 (1967).
[94] Jones, G. O., Martin, D. H., Mawer, P. A., and Perry, C. H., Proc. Roy. Soc. (London) **A261**, 10 (1961).
[95] Kaminow, I. P., and Harding, G. O., Phys. Rev. **129**, 1562 (1963).
[96] Kaminow, I. P., p. 1659, Quantum Electronics proceedings of the third international congress, Columbia University Press, New York 1964.
[97] Kaminow, I. P., Phys. Rev. **138**, A1539 (1965).
[98] Kaminow, I. P., and Turner, E. H., Proc. IEEE **54**, 1374 (1966).
[99] Kamioshi, Miyamoto, Sci. Rept. Res. Inst. Tohoku Univ. ser. A, **2**, 370 (1950).
[100] Kanai, Y., Shohno, K., Japan J. Appl. Phys. **2**, 6 (1963).
[101] Känzig, W., Solid State Phys. **4**, 5 (1957).
[102] Kiriyama, Science (Japan) **17**, 239 (1947).
[103] Kiryashkina, Popov, Bilenko, and Kiryashkina, Sov. Phys.-Solid State **2**, 69 (1957).
[104] Kleinman, D. A., and Spitzer, W. G., Phys. Rev. **118**, 110 (1960).
[105] Kobyakov, I. B., and Pado, G. S., Sov. Phys.-Solid State **9**, 1707 (1968).
[106] Kobyakov, I. B., Sov. Phys.-Crystallogr. **11**, 369 (1966).
[107] Kobayashi, T., Yoshida, K. and Kobayashi, H., Japan J. Appl. Phys. **9**, 846 (1970).
[108] Krainik, N. N., Khuchua, N. P., Zhdanova, V. V., and Evseev, V. A., Sov. Phys.-Solid State **8**, 654 (1966).
[109] Krasnikova, A. Ya., Koptsik, V. A., Strukov, B. A., and Ming, W., Sov. Phys.-Solid State **9**, 85 (1967).
[110] Landolt-Börnstein Numerical Data and Functional Relationships in Science and Technology, New Series, Group III: Crystal and Solid State Physics, edited by Hellwege, K.-H., and Hellwege, A. M. (Springer-Verlag, Berlin, 1969), Vol. 2.
[111] Le Bot, J., Le Montagner, S., and Allain, Y., Compt. Rend. **236**, 1409 (1953).
[112] Le Montagner, S., Le Bot, J., Hagene, M., Lasbleis, F., and Le Page, M., Compt. Rend. **240**, 475 (1956).
[113] Leung, P. C., Andermann, G., Spitzer, W. G., and Mead, C. A., J. Phys. Chem. Solids **27**, 849 (1966).
[114] Liebisch and Rubens, Sitzber. Preuss. Akad. Wiss. Physik-Math. Kl. 876 (1919).
[115] Lilja R., and Stubb, T., Acta Polytech. Scand. Phys. Ser. **28**, 1 (1964).
[116] Lorimer, O. G., and Spitzer, W. G., J. Appl. Phys. **36**, 1841 (1965).
[117] Lowndes, R. P., Phys. Letters **21**, 26 (1966).
[118] Lowndes, R. P., J. Phys. C (Solid St. Phys) **2**, 1595 (1969).
[118a] Lowndes, R. P., and Martin, D. H., Proc. Roy. Soc. **A308**, 473 (1969).
[118b] Lowndes, R. P., and Martin, D. H., Proc. Roy. Soc. Lond. **A316**, 351 (1970).
[119] Makita, Y., J. Phys. Soc. Japan **20**, 1567 (1965).
[120] Malone, M. G., and Ferguson, A. L., J. Chem. Phys. **2**, 99 (1934).
[121] Mariani, E., Eckstein, J., and Rubínová, E., Czech. J. Phys. **B17**, 552 (1967).
[122] Martin, H. J., Die Ferroelektrika (Akademische Verlagsgesellschaft Geest & Portig K.-G., Leipzig, 1964).
[123] Mason, W. P., and Matthias, B. T., Piezoelectric Crystals and Their Application to Ultrasonics (D. Van Nostrand Company, Inc., Princeton, New Jersey, 1950).
[124] Mason, W. P., Phys. Rev. **70**, 529 (1946).
[125] Mason, W. P., Phys. Rev. **88**, 477 (1952).
[126] Midorikawa, M., Ishibashi, Y., and Takagi, Y., J. Phys. Soc. Japan **30**, 449 (1971).
[127] Nanamatsu, S., Kimura, M., Doi, K., Takahashi, M., J. Phys. Soc. Japan **30**, 300 (1971).
[128] Narasimhan, P. T., Proc. Phys. Soc. (London) **B68**, 315 (1955).
[129] Narayana, Rao, D. A. A. S., Proc. Indian Acad. Sci. **30**, 82 (1949).
[130] Nash, F. R., Bergman, J. G., Boyd, G. D., and Turner, E. H., J. Appl. Phys. **40**, 5201 (1969).
[131] Nassau, K., Levinstein, H. J., and Loiacono, G. M., J. Phys. Chem. Solids **27**, 989 (1966).
[132] Nigara, Y., Ishigame, M., and Sakurai, T., J. Phys. Soc. Japan **30**, 453 (1971).
[133] Noguet, C., J. Phys. Radium **31**, 393 (1970).
[134] Nomura, S., J. Phys. Soc. Japan **16**, 2440 (1961).
[135] Ohshima, H., and Nakamura, E., J. Phys. Chem. Solids **27**, 481 (1966).
[136] Omachi, Y., Sawamoto, K., and Toyoda, H., Japan J. Appl. Phys. **6**, 1467 (1967).
[137] Onoe, M., Warner, A. W., and Ballman, A. A., IEEE Trans. on Sonics and Ultrason. **SU-14**, 165 (1967).
[138] Onsager, L., Ferroelectricity, Proceedings of Symposium on Ferroelectricity. General Motors Research Laboratory, 1966, edited by Weller, E. F. (Elsevier Publishing Co., New York, 1967), p. 16.
[139] Parker, R. A., and Wasilik, J. H., Phys. Rev. **120**, 1631 (1960).
[140] Parker, R. A., Phys. Rev. **124**, 1719 (1961).
[141] Patrick, L., and Choyke, W. J., Phys. Rev. B **2**, 2255 (1970).
[142] Patrick, L., and Dean, P. J., Phys. Rev. **188**, 1254 (1969).
[143] Pavlovic, A. S., J. Chem. Phys. **40**, 951 (1964).
[144] Pepinsky, R., Okaya, Y., Mitsui, T., Acta Cryst. **10**, 600 (1957).
[145] Pepinsky, R., and Vedam, K., Phys. Rev. **117**, 1502 (1960).
[146] Petrov, V. M., Kristallografiya [Sov. Phys.-Crystallogr.] **6**, 508 (1961).
[147] Picus, C., Burstein, E., Henvis, B. W., and Hass, M., J. Phys. Chem. Solids **8**, 282 (1959).
[148] Rao, K. J., and Rao, C. N. R., Brit. J. Appl. Phys. **17**, 1653 (1966).
[149] Rao, K. V., and Smakula, A., J. Appl. Phys. **36**, 2031 (1965).
[150] Rao, K. V., and Smakula, A., J. Appl. Phys. **37**, 2840 (1966).
[151] Remeika, J. P., and Glass, A. M., Materials Res. Bull. **5**, 37 (1970).
[152] Reynolds, D. C. Litton, C. W., and Collins, T. C., Phys. Status Solidi **12**, 3 (1965).
[153] Rice, R. R., Fay, H., Dess, H. M., and Alford, W. J., J. Electrochem. Soc. **116**, 839 (1969).
[154] Roberts, S., Phys. Rev. **76**, 1215 (1949).
[155] Robinson, M. C., and Hallet, A. C. H., Can. J. Phys. **44**, 2211 (1966).
[156] Ronich and Nowak, Sitzber. Akad. Wien, Math.-Naturw. Kl. **7011**, 380 (1875).
[157] Rosner, R. D., and Turner, E. H., Appl. Opt. **7**, 171 (1958).
[158] Rushton, E., Brit. J. Appl. Phys. **12**, 417 (1961).
[159] Sakudo, T., and Unoki, H., Phys. Rev. Letters **26**, 851 (1971).
[160] Salo, T., Stubb, T., and Suosara, E., in The Physics of Selenium and Tellurium, Proceedings of the International Symposium held at Montreal, Canada, October 1967; edited by Cooper, W. C. (Pergamon Press, Toronto, 1968).
[161] Samara, G. A., and Anderson, D. H., Solid State Commun. **4**, 653 (1966).
[162] Samara, G. A., Phys. Rev. **165**, 959 (1968).
[163] Samara, G. A., J. Phys. Chem. Solids **26**, 121 (1965).
[164] Samara, G. A., Phys. Rev. B **1**, 3777 (1970).
[164a] Samara, G. A., J. Phys. Soc. Japan **28**, 399, Supplement 1970; Proceedings of the Second International Meeting on Ferroelectricity 1969.
[164b] Samara, G. A., Ferroelectrics **2**, 277 (1971).
[165] Samokhvalov, A. A., Sov. Phys.-Solid State **3**, 2613 (1962).
[166] Sawada, S., Nomura, S., and Fujii, S., J. Phys. Soc. Japan **13**, 1549 (1958).

[167] Schmidt, W., Ann. Physik **9**, 919 (1902).
[168] Schmidt, W., Ann. Physik **11**, 114 (1903).
[169] Schmidt, M., and Sand, T., J. Inorg. Nucl. Chem. **26**, 1189 (1964).
[170] Schupp, P., Z. Physik **75**, 84 (1932).
[171] Schweppe, H., IEEE Trans. on Sonics and Ultrason. SU-16, p. 219 (1969).
[172] Scott, J. F., Phys. Rev. B **1**, 3488 (1970).
[173] Sharma, M. N., and Gupta, S. S., Indian J. Phys. **37**, 33 (1963).
[174] Shirane, G., Danner, H., Parloric, A., and Pepinsky, R., Phys. Rev. **93**, 672 (1954).
[175] Simhony, M., J. Phys. Chem. Solids **24**, 1297 (1963).
[176] Sliker, T. R., and Burlage, S. R., J. Appl. Phys. **34**, 1837 (1963).
[177] Sonin, A. S., and Zheludev, I. S., Sov. Phys.-Crystallogr. **8**, 217 (1963).
[178] Sonin, A. S., and Zheludev, I. S., Sov. Phys.-Crystallogr. **8**, 219 (1963).
[179] Spitzer, W. G., Kleinman, D., and Walsh, D., Phys. Rev. **113**, 127 (1959).
[180] Steulmann, G., Z. Physik **77**, 114 (1932).
[181] Strukov, B. A., Koptsik, V. A., Ligasova, V. D., Sov. Phys.-Solid State **4**, 977 (1962).
[182] Subbarao, E. C., Shirane, G., and Jona, F., Acta Cryst. **13**, 226 (1960).
[183] Tables of Dielectric Materials, Vol. 6, M.I.T. Lab. for Insul. Res. Tech. Rept. 126, June 1958, Von Hippel, A.R.
[184] Tambovtsev, D. A., Skorikov, V. M., and Zheludev, I. S., Sov. Phys.-Crystallogr. **8**, 713 (1963).
[185] Trevelyan, B., Opto-Electron. **1**, 9 (1969).
[186] Tsunekawa, S., Takagi, Y., and Ishibashi, Y., Japan J. Appl. Phys. **9**, 68 (1970).
[187] Turner, W. J., and Reese, W. E., Phys. Rev. **127**, 126 (1962).
[188] Unruh, H. G., Phys. Letters **17**, 8 (1965).
[189] van Daal, H. J., J. Appl. Phys. **39**, 4467 (1968).
[190] van Uitert, L. G. and Egerton, L., J. Appl. Phys. **32**, 959 (1961).
[191] von Hippel, A. R., Dielectric Materials and Applications (John Wiley and Sons, Inc., New York, 1954).
[192] Wagner, H., Z. Physik **193**, 218 (1966).
[193] Waku, S., Hirabayashi, H., Toyoda, H., Iwasaki, H., and Kiriyama, R., J. Phys. Soc. Japan **14**, 973 (1959).
[194] Walther, L., Hochfrequenztechn. u. Elektroak. **74**, 204 (1965).
[195] Wappler, G., Z. Physik. Chem. (Leipzig) **228**, 23 (1965).
[196] Warner, A. W., and Meitzler, A. H., Proc. IEEE **56**, 1376 (1968).
[197] Warner, A. J., Coquin, G. A., and Fink, J. L., J. Appl. Phys. **40**, 4353 (1969).
[198] Warner, A. W., Coquin, G. A., Meitzler, A. H., and Fink, J. L., Appl. Phys. Letters **14**, 34 (1969).
[199] Warner, A. W., Oneo, M., and Coquin, G. A., J. Acoust. Soc. Am. **42**, 1223 (1968).
[200] Weaver, H. E., J. Phys. Chem. Solids **11**, 274 (1959).
[201] Wemple, S. H., Phys. Rev. **137**, A1575 (1965).
[202] Wemple, S. H., Didomenico, M., Jr., and Camlibel, I., J. Phys. Chem. Solids **29**, 1797 (1968).
[203] Wemple, S. H., Jayarman, A., Didomenico, M., Jr., Phys. Rev. Letters **17**, 142 (1966).
[204] Wieder, H. H., J. Appl. Phys. **30**, 1010 (1959).
[205] Wieder, H. H., and Parkerson, C. R., J. Phys. Chem. Solids **27**, 247 (1966).
[206] Willardson, R. K., and Beer, A. C., Semiconductors and Semimetals (Academic Press Inc., New York, 1967), Vol. 1, p. 14.
[207] Wilson, G. J., Chan, R. K., Davidson, D. W., and Whalley, E., J. Chem. Phys. **43**, 2384 (1965).
[208] Wohofsky, O., Ber. Bunsenges. Physik. Chem. **70**, 631 (1966).
[209] Yamada, T., and Niizeki, N., Japan J. Appl. Phys. **7**, 292 (1968).
[210] Yamashita, A., and Asai, K., J. Phys. Soc. Japan **18**, 1247 (1963).
[211] Yoshimoto, J. and Okai, B., J. Phys. Soc. Japan **31**, 307 (1971).
[212] Young, K. F., and Frederikse, H. P. R., J. Appl. Phys. **40**, 3115 (1969).
[213] Yousef, Y. L., and Farag, B. S., Physica **31**, 706 (1965).
[214] Zallen, R., Lucovsky, G., Taylor, W., Pinczuk, A., and Burstein, E., Phys. Rev. B **1**, 4058 (1970).
[215] Data Sheet 571 from Holobeam, Inc., Laser Products Division, 560 Winters Avenue, Paramus, New Jersey 07652.

6. Compound Index

Barium Sodium Niobate ("Bananas")	$Ba_2NaNb_5O_{15}$
Barium Stannate	$BaSnO_3$
Barium Sulfate	$BaSO_4$
Barium Sulfide	BaS
Barium Titanate	$BaTiO_3$
Barium Titanium Niobate	$Ba_6Ti_2Nb_8O_{30}$
Barium Tungstate	$BaWO_4$
Barium Zirconate	$BaZrO_3$
Beryl (Beryllium Aluminum Silicate)	$Be_3Al_2Si_6O_{18}$
Beryllia (Beryllium Oxide)	BeO
Beryllium Aluminum Silicate (Beryl)	$Be_3Al_2(Si_6O_{18})$
Beryllium Carbonate	$BeCO_3$
Beryllium Oxide (Beryllia)	BeO
Bismuth Germanate	$Bi(GeO_4)_3$
Bismuth Germanate	$Bi_{12}GeO_{20}$
Bismuth Iron Oxide	$BiFeO_3$
Bismuth Sesquioxide	Bi_2O_3
Bismuth Titanate	$Bi_4Ti_3O_{12}$
Boracite (Magnesium Borate Monochloride)	$Mg_3B_7O_{13}Cl$
Boron Nitride	BN
CDA (Cesium Dihydrogen Arsenate)	$Cs_2H_2AsO_4$
CDP (Cesium Dihydrogen Phosphate)	$Cs_2H_2PO_4$
Cadmium Arsenide	Cd_3As_2
Cadmium Bromide	$CdBr_2$
Cadmium Fluoride	CdF_2
Cadmium Pyroniobate	$Cd_2Nb_2O_7$
Cadmium Selenide	$CdSe$
Cadmium Sulfide	CdS
Cadmium Telluride	$CdTe$
Calcium Carbonate	$CaCO_3$
Calcium Cerate	$CaCeO_3$
Calcium Fluoride	CaF_2
Calcium Molybdate	$CaMoO_4$
Calcium Niobate	$CaNb_2O_6$
Calcium Nitrate	$Ca(NO_3)_2$
Calcium Oxide	CaO
Calcium Pyroniobate	$Ca_2Nb_2O_7$
Calcium Sulfate Dihydrate	$CaSO_4 \cdot 2H_2O$
Calcium Sulfide	CaS
Calcium Titanate	$CaTiO_3$
Calcium Tungstate	$CaWO_4$
Calumel (Mercurous Chloride)	$HgCl$
Cerium Oxide	CeO_2
Cesium Alum	$CsAl(SO_4)_2 \cdot 12H_2O$
Cesium Bromide	$CsBr$
Cesium Carbonate	Cs_2CO_3
Cesium Chloride	$CsCl$
Cesium Dihydrogen Arsenate (CDA)	$Cs_2H_2AsO_4$
Cesium Dihydrogen Phosphate (CDP)	$Cs_2H_2PO_4$
Cesium Iodide	CsI
Cesium Lead Chloride	$CsPbCl_3$
Cesium Nitrate	$CsNO_3$
Cesium Trihydrogen Selenite	$CsH_3(SeO_3)_2$
Chromic Sesquioxide	Cr_2O_3
Cinnabar (Mercurous Sulfide)	HgS
Cobalt Niobate	$CoNb_2O_6$
Cobalt Oxide	CoO
Cobalt Tungstate	$CoWO_4$
Colemanite	$Ca_2B_6O_{11} \cdot 5H_2O$
Cuprite (Cuprous Oxide)	Cu_2O
Cupric Oxide	CuO
Cupric Sulfate Pentahydrate	$CuSO_4 \cdot 5H_2O$
Cuprous Bromide	$CuBr$
Cuprous Chloride	$CuCl$
Cuprous Oxide (Cuprite)	Cu_2O
DKT (Dipotassium Tartrate)	$K_2C_4H_4O_6 \cdot 1/2H_2O$
Deuterated Rochelle Salt (Potassium Sodium Tartrate Tetrahydrate)	$KNa(C_4D_4O_6) \cdot 4H_2O$
Deuterated Rochelle Salt (Sodium Potassium Tartrate Tetradeuterate)	$NaK(C_4H_2D_2O_6) \cdot 4D_2O$
Deuteroammonium Fluoberyllate	$(ND_4)_2BeF_4$
Deuteroammonium Sulfate	$(ND_4)_2SO_4$
Dextrose Sodium Bromide	$C_6H_{12}O_6 \cdot NaBr$
Diamond	C
Dipotassium Monohydrogen Orthophosphate	K_2HPO_4
Dipotassium Tartrate (DKT)	$K_2C_4H_4O_6 \cdot 1/2H_2O$
EDT (Ethylene Diamine Tartrate)	$C_6H_{14}N_2O_6$
Ethylene Diamine Tartrate (EDT)	$C_6H_{14}N_2O_6$
Europium Fluoride	EuF_2
Europium Molybdate	$Eu_2(MoO_4)_3$
Europium Sulfide	EuS
Ferric Sesquioxide (Hematite)	Fe_2O_3
Ferrosoferric Oxide (Magnetite)	Fe_3O_4
Ferrous Oxide	FeO
Gadolinium Molybdate	$Cd_2(MoO_4)_3$
Gallium Antimonide	$GaSb$
Gallium Arsenide	$GaAs$
Gallium Phosphide	GaP
Germanium	Ge
Germanium Dioxide	GeO_2
HMTA (Hexamethylene Tetramine)	$N_4(CH_2)_6$
Hematite (Ferric Sesquioxide)	Fe_2O_3
Hexamethylene Tetramine (HMTA)	$N_4(CH_2)_6$
Hydrogen Ammonium Dichloroacetate	$H\text{-}NH_4(ClCH_2COO)_2$
Ice	H_2O
Indium Antimonide	$InSb$
Indium Arsenide	$InAs$
Indium Phosphide	InP
Iodic Acid	HIO_3
Iodine	I_2

KDA (Potassium Dihydrogen Arsenate)	KH_2AsO_4
KDDA (Potassium Dideuterium Arsenate)	KD_2AsO_4
KDDP (Potassium Dideuterium Phosphate)	KD_2PO_4
KTN (Potassium Tantalate Niobate)	$KTaNbO_3$
KDP (Potassium Dihydrogen Phosphate)	KH_2PO_4
LAT (Lithium Ammonium Tartrate)	$LiNH_4C_4H_4O_6{\cdot}H_2O$
(LTT) Lithium Thallium Tartrate	$LiTlC_4H_4O_6{\cdot}H_2O$
Lanthanum Scandate	$LaScO_3$
Lead Acetate	$Pb(C_2H_3O_2)_2$
Lead Bromide	$PbBr_2$
Lead Carbonate	$PbCO_3$
Lead Chloride	$PbCl_2$
Lead Cobalt Tungstate	Pb_2CoWO_6
Lead Fluoride	PbF_2
Lead Hafnate	$PbHFO_3$
Lead Iodide	PbI_2
Lead Magnesium Niobate	$Pb_3MgNb_2O_9$
Lead Metatantalate	$PbTa_2O_6$
Lead Molybdate	$PbMoO_4$
Lead Niobate	$PbNb_2O_6$
Lead Nitrate	$Pb(NO_3)_2$
Lead Oxide	PbO
Lead Selenide	$PbSe$
Lead Sulfate	$PbSO_4$
Lead Sulfide	PbS
Lead Telluride	$PbTe$
Lead Titanate	$PbTiO_3$
Lead Tungstate	$PbWO_4$
Lead Zinc Niobate	$Pb(Zn_{1/3}Nb_{2/3})O_3$
Lead Zirconate	$PbZrO_3$
Lithium Ammonium Tartrate (LAT)	$LiNH_4C_4H_4O_6{\cdot}H_2O$
Lithium Bromide	$LiBr$
Lithium Carbonate	Li_2CO_3
Lithium Chloride	$LiCl$
Lithium Deuteride	LiD
Lithium Fluoride	LiF
Lithium Hydride	LiH
Lithium-6 Hydride	Li^6H
Lithium-7 Hydride	Li^7H
Lithium Iodate	$LiIO_3$
Lithium Iodide	LiI
Lithium Metagallate	$LiGaO_2$
Lithium Niobate	$LiNbO_3$
Lithium Sulfate Monohydrate	$Li_2SO_4 \cdot H_2O$
Lithium Tantalate	$LiTaO_3$
Lithium Thallium Tartrate (LTT)	$LiTlC_4H_4O_6 \cdot H_2O$
Lithium Tri-Hydrogen Selenite	$LiH_3(SeO_3)_2$
Lithium Trisodium Chromate	$LiNa_3CrO_4 \cdot 6H_2O$
Lithium Trisodium Molybdate	$LiNa_3MoO_4 \cdot 6H_2O$
MASD (Methyl Ammonium Alum)	$(CH_3NH_3)Al(SO_4)_2 \cdot 2H_2O$
Magnesium Borate Monochloride (Boracite)	$Mg_3B_7O_{13}Cl$
Magnesium Carbonate	$MgCO_3$
Magnesium Niobate	$MgNb_2O_6$
Magnesium Oxide	MgO
Magnesium Sulfate	$MgSO_4$
Magnesium Sulfate Septahydrate	$MgSO_4 \cdot 7H_2O$
Magnesium Titanate	$MgTiO_3$
Magnesium Tungstate	$MgWO_4$
Magnetite (Ferrosoferric Oxide)	Fe_3O_4
Manganese Dioxide	MnO_2
Manganese Niobate	$MnNb_2O_6$
Manganese Oxide (Pyrolusite)	MnO
Manganese Sesquioxide	Mn_2O_3
Manganese Tungstate	$MnWO_4$
Mercuric Chloride	$HgCl_2$
Mercurous Chloride (Calumel)	$HgCl$
Mercurous Selenide	$HgSe$
Mercurous Sulfide (Cinnabar)	HgS
Methyl Ammonium Alum (MASD)	$(CH_3NH_3)Al(SO_4)_2 \cdot 2H_2O$
Mica (Canadian)	$(K,H)Mg_3Al(SiO_4)_3$
Mica (Muscovite)	$(K,H)Al_3(SiO_4)_3$
Neodymium Aluminate	$NdAlO_3$
Neodymium Scandate	$NdScO_3$
Nickel Iodine Boracite	$Ni_3B_7O_{13}I$
Nickel Oxide	NiO
Nickel Niobate	$NiNb_2O_6$
Nickel Sulfate Hexahydrate	$NiSO_4{\cdot}6H_2O$
Nickel Tungstate	$NiWO_4$
Phosphorus (Yellow)	P
Phosphorus (Red)	P
Potassium Alum	$KAl(SO_4)_2{\cdot}12H_2O$
Potassium Bromate	$KBrO_3$
Potassium Bromide	KBr
Potassium Carbonate	K_2CO_3
Potassium Chlorate	$KClO_3$
Potassium Chloride	KCl
Potassium Chromate	K_2CrO_4
Potassium Chrome Alum	$KCr(SO_4)_2{\cdot}12H_2O$
Potassium Cyanide	KCN
Potassium Dideuterium Arsenate (KDDA)	KD_2AsO_4
Potassium Dideuterium Phosphate (KDDP)	KD_2PO_4
Potassium Dihydrogen Arsenate (KDA)	KH_2AsO_4
Potassium Dihydrogen Phosphate (KDP)	KH_2PO_4
Potassium Ferrocyanide	$K_4Fe(CN)_6 \cdot 3H_2O$
Potassium Floride	KF
Potassium Hexathionate	$K_2S_6O_6$
Potassium Iodate	KIO_3
Potassium Iodide	KI

Potassium Niobate	$KNbO_3$
Potassium Nitrate	KNO_3
Potassium Nitrite	KNO_2
Potassium Orthophosphate	K_3PO_4
Potassium Penta-Thionate	$K_2S_5O_6 \cdot H_2O$
Potassium Perchlorate	$KClO_4$
Potassium Selenate	K_2SeO_4
Potassium Strontium Niobate	$KSr_2Nb_5O_{15}$
Potassium Sulfate	K_2SO_4
Potassium Tantalate	$KTaO_3$
Potassium Tantalate Niobate (KTN)	$KTaNbO_3$
Potassium Tetra-Thionate	$K_2S_4O_6$
Potassium Thiocynate	KSCN
Potassium Trithionate	$K_2S_3O_6$
Proustite (Silver Thioarsenate)	Ag_3AsS_3
Pyrolusite (Manganese Oxide)	MnO
RDA (Rubidium Dihydrogen Arsenate)	PbH_2AsO_4
RDP (Rubidium Dihydrogen Phosphate)	PbH_2PO_4
Rochelle Salt (Potassium Sodium Tartrate)	$KNa(C_4H_4O_6) \cdot 4H_2O$
Rochelle Salt (Sodium Potassium Tartrate)	$NaK(C_4H_4O_6) \cdot 4H_2O$
Rubidium Alum	$RbAl(SO_4)_2 \cdot 12H_2O$
Rubidium Bisulfate	$RbHSO_4$
Rubidium Bromide	RbBr
Rubidium Carbonate	Rb_2CO_3
Rubidium Chloride	RbCl
Rubidium Chrome Alum	$RbCr(SO_4)_2 \cdot 12H_2O$
Rubidium Dihydrogen Arsenate (RDA)	RbH_2AsO_4
Rubidium Dihydrogen Phosphate (RDP)	RbH_2PO_4
Rubidium Fluoride	RbF
Rubidium Indium Sulfate	$RbIn(SO_4)_2$
Rubidium Iodide	RbI
Rubidium Nitrate	$RbNO_3$
Rutile (Titanium Dioxide)	TiO_2
Samarium Molybdate	$Sm_2(MoO_4)_3$
Selenium	Se
Silicon	Si
Silicon Carbide	SiC
Silicon Dioxide (α-Quartz)	SiO_2
Silicon Monoxide	SiO
Silicon Nitride	Si_3N_4
Silver Bromide	AgBr
Silver Chloride	AgCl
Silver Cyanide	AgCN
Silver Nitrate	$AgNO_3$
Silver Sodium Nitrite	$AgNa(NO_2)_2$
Silver Oxide	Ag_2O
Silver Thioarsenate (Proustite)	Ag_3AsS_3
Sodium Ammonium Tartrate (Ammonium Rochelle Salt)	$NaNH_4(C_4H_4O_6) \cdot 4H_2O$
Sodium Bromate	$NaBrO_3$
Sodium Bromide	NaBr
Sodium Carbonate	Na_2CO_3
Sodium Carbonate Decahydrate	$Na_2CO_3 \cdot 10H_2O$
Sodium Chlorate	$NaClO_3$
Sodium Chloride	NaCl
Sodium Cyanide	NaCN
Sodium Fluoride	NaF
Sodium Iodide	NaI
Sodium Niobate	$NaNbO_3$
Sodium Nitrate	$NaNO_3$
Sodium Nitrite	$NaNO_2$
Sodium Perchlorate	$NaClO_4$
Sodium Potassium Tartrate (Rochelle Salt)	$NaK(C_4H_4O_6) \cdot 4H_2O$
Sodium Sulfate	Na_2SO_4
Sodium Sulfate Decahydrate	$Na_2SO_4 \cdot 10H_2O$
Sodium Sulfate Pentahydrate	$Na_2S_2O_3 \cdot 5H_2O$
Sodium Potassium Tartrate Tetradeuterate (Deuterated Rochelle Salt)	$NaK(C_4H_2D_2O_6) \cdot 4D_2O$
Sodium Trideuterium Selenite	$NaD_3(SeO_3)_2$
Sodium Trihydrogen Selenite	$NaH_3(SeO_3)_2$
Sodium Uranyl Oxalate	$Na_2UO_2(C_2O_4)_2$
Spinel	$(MgO)_xAl_2O_3$
Stannic Dioxide	SnO_2
Stibnite (Antimonous Sulfide)	Sb_2S_3
Strontium Carbonate	$SrCO_3$
Strontium Chloride	$SrCl_2$
Strontium Chloride Hexahydrate	$SrCl_2 \cdot 6H_2O$
Strontium Fluoride	SrF_2
Strontium Formate Dihydrate	$Sr(COOH)_2 \cdot 2H_2O$
Strontium Molybdate	$SrMoO_4$
Strontium Niobate	$Sr_2Nb_2O_7$
Strontium Nitrate	$Sr(NO_3)_2$
Strontium Oxide	SrO
Strontium Sulfate	$SrSO_4$
Strontium Sulfide	SrS
Strontium Titanate	$SrTiO_3$
Strontium Tungstate	$SrWO_4$
Sulfur	S
TGFB (Triglycine Fluorberllyate)	$(NH_2 \cdot CH_2 COOH)_3 H_2BeF_4$
TGS (Triglycine Sulfate)	$(NH_2 \cdot CH_2$

	$COOH)_3 \cdot H_2SO_4$
TGSe (Triglycine Selenate)	$(NH_2 \cdot CH_2 COOH)_3 \cdot H_2SeO_4$
TTM (Tetramethylammonium Tribromo Mercurate)	$N(CH_3)_4HgBr_3$
TTM (Tetramethylammonium Triiodo Mercurate)	$N(CH_3)_4HgI_3$
TTM (Tetramethyl-Phosphonium Tribromo Mercurate)	$[P(CH_3)_4]HgBr_3$
Tantalum Pentoxide	Ta_2O_5
Tartaric Acid	$C_4H_4O_6$
Tellurium	Te
Terbium Molybdate	$Tb(MoO_4)_3$
Tetramethyl-Phosphonium Tribromo Mercurate (TTM)	$[P(CH_3)_4]HgBr_3$
Tetramethylammonium Tribromo Mercurate (TTM)	$N(CH_3)_4HgBr_3$
Tetramethylammonium Triiodo Mercurate (TTM)	$N(CH_3)_4HgI_3$
Thallous Bromide	TlBr
Thallous Chloride	TlCl
Thallous Iodide	TlI
Thallous Nitrate	$TlNO_3$
Thallous Sulfate	Tl_2SO_4
Thiourea	$SC(NH_2)_2$
Thorium Dioxide	ThO_2
Tin Antimonide	SnSb
Tin Telluride	SnTe
Titanium Dioxide (Rutile)	TiO_2
Titanium Sesquioxide	Ti_2O_3
Topaz (Aluminum Fluosilicate)	$(AlF)_2SiO_4$
Triglycine Fluoberllyate (TGFB)	$(NH_2 \cdot CH_2 COOH)_3 \cdot H_2BeF_4$
Triglycine Selenate (TGSe)	$(NH_2 \cdot CH_2 COOH)_3 \cdot H_2SeO_4$
Triglycine Sulfate (TGS)	$(NH_2 \cdot CH_2 COOH)_3 \cdot H_2SO_4$
Tungsten Trioxide	WO_3
Uranium Dioxide	UO_2
Ytterbium Manganate	$YbMnO_3$
Ytterbium Sesquioxide	Yb_2O_3
Yttrium Manganate	$YMnO_3$
Yttrium Sesquioxide	Y_2O_3
Zinc Oxide	ZnO
Zinc Selenide	ZnSe
Zinc Sulfide	ZnS
Zinc Telluride	ZnTe
Zinc Tungstate	$ZnWO_4$
Zirconium Dioxide	ZrO_2